JACOBS
UNIVERSITY

SELECTED ASPECTS OF THE ARCTIC SEA ICE MOTION AND ITS INFLUENCE ON THE OCEAN

by
Polona Itkin

A thesis submitted in partial fulfillment of the
requirements for the degree of

Doctor of Philosophy
in Geosciences

November 2013

Thesis Committee

Prof. Dr. Rüdiger Gerdes
Jacobs University Bremen

Prof. Dr. Laurenz Thomson
Jacobs University Bremen

Dr. Martin Losch
Alfred Wegener Institute Helmholz Center
for Polar and Marine Research, Bremerhaven

Abstract

A faithful simulation of the sea ice drift in a coupled sea ice-ocean model is one of the key prerequisites for a reliable simulation of the sea ice, ocean and atmosphere interactions. To achieve this goal we should continue improving model physics and constructing parameterizations for relevant sub-gird processes. Also a validation of the simulations against the observational data is essential. The main aim of this work is to demonstrate the importance of the sea ice motion for the underlaying ocean. In the scope of the ongoing and anticipated Arctic climate change it has been demonstrated that the changes in the atmosphere and ocean have large impacts on the sea ice cover. At present, it is still unclear if the changes in the sea ice motion itself can also have a feedback effect on the ocean. In this work we hypothesize that a change in the sea ice motion can cause significant changes in the ocean properties and circulation. To test the hypothesis we use two sensitivity studies that help to isolate sea ice motion processes and quantify the contribution of the process to the Arctic climate system. Our main results show that the immobile landfast ice in the model simulation shifts the flaw polynya, location of strong winter sea ice and brine production away from the coast in the more saline ocean waters and more brine reaches the Arctic halocline. This strengthens the halocline that shields cold surface waters and sea ice from the warm Atlantic Water layer underneath. In addition we find that a general change in the sea ice internal strength leads to substantial changes in the ocean properties and circulation. Under weaker and more mobile sea ice Atlantic Water layer temperatures are reduced by 0.2 K. The Eurasian basin circulation in the Atlantic Water layer is increased and this leads to the volume transports adjustments at the Arctic Straits. This effect shows that the Arctic sea ice properties and motion are not only important for the Arctic ocean, but may have consequences also for the global ocean circulation.

Contents

List of Figures

List of Tables

List of Acronyms

AARI Arctic and Antarctic Research Institute

ADCP Acoustic Doppler Current Profiler

AIW Arctic Intermediate Water

AIW Arctic Intermediate Water

AMOC Atlantic Meridional Overturning Circulation

AMSR-E Advanced Microwave Scanning Radiometer

AO Arctic Oscillation

AOMIP Arctic Ocean Model Intercomparison Project

ARP Arctic Rapid change Pattern

ASAR Advanced Synthetic Aperture Radar

AW Atlantic Water

AWI Alfred Wegener Institute

AWL Atlantic Water Layer

BG Beaufort Gyre

BSBW Barents Sea Branch Water

CERSAT Center for Satellite Exploitation and Research

CMCC Continious Cross Correlation Method

CORE Coordinated Ocean Research Experiment

CTRL control run

IFREMER French Research Institute for Exploitation of the Sea

LF landfast ice run

MITgcm Massachusetts Institute of Technology General Circulation Model

MIZ Marginal Ice Zone

MODIS Moderate Resolution Imaging Spectroradiometer

NAOSIM North Atlantic/Arctic Ocean - Sea Ice Model

NCAR/NCEP National Centers for Environmental Prediction/National Center for Atmospheric Research

NCEP-CSFR NCEP - The Climate Forecast System Reanalysis

NSIDC National Snow and Ice Data Center

OSI-SAF EUMETSAT Ocean and Sea Ice Satellite Application Facility

P compressive sea ice strength

P* maximal compressive sea ice strength empirical constant

QuikSCAT Quick Scatterometer

SLP Sea Level Pressure

SSM/I Special Sensor Microwave/Imager

SST Sea Surface Temperature

T sea ice tensile strength

TD Transpolar Drift

WEAK weak sea ice run

WSC West Spitzbergen Current

z* rescaled vertical coordinate

Chapter 1

Introduction

This thesis is organized in the following way: in this Chapter Sections 1.1 and 1.2 give a brief introduction of the investigated research area, Section 1.3 outlines the aims and research hypothesis, Section 1.3 describes the applied methods, Section 1.4 introduces the papers that form the core of the thesis in Chapters 2, 3 and 4. Finally, Chapter 5 gives a summary of the findings.

1.1 Arctic Ocean

The Arctic Ocean or the Arctic Mediterranean is the wold smallest ocean. On the southern rims it is connected to the Atlantic Ocean through the Fram Strait and through the Canadian Archipelago and to the Pacific Ocean through the Bering Strait. Arctic Ocean has a perennial sea ice cover that reaches its maximal extent in winter when it covers most of the ocean's surface and its minimal extent in summer when the sea ice cover is confined only to the deep basins. Although the Arctic Ocean takes less than 4 % of the global ocean surface is gathers more than 10 % of the global continental river runoff (de Couet and Maurer, 2009).

The Arctic Ocean sea ice and ocean surface circulation is characterized by the anticyclonic Beaufort Gyre (BG) in the Amerasian Basin and the Transpolar Drift (TD) that carries the sea ice and surface water from the Siberian Seas towards Fram Strait (light blue arrows on Figure 1.1). The interannual variability in the strength and location of the ocean surface current system components depends on the Sea Level Pressure (SLP) over the Amerasian Basin and North Atlantic (Govorucha and Gerasimov, 1970; Proshutinsky and Johnson, 1997;

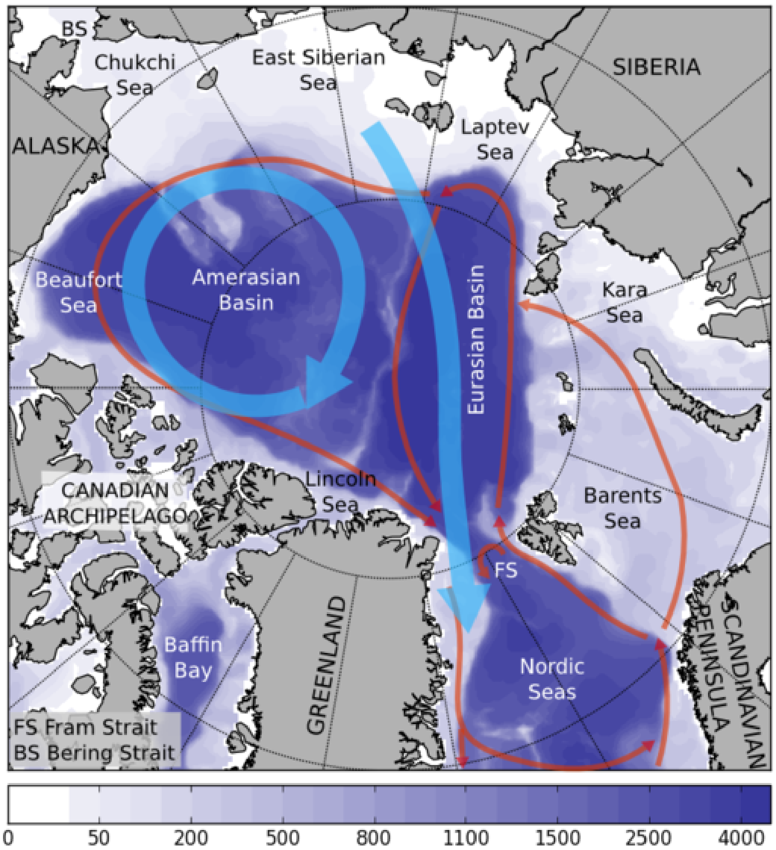

Figure 1.1: The Arctic Ocean and its marginal seas. The sea ice and surface circulation is schematically represented by light blue and mid-depth circulation by red arrows (simplified from Rudels et al (2013)).

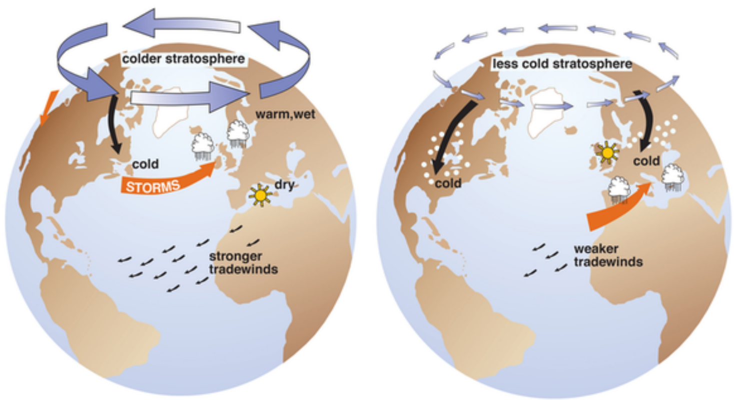

Figure 1.2: Left: Effects of the Positive Phase of the Arctic Oscillation. Right: Effects of the Negative Phase of the Arctic Oscillation. Credit: J. Wallace, University of Washington.

Johnson et al, 1999). If the Islandic Low expands further from the North Atlantic to the Barents and Kara seas, the anticyclonic circulation is weak and the TD widens and slows down. If the anticyclonic circulation over the Amerasian basin is strong, the TD is positioned closer to the Siberian shelfbreak and faster. The corresponding atmospheric circulation anomaly was characterized by Thompson and Wallace (1998) as the Arctic Oscillation (AO). The AO index is defined as the leading principal component of Northern Hemisphere SLP. A strong positive AO index from 1989 till 1995 with weaker Polar High over the Amerasian Basin and therefore weaker anticyclonic circulation and stronger westerlies in the subpolar latitudes was interpreted as the main cause for the steady decrease of the Arctic sea ice extent and sea ice thinning in the 1990s (Rigor et al, 2002). In addition to the local SLP changes in the Arctic, the AO positive phase the stronger westerlies bring more warmth and moisture to Eurasian catchment areas and increase the continental runoff of the Arctic rivers that also influence the Arctic Ocean surface hydrography.

Since 1995 the AO has been predominantly near-neutral or negative, but the sea ice extent and thickness were still decreasing (Comiso et al, 2008; Haas et al, 2008; Kwok et al, 2009). This Arctic Paradox (Overland and Wang, 2005) was addressed by Zhang et al (2008) who pointed out another pattern in the atmospheric circulation, the third principal component of the Northern Hemisphere SLP: a dipole structure between the Eurasian Arctic coast and North Pacific named Arctic Rapid change Pattern (ARP). In recent years the ARP replaced the AO as the leading SPL pattern. The ARP is associated with the meridional winds that transfer more heat from subpolar latitudes into the Arctic (Overland

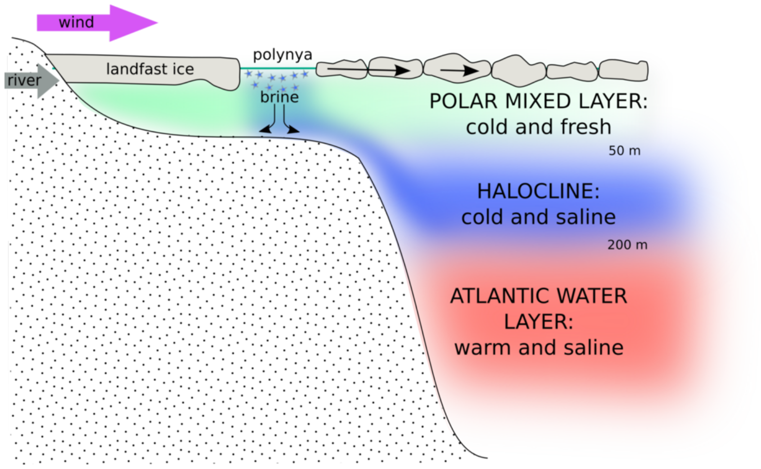

Figure 1.3: Arctic ocean vertical stratification and winter processes maintaining the Arctic halocline.

and Wang, 2010). During ARPs negative phase, an anomalous Eurasian Arctic coast high and North Pacific low occur, resulting in strengthened poleward atmospheric heat transport directly reaching the central Arctic and enhanced Atlantic Water (AW) intrusion into the Arctic Ocean (Zhang et al, 2008).

In the Arctic Ocean surface layer that is driven by these atmospheric circulation patterns the seasonal sea ice melt and freezing cycle maintains the fresh upper ocean waters at the freezing point. In contrast, the ocean temperature below the halocline (Figure 1.3) increases again and at mid-depth the Arctic Ocean has temperatures up to several degrees above zero. The bulk of this warm and salty water is composed of Atlantic Water (AW) that enters the Arctic Ocean though the Fram Strait and the Barents Sea. Also the anticyclonic surface circulation is contrasting the mid depth circulation of the Atlantic Water Layer (AWL) characterized by generally cyclonic motion, most of which occurs in boundary currents along the deep ridges and shelf breaks (red arrows on Figure 1.1, Rudels et al (2013)). Before entering the central Arctic Ocean basins via Fram Strait or the Barents Sea both AW branches experience heat loss and are modified by ice melt and freeze, as well as river runoff. Both branches feed the AWL and after passing through the basins leave the Arctic ocean proper on return through the Fram Strait as Arctic Intermediate Water (AIW). The AIW flows into the Nordic Seas and has an important role in the dense water formation that feed the Atlantic Meridional Overturning Circulation (AMOC) (Schmitz and McCartney, 1993; Swift, 1984).

The cold and fresh surface layers are decoupled form the mid-depth salty and warm AWL by a strong halocline (Figure 1.3) which is maintained by the cold brines formed on the shelf seas (Aagaard et al, 1981; Martin and Cavalieri, 1989; Cavalieri and Martin, 1994a; Winsor and Björk, 2000a) and by winter convection in the northern Barents Sea (Rudels et al, 1996). The cold and fresh waters flow off the shelves and sink along the shelf break, where they mix with the adjacent warm AW. Several authors report about the temperature fluctuations of the AW in the 20^{th} century (Schauer et al, 2004; Polyakov et al, 2005; Dmitrenko et al, 2008). If the warming signal detected in the last decade would continue (Dmitrenko et al, 2008) this could weaken the halocline and some heat could reach the surface layer and contribute to further fast reductions of the Arctic sea ice cover. Also an eastward redirection of the riverine water would result in the surface layer salinification in the Eurasian Basin and halocline weakening as already observed by Johnson and Polyakov (2001) during the positive AO phase in the 1990s. The mid-depth and to some extend also deep water mass modifications detected in the Arctic Ocean in the last decade can exit through the Fram Strait and the Nordic Seas, reach the deep convection areas in the North Atlantic (Karcher et al, 2011) and influence the AMOC.

The combination of the ongoing changes in atmospheric conditions, drifting and landfast ice, and continental runoff are driving the changes in the Arctic Ocean sea ice cover. The Arctic sea ice is getting thinner (Kwok and Rothrock, 2009), more mobile (Rampal et al, 2009; Spreen et al, 2011) and the sea ice extent is shrinking (Stroeve et al, 2012). The reasons for the changes have been under vigorous inspection in the scientific community in various observational and modeling studies (Shimada et al, 2006; Perovich et al, 2008; Kauker et al, 2009; Polyakov et al, 2010; Kattsov et al, 2010; Zhang et al, 2012).

1.2 Siberian Seas

The Eurasian shelf with its shallow seas is the largest shelf in the world and it occupies about 1/3 of the Arctic Ocean area. The eastern part of it, the Siberian shelf which is commonly divided into Kara, Laptev East Siberian and Chukchi Sea, is the shallowest (depth rarely exceeding 200 m) and freshest part of it, as it receives water from the great Siberian rivers: Ob, Yenisei and Lena. Together with smaller rivers they contribute approximately 2100 km^3/year of freshwater (Prange, 2003). This large flux of river water strongly affects temperature, salinity and other ocean parameters. Peterson et al (2002) analyzed the average annual discharge from the six largest Eurasian rivers and discovered an increase of 7% from 1936 to 1999. This agrees with the steady

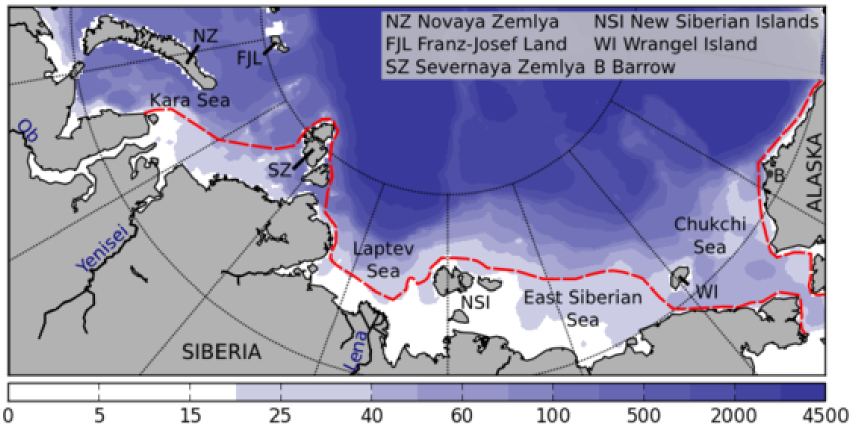

Figure 1.4: Siberian Seas and average position of the landfast ice edge (red dash line).

increase in the northern Eurasian precipitation over the 20th century (Kattsov and Walsh, 2000; McClelland et al, 2004).

Landfast ice (also fast, shore-fast ice) is a dominating feature in the Siberian Seas during winter as it can extend a few kilometers from the coast in the western part of the Laptev Sea or in the Chukchi Sea to several hundred kilometers in the southeastern Kara, Laptev and East Siberian Seas. This creates a vast hydrologically distinct inner shelf region outlined by the landfast ice edge and decoupled from the atmosphere with sea ice that is immobile and mechanically fastened to the coast or to the sea floor. Landfast ice consolidates in late November and remains fixed until early July break up (Rigor and Colony, 1997). For drifting sea ice, the landfast ice edge forms an advanced winter shore line and heavy ridging occurs along this edge during onshore wind events. During the prevailing offshore winds pack ice is advected seaward from the landfast ice edge and narrow stretches of open water and young ice - flaw polynyas, occur. Frequent polynya events, low winter temperatures and prevailing northward ice drift make the Siberian flaw polynya system a major source of the sea ice production for the TD (Eicken et al, 1997; Rigor and Colony, 1997; Alexandrov et al, 2000). The possible contribution of the Siberian flaw polynyas to the formation of dense saline shelf waters was addressed by Aagaard et al (1981); Martin and Cavalieri (1989); Cavalieri and Martin (1994b); Winsor and Björk (2000b); Dmitrenko et al (2005b); Bauch et al (2009); Krumpen et al (2011). The role of this immobile ice cover for the riverine water redistribution was summed up by Proshutinsky et al (2007).

The knowledge about the general circulation patterns in the Siberian Seas is

Figure 1.5: Left: Photo of leveled landfast ice, right: polynya in the Chukchi Sea during SIZONet sea ice campaign at Barrow, Alaska, May 2010.

based on the Russian historical datasets from predominantly summer expeditions. Its main characteristic is the eastward alongshore Siberian Coastal Current that is forced by winds, river runoff and ice melt (Govorucha and Gerasimov, 1970; Weingartner et al, 1999). The current direction is variable and it can revert westward (Münchow et al, 1999). Just north of the shelf break the much better studied TD system begins.

Local atmospheric circulation over the Siberian Seas is governed by the large scale atmospherics circulation over the Arctic Ocean. The Laptev Sea, in particular, is situated within the zero vorticity contour separating the SLP centers over the Amerasian Basin and North Atlantic (Johnson and Polyakov, 2001). This position renders its hydrography very sensitive to the shifts between predominant cyclonic and anticyclonic atmospheric circulation (Dmitrenko et al, 2005a) and several authors distinguish between periods with predominant cyclonic and predominant anticyclonic regimes (Dmitrenko et al, 2005a; Bauch et al, 2009; Abrahamsen et al, 2009). The winds are parallel to the isobars and the Coriolis force deflects the ocean and sea ice motion on the Northern hemisphere to the right. The mean surface current direction is usually perpendicular to the wind direction. On the shallow shelf, however, the current is essentially controlled by wind stress and bottom friction and the Coriolis force becomes insignificant. The surface current aligns almost completely with the wind direction. Thus, the cyclonic regime on the Laptev Sea shelf drives ”onshore” surface currents that divert the riverine water eastward towards the East Siberian Sea. In the ”offshore” anticyclonic regime the riverine water is advected northward.

The declining summer sea ice cover is opening large areas of open water in the Siberian Seas (Comiso et al, 2008; Stroeve et al, 2012). The modified surface fluxes should lead to warmer and fresher surface layer. Decadally averaged temperatures (1950s-1980s) for various water depths in the Arctic Ocean available from the National Snow and Ice Data Center (NSIDC) in Boulder, Colorado (Timokhov and Tanis, 1997, 1998) indicate that there have been decadal scale changes of a degree or more in the temperatures of surface water, and smaller changes in deeper water. Interdecadal variability is apparent along the Beaufort shelf (warmer in the 1960s and 1980s) and the Laptev Sea shelf (cooler in the 1980s) (Slanina, 2007). Dmitrenko et al (2010), however analyzed the same historical dataset with addition of the data from Russian-German expeditions in the 1990s and 2000s and report no significant warming over the Laptev Sea shelf deeper than 10-15 m. In summer 2007, when a prominent minimum in sea ice extent was observed, the atmospheric circulation over the Siberian Seas was cyclonic (Abrahamsen et al (2009); Hölemann et al (2011)) -"onshore". Most of the seas were ice free and absorbed unusual amount of heat. (Steele et al, 2008) and (Frolov et al, 2009) report a $+2°C$ to $+5°C$ anomaly in the sea surface temperature (SST). The bottom water temperatures anomaly on the mid-shelf was more than $+3°C$ (Hölemann et al, 2011). The possible reduction of landfast ice cover extent or duration in the future would result in flaw polynyas located in the more fresh coastal waters and less brine would reach the Arctic halocline. The modifications of the shelf water masses that feed the Arctic Ocean surface and partly intermediate layers might lead to changes in the Arctic Ocean stratification (Figure 1.3).

1.3 Scope of this work

The main aim of this work is to demonstrate the importance of the sea ice motion for the underlaying ocean. Sea ice motion is transporting sea ice from the area where the sea ice formed in through the freezing processes to the area where it melts and releases freshwater and takes up latent heat from the ocean and atmosphere. The sea ice drift, and in particularly the divergent sea ice motion causes opening of leads and polynyas, where more sea ice is formed and the ocean's freshwater is removed, stored in solid form in the sea ice and latent heat is released to the atmosphere. The remaining surface ocean water depleted in freshwater still contains the salt and thus has a higher density than the underlaying water and therefore sinks to the depth where its buoyancy is neutral.

The sea ice is also a layer between the atmosphere and ocean and is transmitting and transforming the wind stress to the ocean surface. How much momentum is transfered from the atmosphere to the ocean depends on the sea ice internal stress. The main tool for our investigations is a numerical sea ice-ocean coupled model described in Section 1.3 where processes outlined above are represented by equations.

A faithful simulation of the sea ice drift in a coupled sea ice-ocean model is one of the key prerequisites for a reliable simulation of the sea ice, ocean and atmosphere interactions. Apart from improving model physics and constructing parameterizations for relevant sub-gird processes also validation of the simulations against the observational data is essential. But the Arctic Ocean is a remote region, generally inaccessible during the severe winter weather conditions. Satellite remote sensing products (Ezraty et al, 2006; Lavergne et al, 2010) offer a large improvement in the spatial and temporal availability of observational ice drift data, but they also need to be validated with the in-situ data. For the remote coastal regions such as the Siberian Seas there are even fewer ice drift field observations available, as the manned stations and drifting buoys are usually positioned in the thicker sea ice of the Central Arctic. Alternatively a numerical model simulation offers temporally and spatially holistic view on the processes in the Arctic Ocean. At this point the model simulations, satellite and in-situ observations should be seen as complimentary research approaches that benefit from each other and not as alternatives.

In the scope of the ongoing and anticipated Arctic climate change (Kwok and Rothrock, 2009; Spreen et al, 2011; Stroeve et al, 2012) it has been demonstrated that the changes in the atmosphere (Shimada et al, 2006; Perovich et al, 2008) and ocean (Polyakov et al, 2010) have a large impact on the sea ice cover. It has also been shown that the thinning of the sea ice is preconditioning further fast reductions in the sea ice (Haas et al, 2008; Zhang et al, 2012). The hypothesis of the sea ice positive feedback where the loss of the Arctic sea ice will lead to albedo increase and consequently to even faster warming of the Arctic has been widely accepted by the scientific community. At present, it is still unclear if the changes in the sea ice motion itself can also have a feedback effect on the ocean. In this work we hypothesize that a change in the sea ice motion will cause significant changes in the ocean properties and circulation. To test the hypothesis we use two sensitivity studies that help to isolate sea ice motion processes and quantify the contribution of the process to the Arctic climate system.

Data and Methods

The main tool for our investigations is a numerical sea ice-ocean coupled model. State-of-the-art sea ice models are all based on the same set of primitive equations that are simplified descriptions of the processes in nature. The sea ice is usually simulated by a dynamical-thermodynamical models such as Hibler III (1979) or Hunke and Dukowicz (1997). The base of the thermodynamical model is the energy balance of the sea ice:

$$Q_a + Q_w + \rho_i L_i \frac{\partial h}{\partial t} = 0 \tag{1.1}$$

where Q_a is the heat exchange of the sea ice with the atmosphere and Q_w with the ocean. ρ_i is the sea ice density. L_i is the latent heat taken up or released during sea ice growth: $\frac{\partial h}{\partial t} > 0$ or sea ice melt: $\frac{\partial h}{\partial t} < 0$, where h is sea ice thickness and t is time.

The base of the sea ice dynamical model is the momentum balance (Hibler III, 1979):

$$m_i(\frac{\partial \vec{u}}{\partial t} + \vec{u} \cdot \nabla \vec{u}) = \tau_a + \tau_w - m_i f \vec{k} \times \vec{u} - m_i g \nabla H_{tilt} + \nabla \cdot \sigma \tag{1.2}$$

where m_i is the sea ice mass per unit area and $\vec{u}$ is the sea ice velocity. On the right side of the equations the terms are τ_a - atmospheric stress, τ_w - oceanic stress, $m_i f \vec{k} \times \vec{u}$ - Coriolis term (f is the Coriolis parameter and k is the unit vector normal to the surface), $m_i g \nabla H_{tilt}$ - horizontal tilt term (g is gravitational acceleration and H_{tilt} is the sea surface tilt) and finally the divergence of the ice stress tensor $\nabla \cdot \sigma$ that describes the internal sea ice forces stemming from ice interactions like rafting, ridging and fracturing. This is the only term in the equation which depends directly on the sea ice properties itself.

Hibler III (1979) uses rheology which connects σ with the strain rate tensor $\dot{\epsilon}$, a basic variable describing the sea ice behavior, and considers the sea ice as a viscous plastic fluid. This means that at small σ and $\dot{\epsilon}$ acting upon sea ice, sea ice behaves like a viscous fluid and undergoes no deformation. But when a certain threshold is reached sea ice behaves like a plastic material and is permanently deformed. σ is defined as:

$$\sigma_{ij} = 2\eta\dot{\epsilon}_{ij} + ((\eta - \zeta)(\dot{\epsilon}_{11} + \dot{\epsilon}_{22}) - \frac{P}{2})\delta_{ij}, \tag{1.3}$$

where σ_{ij} and $\dot{\epsilon}_{ij}$ are two-dimensional stress and strain rate tensors and δ_{ij} is Kroeneker delta function. ζ - bulk viscosity, η - shear viscosity and P - sea ice strength are defined as:

$$\zeta = P/2\Delta, \tag{1.4}$$

$$\eta = \zeta/e^2, \tag{1.5}$$

and

$$P = P^* h \exp(-C^*(1 - A)), \tag{1.6}$$

where $\Delta = \sqrt{(\dot{\epsilon}_{11}^2 + \dot{\epsilon}_{22}^2)(1 + e^{-2}) + \frac{4}{e^2}\dot{\epsilon}_{12}^2 + 2\dot{\epsilon}_{11}\dot{\epsilon}_{22}(1 - e^{-2})}$ is a term introduced for brevity and e is eccentricity constant. The sea ice internal stress P in this rheology varies with the sea ice thickness and concentration (A), whereas P^* and C^* - sea ice strength parameters are empirical constants.

To track the consequences of the perturbing the sea ice motion the sea ice model is coupled to a regional ocean model. In this study we use two models: The North Atlantic/Arctic Ocean - Sea Ice Model (NAOSIM) and the Massachusetts Institute of Technology general circulation model (MITgcm). Both models cover the same domain enclosing the northern North Atlantic, the Nordic Seas and the Arctic Ocean (Figure 1.6) on a rotated grid with the grid equator passing through the geographical North Pole. Both models have similar numerics, but differ in the spatial resolution.

NAOSIM is a coupled ocean-sea ice model developed at the AWI (Gerdes et al, 2003; Karcher et al, 2003; Fieg et al, 2010). Here we use the highest resolving version of NAOSIM (Fine Resolution Model), that has a horizontal grid spacing of 1/12°. In the vertical, the model has 60 levels. Near the surface, the vertical resolution is 10 m. There is a minimum number of three grid cells in the vertical, limiting the representation of shallow topography. The ocean component of the model is based on the Modular Ocean Model MOM-2 of the Geophysical Fluid Dynamics Laboratory (Pacanowski, 1995). It is coupled, following the scheme developed by Hibler and Bryan (1987), to a dynamic-thermodynamic sea ice model (Hibler III, 1979) which employs a viscous-plastic rheology. River water discharge is incorporated as in Prange and Gerdes (2006). River water influx is distributed over the first three levels in the vertical to improve vertical mixing

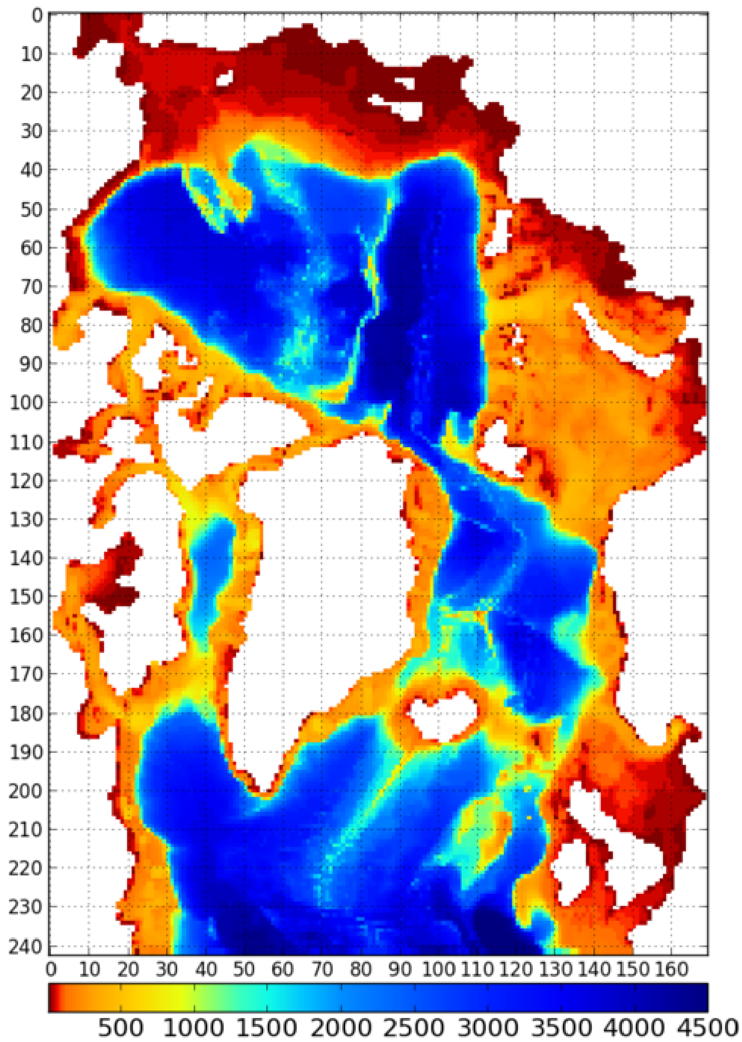

Figure 1.6: Model domain of NAOSIM and MITgcm and the bathymetry of the MITgcm.

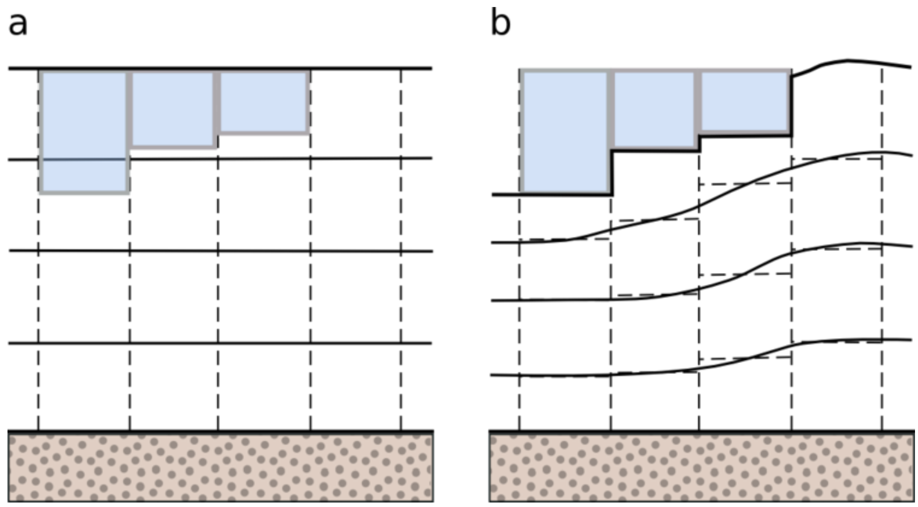

Figure 1.7: Schematic view of two vertical coordinate options under thick sea ice: a - z vertical coordinate with rigid lid, b - z* vertical coordinate with non-linear free surface. In a the first layer is a mixture of sea ice and water with the first level empty, while in b the sea surface position is depressed by the weight of sea ice and the tilt of the coordinate in avoids the problem of disappearing level. The figure is adopted from Campin et al (2008).

of the fresh water near the river mouths (Fieg et al, 2010). The model includes a passive salinity tracer to follow the spreading of the river water. NAOSIM is an established model in the Arctic community participating in the Arctic Ocean Model Intercomparison Project (AOMIP, `http://www.whoi.edu/projects/AOMIP/`).

Massachusetts Institute of Technology General Circulation Model - MITgcm (Marshall et al, 1997) is a community effort model available at `http://mitgcm.org/`. The numerous users of the code update, develop, maintain and document the model code on a regular basis. The model configuration we have used is similar to the NAOSIM, but it has a coarser horizontal resolution of 1/4° (∼28 km). The vertical resolution is adjusted to the surface and halocline studies and its 36 levels are unevenly distributed in a way that the top 500 m of the water column is divided into 20 levels and the depths below 2000 m have only 6. The very thin surface layer thickness under sea ice requires a non-linear free surface and the use of the rescaled vertical coordinate z* (Figure 1.7, (Campin et al, 2008)). Non-linear free surface and z* are an example of options that are not available at NAOSIM. The MITgcm sea ice model is based on a version of the viscous-plastic dynamic-thermodynamic sea ice model of Zhang and Hibler III (1997) with some adaptations and many further numerical options and parameterizations described by Losch et al (2010).

To validate our sea ice drift simulation in the Laptev Sea we have used a unique mooring (Figure 1.8) dataset from winter 2007/08 and a self produced sea motion product. Other data used for the validation in our research are publically available remote sensing sea ice products and sea ice and ocean databases.

1.4 Overview of the Papers

The main aim of this thesis is to investigate the effect of the sea ice motion on the underlaying ocean.

In the first paper:

Polona Rozman, Jens Hölemann, Thomas Krumpen, Rüdiger Gerdes, Cornelia Köberle, Thomas Lavergne, Susanne Adams and Fanny Girard-Ardhuin, 2011: **Validating Satellite Derived and Modeled Sea Ice Drift in the Laptev Sea with In-Situ Measurements of Winter 2007/08**. Polar Research, 30, 7218, DOI: 10.3402/polar.v30i0.7218.

we address the challenge of cross-validating the point observations, remote sensing products and model simulations. Our research area is the Southeastern Laptev Sea, a coastal region that is especially difficult to simulate due to the partial cover with the immobile landfast sea ice. The land contamination of the satellite sea ice grid points close to the coast and a general lack of the in-situ data make this validation attempt especially difficult. To address the latter problem we present a unique dataset composed of two points with mooring measurements over the winter 2007/08. We use an approach novel in the sea ice research: circular statistics to compare the sea ice drift directions.

Our main findings are that correlations of sea ice direction between the in situ data and the remote sensing products are high, about 0.8. Similar correlations are achieved by the model simulations. The sea-ice drift speed is the more challenging variable as some of the satellite products and model have have only moderate correlations of about 0.6 to the in situ records. The landfast ice parameterization implementation in the model was successfully tested for its influence on the sea-ice drift. In contrast to the satellite products, the model drift simulations have a full temporal and spatial coverage and results are reliable enough to be used as sea-ice drift estimates on the Laptev Sea Shelf.

As our main aim remains to study the impact of the sea ice motion on the ocean we then attempted to develop a landfast ice paramterization that would

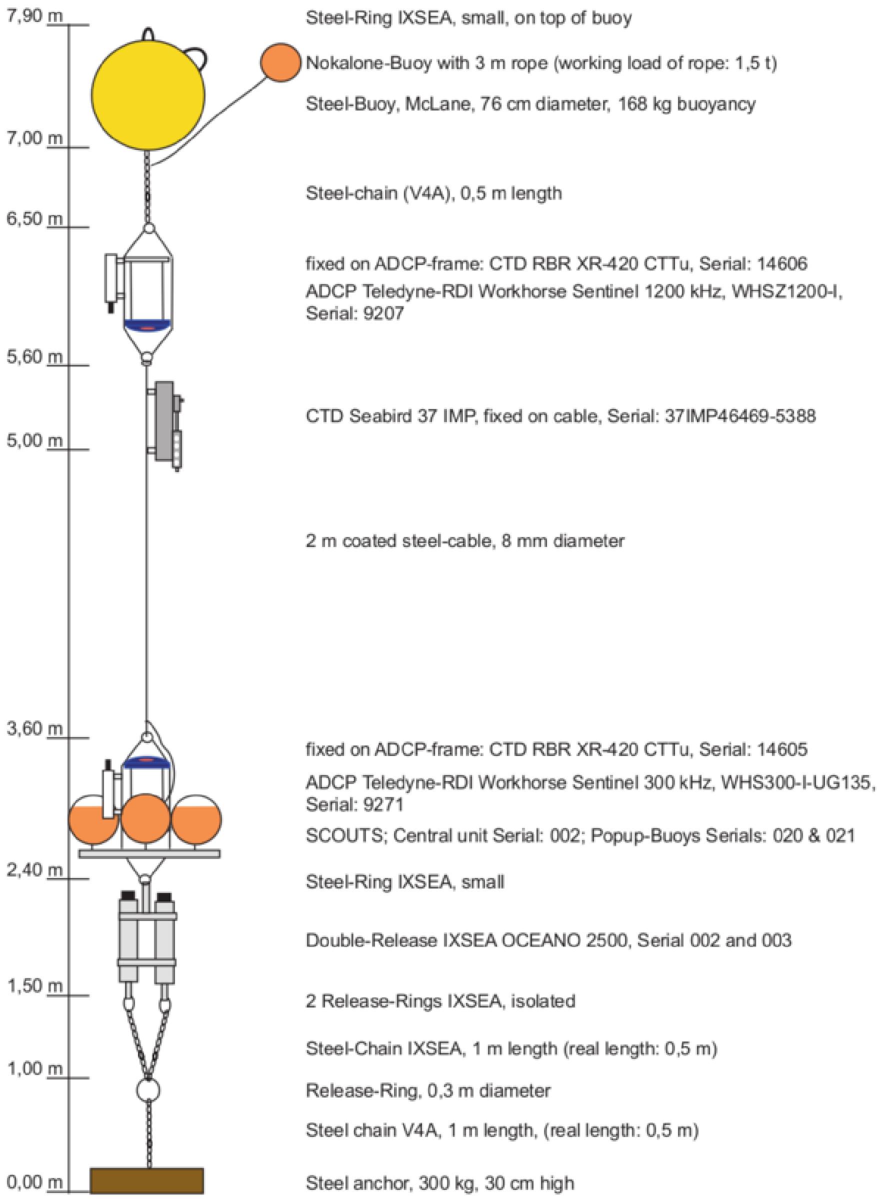

Figure 1.8: Mooring scheme of the two moorings which data forms the dataset. The instrument monitoring the sea ice drift is the ADCP (Acoustic Doppler Current Profiler) at 3 m above the bottom. Credit: Torben Klagge, IFM-Geomar, Kiel.

be applicable for more than a single winter and dependent as well on the sea ice properties. Landfast ice is immobile level sea ice (Figure 1.5) and the most logical property to use was the compressive sea ice strength (P) that prevents the sea ice from deforming. To inspect a general impact of P on the sea ice and ocean we performed a sensitivity study that was motivated also by the observed changes of sea ice motion due to the climate change.

Our second paper is therefore:

Polona Itkin, Michael Karcher and Rüdiger Gerdes, 2013: **Is weaker Arctic sea ice changing the Atlantic water circulation?** Submitted to the Journal of Geophysical Research - Oceans.

In this paper we perform a sensitivity study by comparing two MITgcm model simulations that differ only in the P* constant: 25700 N/m^2 (control run: CTRL) and 15000 N/m^2 (weak sea ice run: WEAK). In WEAK the sea ice velocities are generally higher than in CTRL. Through the momentum transfer to the ocean and difference in the sea ice cover distribution these differences are reflected not only in the surface layer, but also in the mid-depth AWL of the ocean. Differences in the sea ice extent in the marginal sea ice zone (MIZ) lead to a reduction of the AWL temperatures by 0.2 K in WEAK comparing to CTRL. The increased sea ice mobility in the central Arctic in WEAK results in faster and deeper ocean's anticyclonic BG which hampers the cyclonic AW circulation beyond the Lomonosov Ridge and enhances the loop of the AW in the Eurasian Basin. As a results of both mechanisms, the Fram Strait net outflow increases by 0.46 Sv whereas as a reaction the Davis Strait net outflow is weaker by 0.28 Sv.

The main lesson that we learn with this study for our landfast ice parametrization development is that the P* parameter choosing (and P definition) should be done with care and that a uniform change of P* to achieve the immobile landfast ice in the Siberian Seas would have Arctic wide consequences for the ocean properties. Therefore we decided for a parameterization that would only effect the local sea ice properties in the shallow and river runoff characterized Siberian Seas.

In our third paper:

Polona Itkin, Martin Losch and Rüdiger Gerdes, 2013: **Role of the landfast ice for the Arctic halocline stability.** Manustript in preparation,

we return to the research problem of the sea ice drift and landfast ice in the Siberian Seas. We present a landfast parametrization depending on the bathymetry, where we double the P* and introduce the sea ice tensile strength T (resistance to divergence) König Beatty and Holland (2010) in the coastal regions shallower than 30 m. This creates an immobile sea ice cover that shields the river plume residing on the shelf from the wind stress and positions the polynyas further offshore in the more saline waters. A sensitivity study where we compare a control run (CTRL) to a run with the landfast ice parametrization (LF) shows that the landfast ice has local impact on the sea ice thickness and Arctic wide impact on the halocline stability. We recommend to include our simple landfast parametrization into the regional climate and biogeochemical models that study freshwater distribution, water column stability and nutrient availability.

Chapter 2

Validating Satellite Derived and Modeled Sea Ice Drift in the Laptev Sea with In-Situ Measurements of Winter 2007/08

Abstract

A correct representation of the ice movement in an Arctic sea ice - ocean coupled model is essential for a realistic sea ice and ocean simulation. The aim of this study is to validate the observational and simulated sea ice drift for the Laptev Sea shelf region with in-situ measurements of winter 2007/08. Several satellite remote sensing datasets are first compared to the mooring measurements and afterwards to the sea ice drift simulated by the coupled sea ice-ocean model. The different satellite products have a correlation to the in-situ data ranging from 0.56 to 0.86. The correlations of sea ice direction or individual drift vector components between the in-situ data and the observations are high, about 0.8. Similar correlations are achieved also by the model simulations. The sea ice drift speed of the model and of some satellite products have only moderate correlations of about 0.6 to the in-situ record. The standard errors for the satellite products and model simulations drift components are similar to the errors of the satellite products in the central Arctic and are in the range of 0.03 m/s. The fast ice parameterization implementation in the model was also successfully tested for its influence on the sea ice drift. The model drift simulation have contrary to the satellite products a full temporal and spatial coverage and results are reliable enough to use them as sea ice drift estimates on the Laptev Sea shelf.

2.1 Introduction

A faithful simulation of the sea ice velocities in a coupled sea ice-ocean model is one of the key prerequisites for a reliable simulation of the sea ice, ocean and atmosphere parameters. To achieve it, data gathered by manned stations, drifting bouys and lately satellite sensors have been used extensively in pan-Arctic sea ice model validations (Lemke et al, 1997; Kreyscher et al, 2000a; Martin and Gerdes, 2007) and data assimilations (Meier et al, 2000; Rollenhagen et al, 2009). For the remote coastal regions such as the Laptev Sea shelf there are very few ice drift field observations available. Satellite remote sensing products offer a large improvement in the spatial and temporal availability of observational data, but the retrieval algorithms give products with discontinuous temporal coverage at the grid points closest to the coast (Ezraty et al, 2006; Lavergne et al, 2010) that are consequently hard to inspect for inconsistency.

Sea ice motion is important as a transport of fresh water and latent heat. Its

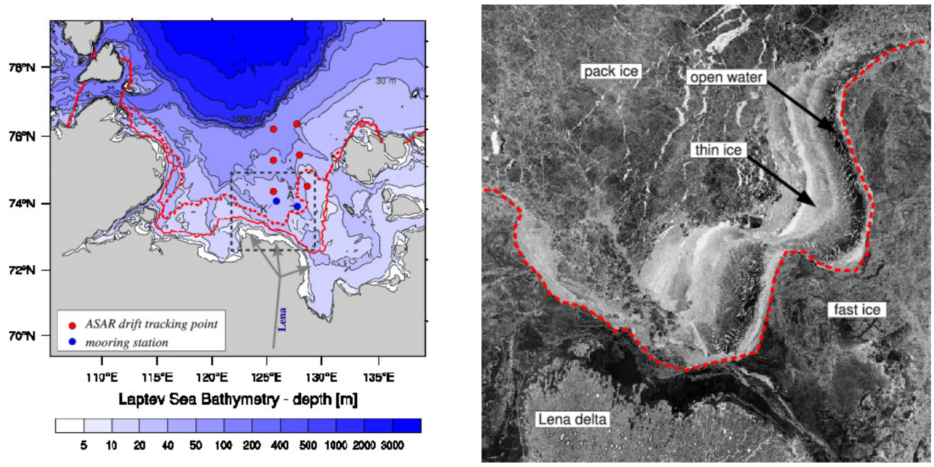

Figure 2.1: Left: Laptev Sea bathymetry (Jakobsson et al, 2008). The fast ice extents in December 2007 (solid red line) and in May 2008 (dashed red line) determine the position of the mid-shelf flaw polynya. The mooring stations Anabar and Khatanga are labeled by letters "A" and "K", respectively. The distance from the fast ice edge to the mooring stations changes from about 100 to 20 km, while the distance to the furtherest ASAR tracking point changes from about 300 to 250 km during the winter. The black dashed box represents the area of the ASAR image on the right. Right: ASAR (Advanced Synthetic Aperture Radar) satellite image from 30th April 2008 showing the fast ice in the southeastern Laptev Sea. The Lena delta is at the bottom of the image. An advanced flaw polynya with low backscatter values in the open water area (dark area) developed at the fast ice edge (marked by dashed red line). The high backscatter values (bright area) in the polynya indicates presence of the newly formed ice.

shear and convergent motion causes dynamical ice growth and influences the ice thickness distribution. The sea ice drift, and in particularly the divergent sea ice motion causes opening of leads and polynyas. The extensive Laptev Sea polynya system (Figure 2.1) is estimated to contribute as much as 20% of the sea ice area transported through Fram Strait (Rigor and Colony, 1997) Despite this there was so far no validation of the sea ice drift focusing on the Laptev Sea shelf, where low ice concentrations and fast movements in the polynya zones could influence the quality of the ice drift products (Ezraty et al, 2006).

North Atlantic/Arctic Ocean Sea Ice Model (NAOSIM) that we use in this paper (model is described in more detail in section Model Description) gives a relatively good representation of the large scale Arctic sea ice features such as Beaufort Gyre, Transpolar Drift and sea ice export out of Fram Strait (Karcher et al, 2003; Martin and Gerdes, 2007). However, the performance of this pan-Arctic model in the sea ice drift over the shelf has yet not been validated. The primary aims of this paper is to examine the quality of the available ice drift data and use it for a simple validation of the model results on the Laptev Sea shelf.

Similarly to other sea ice models NAOSIM is not able to simulate the formation of fast ice (König Beatty and Holland, 2010; Adams et al, 2011). Due to this deficiency the simulated flaw polynya does not occur at the fast ice edge, but directly at the coast instead. The dislocation of the polynya results in severe regional biases in sea ice concentration, ice growth, ice thickness, winter temperature and salinity distribution. A significantly improved representation of sea ice concentration as well as ocean temperature and salinity distribution was obtained by including the fast ice in the model (Rozman, 2009; Adams et al, 2011). The fast ice edge region is usually refered to as the mid-shef, while the regions coastward and seaward from the edge are refered to as inner and outer shef, respectively. The secondary aim of this paper is to show that in the outer shelf the parameterization does not have a significant impact on the sea ice drift.

2.2 Observational Data

Observational data analyzed in this study are in-situ data from two moored stations as well as satellite remote sensing products. Mooring data were retrieved from upward-looking Acoustic Doppler Current Profilers (ADCP Teledyne-RDI Workhorse Sentinel 300 kHz) deployed by the "Laptev Sea System Project" in the eastern Laptev Sea mid-shelf. The mooring station "Anabar" was deployed at 74.33°N, 128.00°E at a depth of 30 m and station "Khatanga" at 74.71°N, 125.29°E at a 43 m depth (Figure 2.1). The devices were operating from September 2007 until August 2008 and they were recording the ice movements at the sea surface above them as described by Belliveau et al (1990).

All available sources of satellite-based ice drift products regardless the spatial resolution were used for the validation of the model simulations. Table 2.1 shows an overview of the used data.

The sea ice drift vectors distributed by Center for Satellite Exploitation and Research (CERSAT), at the French Research Institute for Exploitation of the Sea (IFREMER), Plouzané (France), were processed from pairs of Advanced Microwave Scanning Radiometer aboard EOS/Aqua (AMSR-E) images acquired by the 89 GHz channels and with 6.25 km pixel size (Ezraty et al, 2006) - from here on we name the product IFREMER. The gridded drift data has a spatial resolution of 31.25 km. For this study, 3-day drift vectors were used. The dataset is only available from October until the onset of ice melt at the beginning of May and has quality flags indicating the input data and method used for the drift estimation.

The second ice drift product used for the validation is the low resolution sea ice drift dataset (62.5 km equally spaced grid) of the EUMETSAT Ocean and Sea Ice Satellite Application Facility (OSI-SAF) (Lavergne et al, 2010), also processed from AMSR-E images and available from October till May. Conversely to the IFREMER product, it computes 2-day ice motion vectors from the 37 GHz channels (12.5 km pixel size), hence the coarser spatial resolution. The Laptev Sea has many coastal areas and two vast archipelagos. Consequently, the coarse resolution of the latter product considerably limits its use for comparison in the southernmost parts of the sea. At the Khatanga mooring location no OSI-SAF data are available and a point more northward had to be analyzed instead.

The third ice drift product we generated from Advanced Synthetic Aperture Radar (ASAR) satellite images. An ASAR image covers an area of approximately $400 \times 800\ km^2$ with a spatial resolution of $150 \times 150\ m^2$ (Cordey et al, 2004). We used the ASAR scenes for the sea ice drift detection at the mooring locations and at six locations in the eastern Laptev Sea outer shelf (Figure 2.1) chosen in a way to form a 1° grid. We manually tracked the movements of remarkable ice floes in the vicinity of these points to obtain drift vectors. The floes were tracked inside a search window with a radius proportional to the scale of the ice drift and preferably chosen in a way that they drifted directly through the grid points. On average the search window radius was under 5 km. The ASAR images were available from November until April with major gaps in January and March. The time difference between two images varies from 2 to 4 days.

	temporal availability	initial temp. resolution	source	spatial resolution	type	quality flags	error estimate
ADCP	September 2007- August 2008	30 min	mooring	2 points	E	no	0.0004 m/s
IFREMER	October- April	3 days	AMRS-E/ EOS-Aqua	31.25 km	L	yes	0.026 m/s, 35°
OSI-SAF	October- April	2 days	AMRS-E/ EOS-Aqua,	62.5 km	L	yes	0.015 m/s
ASAR	November- April	12 h - 4 days	ASAR/ ENVISAT	1° (5 km)	L	no	0.004 - 0.002 m/s

Table 2.1: The overview of the datasets used in the validation. Type 'E' stands for Eulerian type of motion and type 'L' for Lagrangian. The error estimate for the ADCP instrument given here is a mean error velocity of the Khatanga mooring record. This error is estimated on the basis of the difference between the velocities measured by the four beams of the device and is a measure of combination of a horizontal homogeneity and errors caused by malfunctioning equipment (Instruments, 1996). The error for the Anabar mooring which was later corrected for the compass bias is larger - 0.001 m/s.

The estimated errors of the satellite remote sensing data are low. Validation of both, the IFREMER 3-day ice drift and the OSI-SAF 2-day product have been conducted against drifting buoys in the central Arctic (Ezraty et al, 2006; Lavergne et al, 2010). For the IFREMER product Girard-Ardhuin and Ezraty (2005) report standard deviations of 6.7 km and 35°, which corresponds to 0.026 m/s uncertainty on the drift speed. For the OSI-SAF product Lavergne et al (2010) document a standard deviation of 2.6 km, which translates into 0.015 m/s uncertainty on the zonal and meridional drift component. One should note, however, that the reference dataset used for both validation exercises were different, as well as the collocation methods and time period.

ASAR drift was extracted from the geolocated images. The geolocation uncertainty could result in an error of up to 2 pixels (300 m) (Rosich and Meadows, 2004). We estimate that the deformation of the tracked ice floe could contribute to an error of another 1-3 pixels and therefore result in a drift error for the tracked floe of around 0.004 m/s. The true error of the ASAR drift compared to the real velocities at the tracking points (position of the tracked ice floe was not exactly at the tracking point) is unknown. The ice drift situation in the northern 4 points was homogeneous, while the southern most points were very close to the flaw polynya where the sea ice drift is more heterogeneous.

2.3 Model Description

NAOSIM is a coupled ocean-sea ice model developed at Alfred Wegener Institute for Polar and Marine Research (Gerdes et al, 2003; Karcher et al, 2003; Fieg et al, 2010). The model domain encloses the northern North Atlantic, the Nordic Seas and the Arctic Ocean. The highest resolving version of NAOSIM (Fine Resolution Model) has a horizontal grid spacing of 1/12° on a rotated spherical grid where the equator runs across the North Pole. Near the surface vertical resolution is 10 m. The ocean component of the model is based on the Modular Ocean Model MOM-2 of the Geophysical Fluid Dynamics Laboratory (Pacanowski, 1995). It is coupled to a dynamic-thermodynamic sea ice model (Hibler III, 1979) which employs a viscous-plastic rheology. The wind forcing in this experiment was taken from the 6-hourly NCAR/NCEP (National Centers for Environmental Prediction/National Center for Atmospheric Research) reanalysis data. Fast ice information (Figure 2.1: left) was integrated in the model in a way that the fast ice covered cells were excluded from the calculation of the sea ice momentum balance. Fast ice remained at rest while all thermodynamic calculations were performed as usual. Such procedure was already successfully applied by Lieser (2004). There a fast ice parameterization on the basis of sea ice thickness and bathymetry in a 1/4° model was used. To enable a realistic representation of the flaw polynya processes in our high resolution model, we used prescribed high resolution fast ice area instead. Monthly fast ice masks for winter 2007/08 (from December to May) were obtained from thermal bands of Moderate Resolution Imaging Spectroradiometer (MODIS) sensor aboard EOS/Aqua (Adams et al, 2011).

2.4 Data Analysis Methods

All ice drift data, modeled and observed, were converted to 3-day running mean ice drift to average out tidal and inertial movements of sea ice and obtain comparable quantities. The OSI-SAF 2-day means were first divided into daily means and then re-averaged to 3-day means. The low temporal resolution did not allow a complete averaging of the ASAR drift estimates for which in some cases single values were used to represent the 3-day period. The satellites carrying AMSR-E and ASAR sensors fly over the Laptev Sea twice per day, usually at noon and midnight. The three day means in all of the AMSR-E products are calculated from noon first day until noon of the fourth day (in total 3 to maximum 8 overflights as the neighboring scenes overlap in high latitutes). To avoid a phase shift between the datasets also the mooring and modeled ice drift was calculated for the same time window. As noon images of ASAR are rare most of the images we analyzed were taken at midnight (typically 2-3am UTC) and consequently the ASAR time series still have a small time shift compared to other time series.

We converted the data on the meridional and zonal sea ice movement to two sea ice drift properties: speed (magnitude) and direction (angle) and analyzed them separately. We first examined the time series of speed and sine of direction for all datasets and checked that there is no or minimal time shift between them. In section Observed Sea Ice Drift we show results of the linear regression analysis for the correlations between the observational datasets for speed and circular regression for the directional correlations. The ADCP record has the full time coverage and is the only dataset measured in-situ at the drifting ice surface. Despite this the mooring record represents a point measurement, while the satellite products represent gridded information (as also the model output is) produced from individual daily snapshots. No mooring with ice drift recording device has ever been recovered in the Laptev Sea outer shelf. In this paper we therefore compared the ADCP data to all other observational datasets in the mid-shelf. In the outer shelf, where no such data is available, we made a cross-comparison of all other data. In section Simulated Sea Ice Drift we then show the correlations between the observational data and the model simulations. If available we also analyzed the observational data with the best quality flags only. Finally, in section Drift Vector Validation we compare the zonal and meridional drift vectors of all satellite remote sensing products and model simulations to the in-situ data. This eases the comparison with previously published validation statistics for the central Arctic.

Statistics such as linear regression analysis are not appropriate for the analysis of the circular data where the numerical value for the parameter depends on the assignment of zero-direction and direction of rotation. The angles such as $0°$ and $359°$ are as numerical values very distant and would result in erroneous mean values if regular arithmetic mean is applied. Various circular (directional) statistics methods have been suggested and used over the past decades to overcome this problem (Fisher, 1996; Jammalamadaka and Sengupta, 2001). The mean of an angular dataset is computed by treating all angular measurements as points on a unit circle, and computing the resultant vector of the unit vectors determined by the data points (Fisher, 1996; Jammalamadaka and Sengupta, 2001). The mean direction is the direction of this resultant vector, and the mean resultant length provides a measure of concentration of the circular data. For the angular data α with statistical population n, mean direction $\bar{\alpha}$ is defined as

$$\bar{\alpha} = \begin{cases} \arctan\left(\frac{S}{C}\right) & \text{if } S > 0,\, C > 0 \\ \arctan\left(\frac{S}{C}\right) + \pi & \text{if } C < 0 \\ \arctan\left(\frac{S}{C}\right) + 2\pi & \text{if } S < 0,\, C > 0 \end{cases} \tag{2.1}$$

where S and C are

$$S = \sum_{i=0}^{n} \sin(\alpha_i) \tag{2.2}$$

$$C = \sum_{i=0}^{n} \cos(\alpha_i) \tag{2.3}$$

The circular variance is defined as $1 - \bar{R}$ where $R = \sqrt{S^2 + C^2}$ and $\bar{R} = R/n$. Its values fall in the interval $[0, 1]$, where data highly concentrated around one direction take values close to 0, while widely dispersed data have values close to 1. Statistical mean and variance for linear variables x,y or circular variables α,β were then used for calculation of statistical bias ($\bar{x} - \bar{y}$ or $\bar{\alpha} - \bar{\beta}$) and variance ratio F (var_x/var_y or var_α/var_β).

One of the possible measures of correlations between two circular variables was suggested by Jammalamadaka and Sengupta (2001) where for two angular data sets α and β the circular correlation coefficient $r_{\alpha\beta}$ is defined as

$$r_{\alpha\beta} = \frac{\sum_{i=1}^{n} \sin(\alpha_i - \bar{\alpha}) \sin(\beta_i - \bar{\beta})}{\sqrt{\sum_{i=1}^{n} \sin^2(\alpha_i - \bar{\alpha}) \sin^2(\beta_i - \bar{\beta})}} \tag{2.4}$$

If α and β are independent, $r_{\alpha\beta}$ is close to 0 and if the two variables are rotationally dependent the $r_{\alpha\beta}$ would be close to ± 1. The correlation is then defined as $r^2_{\alpha\beta}$. This is an analogue formula to the classical linear regression correlation coefficient where for two linear variables x and y the correlation coefficient r_{xy} is defined as $r_{xy} = \sum_{i=1}^{n}(x_i - \bar{x})(y_i - \bar{y})/\sigma_x\sigma_y$.

2.5 Observed Sea Ice Drift

Figure 2.2 shows scatter diagrams and statistical coefficients for the Khatanga and Anabar mooring locations in the mid-shelf. The ADCP and IFREMER datasets agree well in the direction of the drift. The statistical correlation between datasets are high ($r^2 = 0.8$), statistical bias is low and and variance ratio (F) is close to 1. The correlations of ASAR and OSI-SAF datasets to the ADCP record are lower ($r^2 = 0.6$) with both, ASAR and OSI-SAF datasets underestimating the ADCP measured speeds. There was no OSI-SAF drift point available for the exact Khatanga location and a point further off-shore was analyzed instead. Consequently it is not surprising that the correlations of all datasets with the OSI-SAF are moderate.

On the outer shelf correlations between the datasets are higher than in the mid-shelf region (r^2 from 0.65 to over 0.8). In Figure 2.3 we show scatter diagrams and statistical coefficients for the combination of data for all six points on the ASAR grid.

2.6 Simulated Sea Ice Drift

The time series of sea ice drift speed and direction in Figures 2.4 and 2.5 show that the model is simulating the ice drift in comparison with the observed drift well. The model is underestimating the ADCP velocities, but is simulating all of the peak speed events from the consolidation of the sea ice cover in November on. The directions during the high speed events are represented correctly. Erroneous drift directions occur mainly during the events with low drift speed. The speeds lower than 0.035 m/s would contribute to a displacement up to 9 km during the 3-day averaging period. As this movement is a subgird process for a model with $1/12°$ horizontal grid resolution we excluded this directions from the circular regression analysis. The displacements smaller than half of a pixel (3.12 km for IFREMER product and 6.25 km for OSI-SAF) are also not detectable by the tracking algorithms. Apart from a slight reduction in speed in the second part of the winter there is no significant change in ice drift

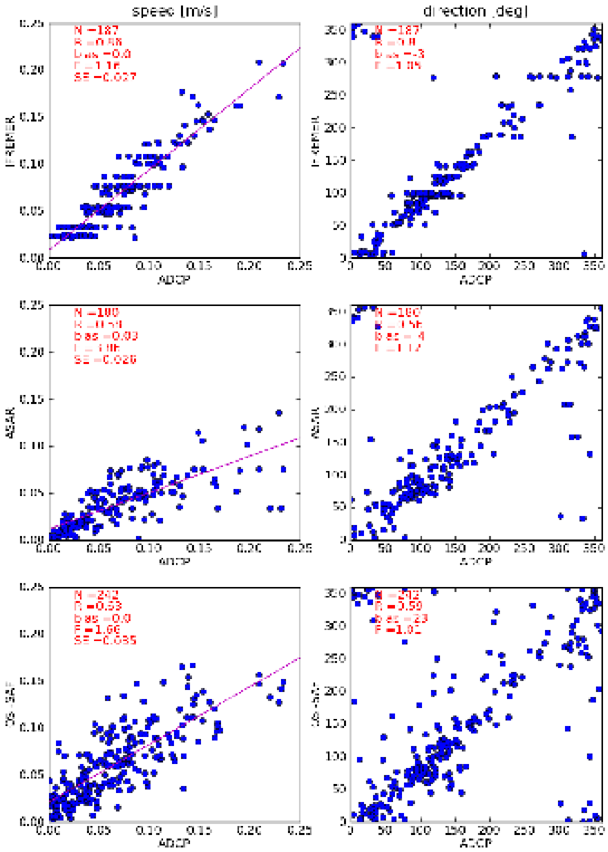

Figure 2.2: Scatter plots of sea ice drift speed and direction at the Anabar and Khatanga mooring locations for observational data comparison from November 2007 till May 2008. The numbers on the plots show number of data pairs in the analysis - N, correlation value (r^2) - R, statistical bias - $bias$, variance ratio - F, standard deviation of the error - SE. Speed units are m/s and direction values are degrees. All correlations shown are statistically significant at probability 0.99 (P value less than 0.001).

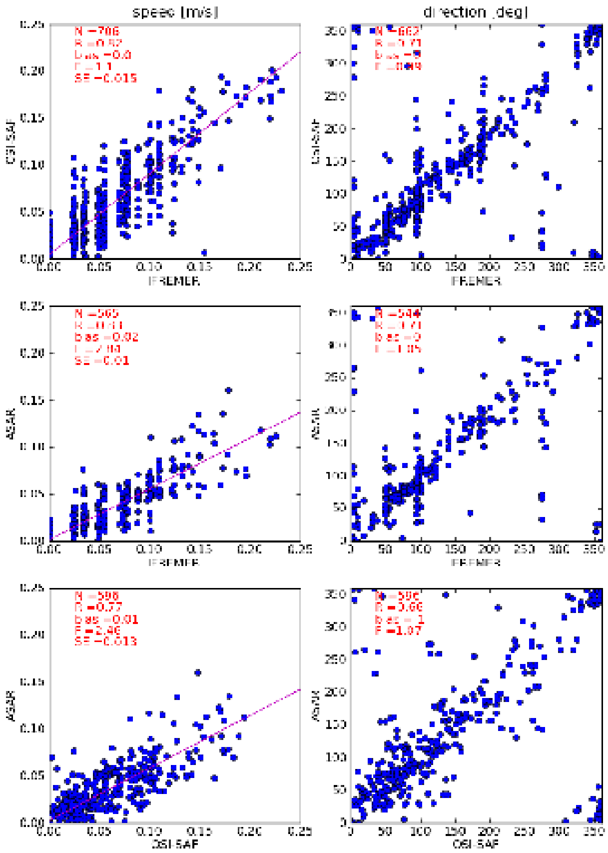

Figure 2.3: Scatter plots of sea ice drift speed and direction in the outer shelf for observational data comparison from November 2007 till May 2008. The numbers on the plots show number of data pairs in the analysis - N, correlation value (r^2) - R, statistical bias - $bias$, variance ratio - F, standard deviation of the error - SE. Speed units are m/s and direction values are degrees. All correlations shown are statistically significant at probability 0.99 (P value less than 0.001).

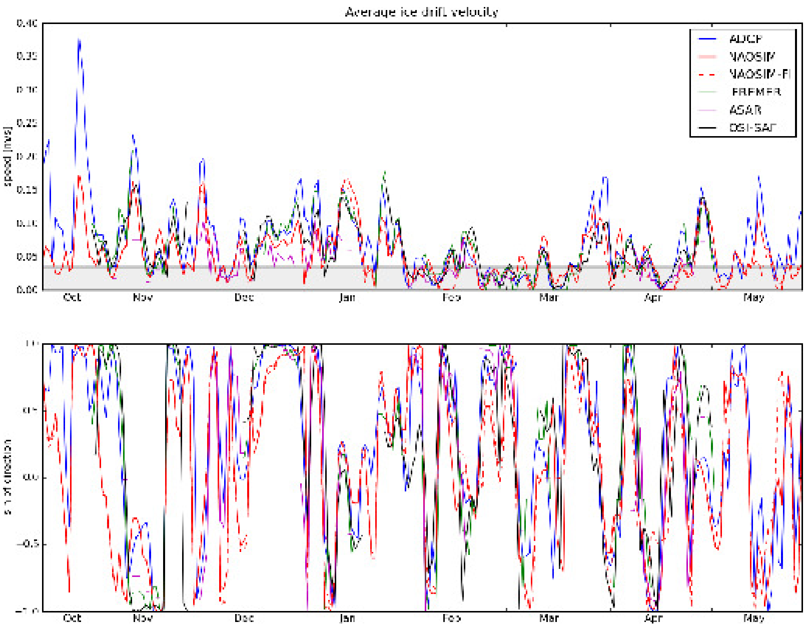

Figure 2.4: Simulated sea ice drift speed (top) and direction (bottom) without (full red line) and with (dashed red line) integrated fast ice compared to observational and remote sensing drift for the Khatanga mooring location from 15th October 2007 till 15th May 2008. The gray box in the top graphs marks the speeds that were not included into the directional correlation analysis.

simulation after the integration of the fast ice for any of the analyzed locations on the mid- or outer shelf (Figures 2.4 and 2.5).

Figures 2.6 and 2.7 show scatter diagrams and statistical coefficients of the observational data and the model simulations. The model speed simulations have low statistical bias compared to all observational data, but the variance ratio (F) is high when compared to all of the datasets, except compared to the ASAR drift speed. The simulated directions have a moderate bias, but variance ratio (F) slightly lower than 1.

The simulated sea ice speed at the mooring locations and in the outer shelf is moderately correlated to the observational speeds (r^2 from 0.4 to 0.7). The regression line shows a general underestimation of the speed compared to observations. Once the directions simulated at low speeds were removed from the statistical analysis the circular correlations to the observational datasets are moderate to high (r^2 from 0.5 to 0.9). Using only the best quality flags for the IFREMER and OSI-SAF datasets the number of data points in time reduces, but the correlations do not improve.

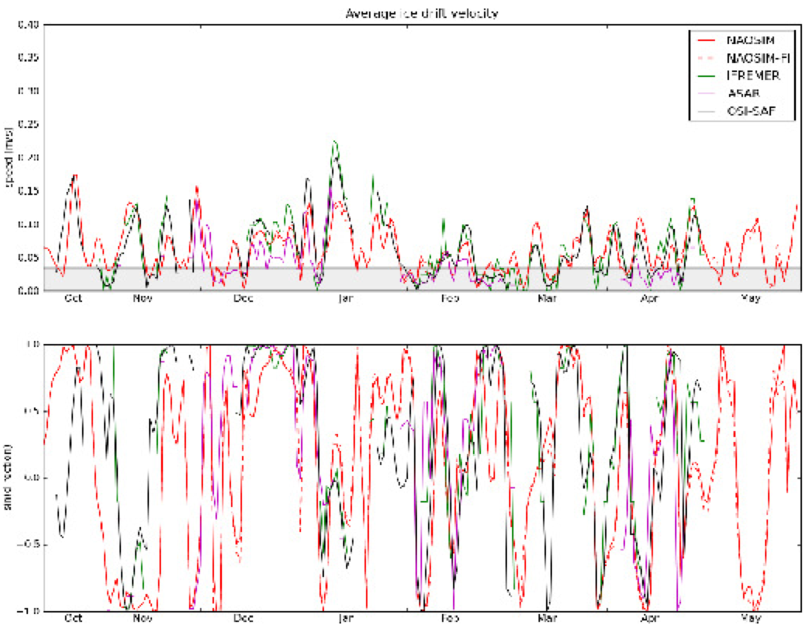

Figure 2.5: Simulated sea ice drift speed (top) and direction (bottom) without (full red line) and with (dashed red line) integrated fast ice compared to observational and remote sensing drift for the for a point in the outer shelf ($77°N$, $125°E$) from 15th October 2007 till 15th May 2008. The gray box in the top graphs marks the speeds that were not included into the directional correlation analysis.

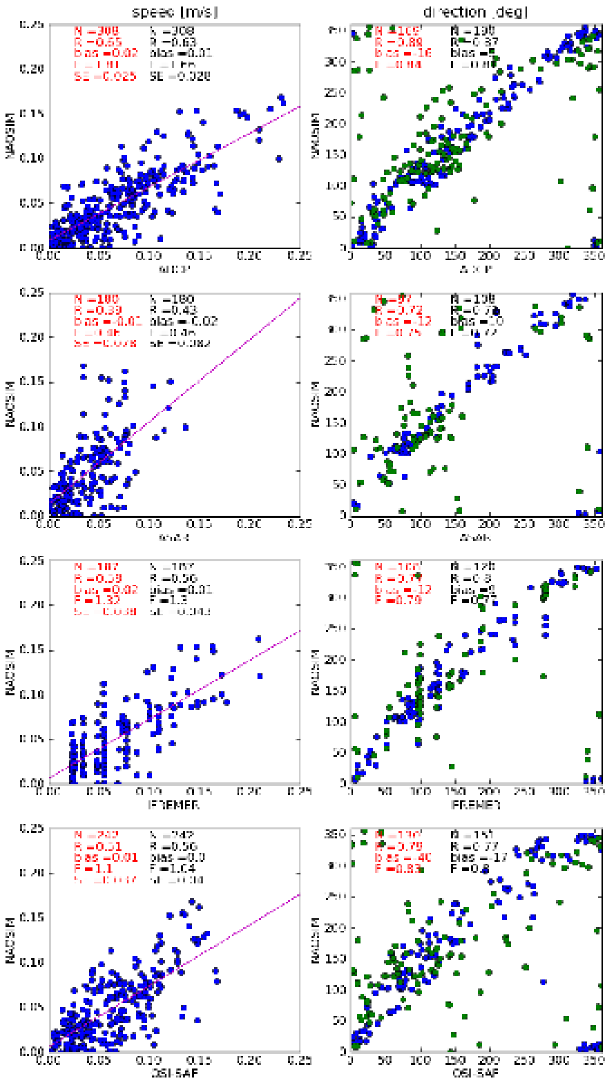

Figure 2.6: Scatter plots of sea ice drift speed and direction at the Anabar and Khatanga mooring locations for model simulation with the fast ice and observational data comparison from November 2007 till May 2008. The data points included into the statistical analysis are marked by blue dots. The points with drift speed under 0.035 m/s at the drift direction scatter plots are marked by green dots. The numbers on the plots show number of data pairs in the analysis - N, correlation value (r^2) - R, statistical bias - *bias*, variance ratio - F, standard deviation of the error - SE. Speed units are m/s and direction values are degrees. All correlations shown are statistically significant at probability 0.99 (P value less than 0.001). Numbers printed in red (black) show the statistical characteristics of the model simulations with (without) the fast ice.

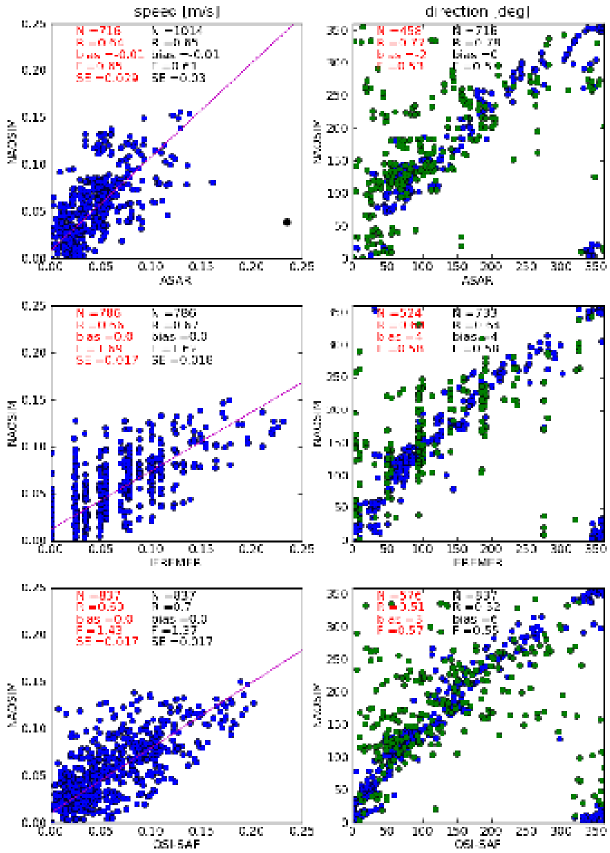

Figure 2.7: Scatter plots of sea ice drift speed and direction at in the outer shelf for model simulation with the fast ice and observational data comparison from November 2007 till May 2008. The data points included into the statistical analysis are marked by blue dots. The points with drift speed under 0.035 m/s at the drift direction scatter plots are marked by green dots. The numbers on the plots show number of data pairs in the analysis - N, correlation value (r^2) - R, statistical bias - $bias$, variance ratio - F, standard deviation of the error - SE. Speed units are m/s and direction values are degrees. All correlations shown are statistically significant at probability 0.99 (P value less than 0.001). Numbers printed in red (black) show the statistical characteristics of the model simulations with (without) the fast ice.

2.7 Drift Vector Validation

	N	$bias_{\vec{u}}$	$bias_{\vec{v}}$	$SD_{\vec{u}}$	$SD_{\vec{v}}$	$r^2_{\vec{u}}$	$r^2_{\vec{v}}$
IFREMER	187	-0.006	0.002	0.030	0.027	0.90	0.93
OSI-SAF	242	0.040	0.006	0.040	0.031	0.69	0.84
ASAR	180	0.003	0.005	0.027	0.021	0.73	0.86
NAOSIM	190	0.005	0.014	0.033	0.025	0.85	0.87
NAOSIM - FI	169	0.009	0.014	0.037	0.025	0.84	0.87

Table 2.2: The validation results of the drift vector components of the satellite products and model simulations with the in-situ measurements for the Laptev Sea mid-shelf in winter 2007/2008. The columns show statistical parameters for the zonal ($\vec{u}$) and meridional ($\vec{v}$) components of the drift: number of data pairs in the analysis - N, statistical bias - $bias$, standard deviation of the error - SE and correlation value - r^2. Velocity units are m/s. All correlations shown are statistically significant at probability 0.99 (P value less than 0.001).

The comparison of the zonal and meridional drift component of satellite products and model simulations to the in-situ data shows high correlations (r^2 higher than 0.7, Table 2.2), but higher standard deviations of errors as in the central Arctic basin (Table 1). The mean measured error velocity for the Khatanga mooring ADCP is 0.0004 m/s (Table 1), while the error velocity for the Anabar, which compass bias was calibrated only after the instrument was recovered, is 0.001 m/s. For the model again only the drifts with speed higher than 0.035 m/s were analyzed.

2.8 Discussion

The observational data and model simulations were compared at two mooring locations in the mid-shelf dominated by the polynya activity and at six regularly spaced points in the outer shelf region where the thin ice gradually grows into the pack ice.

The comparison of the satellite observational data shows that ice drift directions are all moderatelly to highly correlated to the ADCP record. The IFREMER product is also highly correlated in speed. The ASAR and OSI-SAF speeds are only moderately correlated, regarding the temporal and spatial mismatch a relatively good result. While the ASAR datasets still have a small phase shift due to prevailing midnight overflights and 3-day averages based on a small number of images, the OSI-SAF product does not cover the Khatanga mooring location and an alternative location further offshore was used in comparison.

The scatter diagrams on Figures 2.2 and 2.3 show that the IFREMER dataset only occupy certain discrete values. This "quantization noise" is a well known effect of the robust Maximum Cross Correlation method (Kwok et al, 1998; Girard-Ardhuin and Ezraty, 2005; Lavergne et al, 2010) that the IFREMER dataset algorithm is using for the ice drift estimation. The effect causes no obvious problems at this stage of the model validation. The OSI-SAF product is using the Continious Cross Correlation Method (CMCC) (Lavergne et al, 2010) which avoids this problem.

For the mooring locations the model simulation is in good agreement with the ADCP and satellite remote sensing data (Figure 2.4). The simulated ice drift speeds compared to these datasets are very similar starting from November, when the sea ice cover in the Laptev Sea becomes relatively stable. It is remarkable that the simulated and ADCP speeds match not only in phase, but also in magnitude and the model is able to simulate the early winter extreme velocities (peaks in Figure 2.4). The ice drift directions are similar for the whole observation period and especially during the high speeds. The time series also show the scarcity of the satellite retrieved data, which can be unavailable on the scale of weeks.

The statistical bias of the model results is much lower on the outer shelf than on the mid-shelf. The variance ratio (F) of directions decreases on the outer shelf as well and shows that the simulated model directions are more disperse than observed.

The correlations between all of the observational data and the model simulations are slightly higher on the mid-shelf than on the outer shelf. This is surprising as in the dynamic mid-shelf environment, dominated by polynya events, the model should have more difficulties with correct simulations than on the relatively homogeneous outer shelf. The reason for this unexpected result is probably a smaller number of observations analyzed on the mid-shelf. As we decided to exclude all of the drift directions for drift speed lower than 0.035 m/s, a relatively larger part of the data was excluded on the mid-shelf where the ice velocity is generally lower and only the fastest movements (top 50%) of the data entered the analysis. In the outer shelf almost 70% of all data entered the analysis.

There is still some remaining phase shift (Figure 2.4) between the model and the observations due to the temporal resolution of the wind forcing data. The 6-hour wind situation does not represent the wind changes during the 6 hour interval. The time shift error is occurring randomly and depends on the timing of the wind direction change. This error can only be excluded by a high enough temporal resolution of the forcing data or by full coupling of the model.

Furthermore, differences in observed drift arise also because the measurement techniques are principally different. The model and the mooring velocities are Eulerian while the remote sensing velocities are Lagrangian. The high correlation between the ADCP and the IFREMER data shows that the averaged Lagrangian velocities around the mooring location are comparable to the Eulerian velocities measured over the mooring station. The classical sea ice drift validation was done with the drifting buoys that also represent a Lagrangian type of measurements (Ezraty et al, 2006; Lavergne et al, 2010). IFREMER and OSI-SAF drift products are spatial averages, while the ADCP record and ASAR drift data represent a non-averaged single point/floe drift. Each drift vector from the OSI-SAF product pertains to an area of approximately 120×120 km^2 while the IFREMER vectors pertain to roughly 60×60 km^2 (4 times less), thanks to the higher resolution of the 89 GHz channels. This results were then gridded to the spatial resolutions of 62.5 km and 31.25 km, respectively.

The model simulations and the ASAR dataset are systematically underestimating the in-situ measured speed, when velocities are higher than 0.1 m/s. The reasons for too low simulated drift speeds could be found in a too low wind stress or to high ocean drag influencing momentum balance of the sea ice in the model. The ASAR dataset peak speeds are systematically lower than the ones of IFREMER, OSI-SAF and ADCP by about a half. For the ASAR drift only remarkable features in sea ice such as big pressure ridges and hummocks were used for tracking. Despite a great surface roughness, detectable also by high backscatter signatures on the ASAR images, these features are not drifting as fast as one would expect from a greater wind stress acting on their sails. It seems that the friction between rough jagged floes is an important sink of energy for shearing at floe boundaries (Rothrock, 1975). The big ice floes, as used for tracking on the ASAR images, are therefore less appropriate for the estimation of the prevailing ice drift situation. The ASAR velocities which have been retrieved specifically for this research have still been proven to be an useful alternative source of information, independent from other satellite remote sensing products. In November and December, when there are occasionally no AMSR-E ice drift products available (Figures 2.4 and 2.5), ASAR derived speed and direction are similar to the in-situ measured and to the simulated.

The standard deviations of the error for the satellite products and model simulations validated with the ADCP record are in the range of 0.03 m/s (Table

2.2). Compared to the buoy validation performed in the central Arctic and Canadian Archipelago this errors are slightly higher (for 0.005 m/s) for the IFREMER (Ezraty et al, 2006) and double for the OSI-SAF product (Lavergne et al, 2010). This confirms our hypothesis that the errors of the estimates are higher over the shelf seas. The in-situ ice drift velocities measured in the Laptev Sea mid-shelf are relatively higher then in the buoy validation set that was used by Ezraty et al (2006) and Lavergne et al (2010). A part of this error can be certanly attributed to the inhomogeneous drift environment in the mid-shelf. The datasets used in this paper also exhibit frequent peaks in speeds over 0.1 m/s, while such events in the buoy datasets were not common. This suggests that despite the larger errors the satellite and simulated velocities are still relatively good estimates.

The fast ice parameterization has no major impact on the ice drift simulations apart from additionally reducing the drift speed in the mid shelf region during the periods with low speeds (in our case: from February on). This effect is hardly detectable further offshore (Figure 2.5). The correlations of model results with and without fast ice parameterization with the observational data are similar (Figures 2.6, 2.7).

NAOSIM was already validated by Martin and Gerdes (2007) with the product merged from Quick Scatterometer (QuikSCAT) and Special Sensor Microwave/Imager (SSM/I) drift estimations provided by CERSAT/IFREMER. The product has a spatial resolution of 62.5 km and is available for the central Arctic only. Using monthly means from 3- or 6-day products the validation was preformed for the period 1992 - 2001. NAOSIM, similarly to other models in the Arctic Ocean Model Intercomparison Project (AOMIP), slightly overestimated the drift speeds. The model also had a slight deviation of the drift angles to the right. On the other hand, NAOSIM on the Laptev shelf underestimates the drift speed and has a slight angle deviation to the left. This again points at the systematic differences between the central Arctic and the shelf seas.

The above mentioned AOMIP intercomparison also revealed the differences between the simulations of different sea ice-ocean coupled models. Although it has been estimated that the 70 % of short term ice drift variability is explained by the wind variability (Thorndike and Colony, 1982) and the models in the project all used identical atmospheric forcing, the resulting sea ice drift simulations differed substantially (Martin and Gerdes, 2007). To explain the differences in the model performances Martin and Gerdes (2007) pointed out the differences in the implementation of the atmospheric and oceanic forcing, among them the actual prescription of the wind stress and the implementation of the ocean-ice drag term.

For the NAOSIM in this case study the correlation of simulated sea ice drift to the in-situ data in sea ice direction or in individual vector components largely exceeds the 70 % of the variability that should be explained by the wind variability (Thorndike and Colony, 1982). This means that not only wind stress, but also other important contributors to the sea ice momentum balance such as the ocean-ice drag, the internal sea ice stress and the Coriolis force (Harder et al, 1998), are realistically implemented in the model. Another evidence for the role of the ocean and ice dynamics in the model is the spatial variability between the drift records at the Khatanga mooring location (Figure 2.4) and in the outer shelf (Figure 2.5). The difference between the both time series is much larger as expected from a difference between two grid points of the wind forcing data with a spatial resolution of 1.875° (Kanamitsu et al, 2002).

2.9 Conclusions

In this paper we used unique in-situ sea ice drift records from the Laptev Sea shelf to validate the satellite remotes sensing products and model simulations. Our results show that:

1. The fast ice parameterization in the model has no major impact on the sea ice drift simulations and it's smoothing effect disappears already at distance larger than 100 km (about 10 model grid points).

2. The standard deviations of the error for the satellite products validated with the in-situ record are larger on the shelf than in the central Arctic. The errors for the satellite products and model simulations are in the range of 0.03 m/s.

3. The sea ice drift remote sensing products compared to the in-situ mooring records give good estimates for the shelf regions. Especially the high resolution IFREMER product has a high correlation and low standard deviation compared to the in-situ data.

4. For the validation of the sea ice drift on the Eurasian shelf simulated by the eddy resolving sea ice models we recommend the use of the in-situ data and high resolution satellite retrieved products. Because of the

differences between the products in our validation we recommend to use more than one satellite product for the validation.

5. The correlation of simulated sea ice drift to the in-situ data in sea ice direction or in individual vector components is at least 0.84. To achieve a more realistic simulations of the drift speed, the calculation of the wind stress and ocean drag terms should be studied closely. The model drift simulation have contrary to the satellite products a full temporal and spatial coverage and the correlations to the in-situ data are high enough to use them as sea ice drift estimates on the Laptev Sea shelf.

Acknowledgments

This research was conducted as part of the BMBF project "System Laptev Sea" (03G0639A). ENVISAT/ASAR satellite images were obtained through ESA Project EO-500 "Formation, transport and distribution of sediment-laden sea-ice in the Arctic Shelf seas". P.R. would like to express her gratitude to the Slovenian Academy of Science and Art, to the Municipality of Ljubljana, Slovenia and to the Otto-Schmidt-Laboratory, Saint Petersburg, Russia for supporting her master studies with scholarships and grants. The authors would like to thank the anonymous reviewers whose helpful comments and criticism provided substantial improvements of the manuscript.

Chapter 3

Is weaker Arctic sea ice changing the Atlantic water circulation?

Abstract

The Arctic sea ice is getting weaker and more mobile. We attempt to mimic two sea ice strength modes, prior to and during climate change, in a sensitivity study where we compare sea ice-ocean model simulations with two maximal compressive sea ice strength (P*) values: 27500 N/m^2 in the control run (CTRL) and 15000 N/m^2 in the weak sea ice run (WEAK). The differences in the sea ice simulations are the largest in the winter sea ice concentration in the Barents Sea and in the Nordic Seas and in the sea ice motion in the central Arctic. In addition we also find differences in the ocean mid-depth circulation and temperature. Our analysis shows that the low sea ice concentration in the Barents Sea contributes to high negative ocean surface heat fluxes and to formation of cooler (by 0.2 K) and stronger (by 0.19 Sv) Barents Sea branch. The increased sea ice mobility in the central Arctic in WEAK results in an increasing circulation strength in the anticyclonic Beaufort Gyre which reduces the cyclonic AW circulation beyond the Lomonosov Ridge and enhances the loop of the AW in the Eurasian Basin. As a result of both mechanisms, the Fram Strait net outflow increases by 0.46 Sv whereas as a reaction the Davis Strait net outflow is weaker by 0.28 Sv. This shows that the Arctic sea ice mobility is important also for the water masses feeding the Atlantic Meridional Overturning in the North Atlantic.

3.1 Introduction

The Arctic sea ice is changing: it is getting thinner (Kwok and Rothrock, 2009), more mobile (Rampal et al, 2009; Spreen et al, 2011) and the sea ice extent is shrinking (Stroeve et al, 2012). The reasons for the changes have been investigated in various observational and modeling studies (Shimada et al, 2006; Perovich et al, 2008; Polyakov et al, 2010; Kattsov et al, 2010; Zhang et al, 2012). It is likely that the reasons for the observed changes are numerous and connected with feedbacks. In an attempt to isolate the response to only one changing sea ice characteristic, sea ice mobility, we perform a sensitivity experiment by changing the value of a single numerical parameter: the maximal compressive sea ice strength (P*).

P* is an empirical parameter that is used in the rheology of sea ice models and controls the response of the sea ice to stresses. Its value has a considerable effect on the sea ice motion, thickness and concentration. P* is hard to measure in nature (although Tremblay and Hakakian (2006)) made an attempt to estimate it by the remote sensing sea ice drift products and sea level pressure from reanalysis data) - its value is commonly fitted to optimize sea ice drift (Hibler and Walsh, 1982; Kreyscher et al, 2000b). In our study we compare a model simulation with a standard value to a simulation with a relatively low value of P* that results in weak and very mobile sea ice.

Where the Arctic Ocean is covered by sea ice, its fresh upper ocean waters are at the freezing point. At mid-depth the Arctic Ocean has temperatures up to several degrees above zero. The bulk of this warm and salty water is composed of Atlantic Water (AW) that enters the Arctic Ocean though the Fram Strait and the Barents Sea. The surface circulation is characterized by an anticyclonic Beaufort Gyre in the Amerasian Basin and a Transpolar drift that transports the sea ice and surface water from the Eurasian shelves towards the Fram Strait (light blue arrows on Fig. 2.1). In contrast, the mid-depth circulation of the Atlantic Water Layer (AWL) is characterized by generally cyclonic motion, most of which occurs in boundary currents along the deep ridges and shelfbreaks (red arrows on Fig. 2.1). Before entering the central Arctic Ocean basins via Fram Strait or the Barents Sea both branches experience heat loss and are modified by ice melt and freeze-up, as well as river runoff. Both branches feed the AWL and after passing through the basins leave the Arctic ocean proper on return through the Fram Strait as Arctic Intermediate Water (AIW). The AIW flows into the Nordic Seas and has an important role in the dense water formation that feeds the Atlantic Meridional Overturning circulation (Schmitz and McCartney, 1993; Swift, 1984).

It has been hypothesized that the inflow of the warm AW to the Arctic Ocean has an influence on the decline of the sea ice extent and thickness (Polyakov et al, 2010; Ivanov et al, 2012). In our study we investigate if there is any reverse connection: can a change in the Arctic sea ice characteristics influence the flow in the AWL and the AIW outflow?

The outline of this paper is as follows. In section 3.2 we describe the employed numerical model. Section 3.3 contains a brief comparison of the performance of our model to observations. In sections 3.4, 3.5 and 3.6 we present and discuss our sea ice and ocean mid-depth simulation results. A summary of our findings and final remarks are in section 3.7.

3.2 Model setup

Our model is a regional coupled sea ice - ocean model based on the Massachusetts Institute of Technology General Circulation Model code - MITgcm (Marshall et al, 1997) with a model domain covering the Arctic Ocean, Nordic Seas and northern North Atlantic (Fig. 3.1). The horizontal resolution is 1/4° (∼28 km) on a rotated grid with the grid equator passing through the geographical North Pole (along 30°N. The model has 36 vertical levels unevenly distributed in a way that the top 500 m of the water column is divided into 20 levels and the depths below 2000 m have only 6. The AWL in our model is spanning from 212 to 1200 m, the depth with is resolved in 13 vertical layers with thickness increasing from 42 to 100 m. The very thin surface layer thickness under sea ice requires a non-linear free surface and the use of the rescaled vertical coordinate z* (Campin et al, 2008). Vertical mixing in the ocean interior is parameterized by a K-Profile Parameterization (KPP) scheme (Large et al, 1994) and tracers (temperature and salinity) are advected with an unconditionally stable seventh-order monotonicity preserving scheme (Daru and Tenaud, 2004) that requires no explicit diffusivity. The sea ice model is a dynamic-thermodynamic sea-ice model with a viscous-plastic rheology (Losch et al, 2010). The same set-up for the sea ice model has been used in the study by Castro-Morales et al (submitted).

The model is initialized by the PHC climatology (Steele et al, 2001) and has initially no sea ice cover. For the spin-up we run the model for 30 years with atmospheric climatology from the Coordinated Ocean Research Experiment (CORE) version 2 based on the reanalysis from the National Center for Atmospheric Research/National Centers for Environmental Prediction (NCAR/NCEP) (Large and Yeager, 2009). Subsequently the model is driven from 1948 to 2007 by realistic daily atmospheric data also provided by CORE. Surface salinity in ice free regions is restored to a mean salinity field (PHC climatology) with a time scale of 180 days to avoid model drift. River runoff was prescribed for the main Arctic rivers according to the Arctic Ocean Model Intercomparison Project (AOMIP, `http://www.whoi.edu/projects/AOMIP/`) protocol and treated like a surface volume flux. Open boundaries are formulated following Stevens (1990) and are located at 50°N in the Atlantic and just south of the Bering Strait. Temperature and salinity are taken from the PHC climatology. The Bering Strait inflow is prescribed to 0.8 Sv and the stream function at the open boundary in the Atlantic Ocean is formulated in way that it compensates the sea surface height fluctuations in the model domain.

In this study we are comparing two identical experiments with the only difference being the P* parameter of the sea ice model:

- control run (CTRL): P*=27.500 N/m^2 (the value estimated by Hibler and Walsh (1982))
- low P* run (WEAK): P*=15.000 N/m^2 (the value estimated by Kreyscher et al (2000b))

The first 20 years of the simulations (1948-1967) are considered to be influenced by adjustment processes in the sea ice and are excluded from the calculation of temporal means for the analysis, but are still shown in the time series to track the development of the differences between the runs.

3.3 Comparison to observations

Although this paper is a sensitivity study of two model runs, we perform a brief comparison of CTRL to observational data. We have chosen to compare sea ice concentration and temperature time series at the inflow points of the mid-depth water into the Arctic. The sea ice concentration data for the model validation are obtained from EUMETSAT Ocean and Sea Ice Satellite Application Facility: Global sea ice concentration reprocessing dataset (OSI-SAF, 2013). The model tends to overestimate the sea ice extent in the Marginal Ice Zone (MIZ) and underestimate the summer sea ice concentration in the Central Arctic (Fig. 3.2).

Hydrographic data for the Kola section (1958-2007) are from the Knipovich Polar Research Institute of Marine Fisheries and Oceanography (PINRO, `http://www.pinro.ru`). The section comprising 5 CTD stations in total is located in the Murman Current along 33°30′E between 71°N and 73°N. The data is averaged over 0 to 200 m depth. While our simulation has a low temperature bias of about 1 K (Fig. 3.3), it shows an interannual variability resembling the observations.

To compare the simulated temperature of the Fram Strait inflow we have chosen a region in the West Spitzbergen Current (WSC) between 78°30′ - 79°12′N and 5° - 9°E. We used hydrographic data from the World Ocean Database 2009 (`http://www.nodc.noaa.gov/OC5/WOD`), HydroBase3 (`http://www.whoi.edu/science/PO/hydrobase`) and from cruises of the Alfred Wegener Institute and the Norwegian Polar Institute (Schauer et al, 2008; Hughes

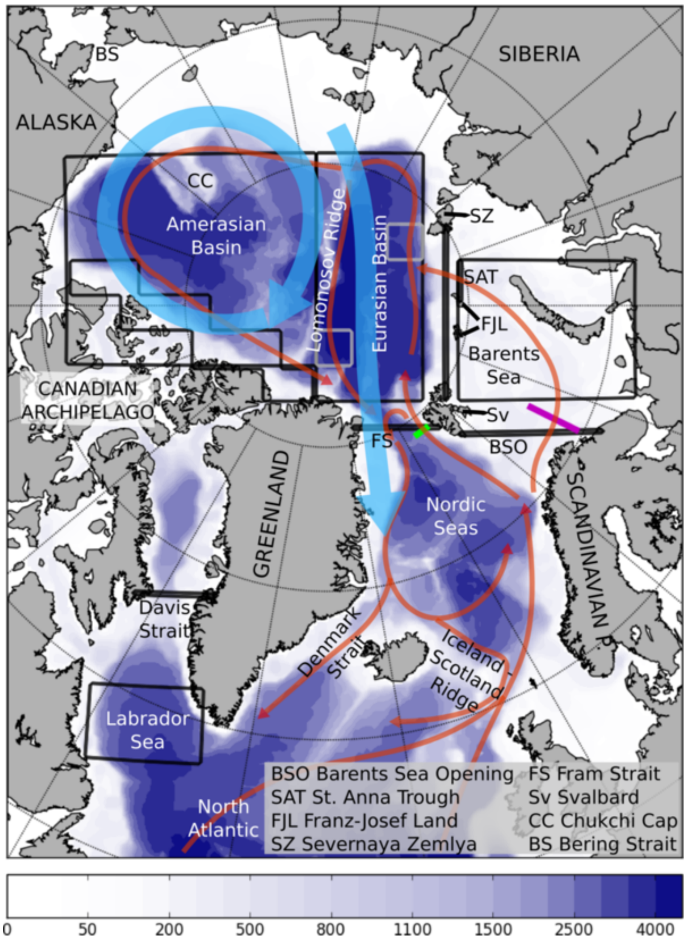

Figure 3.1: The model domain and bathymetry. The sea ice and surface circulation is schematically represented by light blue arrows and the mid-depth circulation by red arrows (for the Arctic Ocean simplified from Rudels et al (2013) and for the Nordic Seas and North Atlantic from Eldevik et al (2005)). The oceanographic sections for the comparison with the observational data in the West Spitzbergen Current and the Kola section in the Barents Seas are marked by green and purple color, respectively. The black lines and black and grey boxes mark the sections and regions used in the model analysis.

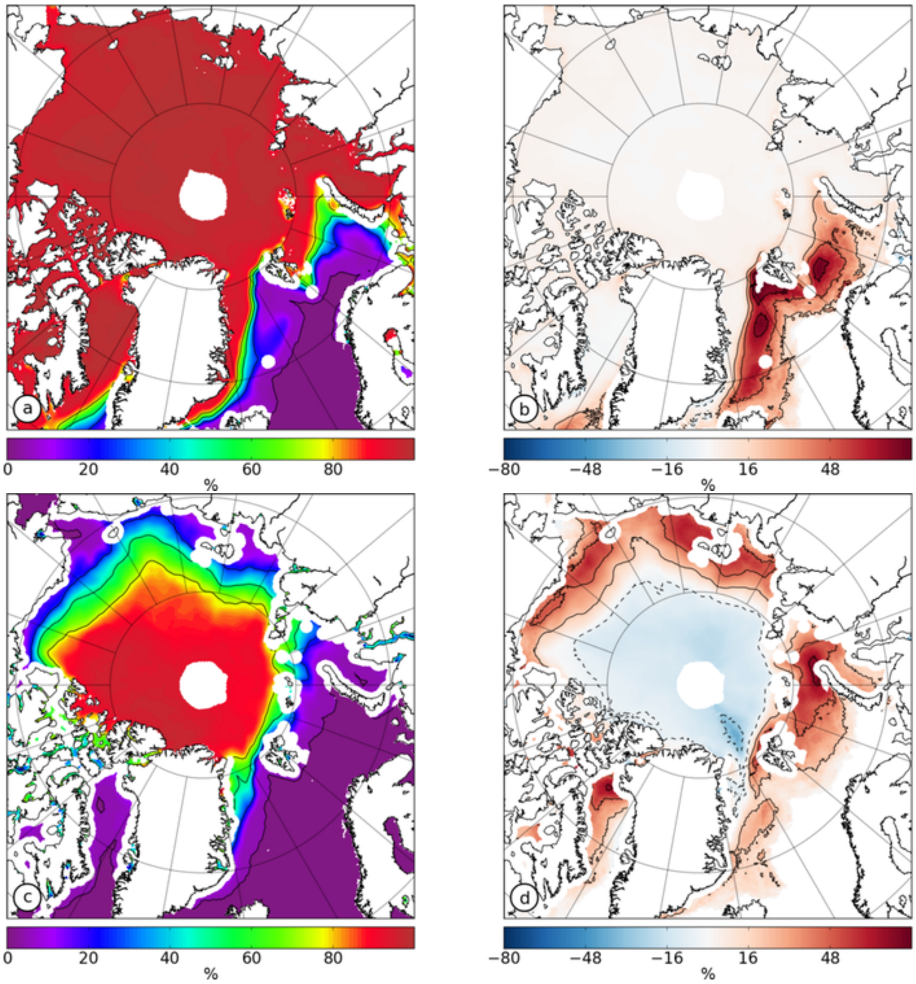

Figure 3.2: March (a,b) and September (c,d) mean (1988-2007) sea ice concentration observations by OSI-SAF and the differences model minus OSI-SAF. On b and d: blue color means model is underestimating sea ice concentration, red color means model is overestimating sea ice concentration.

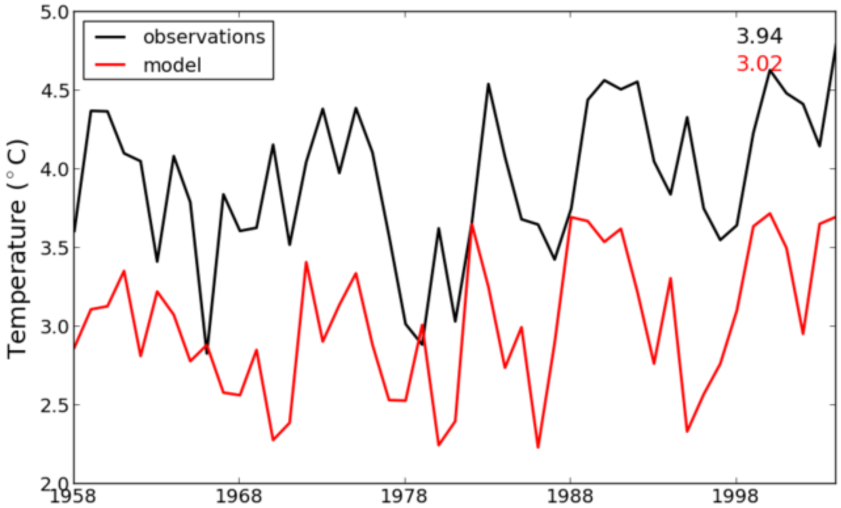

Figure 3.3: Vertical mean 0-200 m annual temperature at the Kola section in the central Barents Sea. The temporal mean from 1958 to 2007 is printed in the colors corresponding to the legend. The model section is shortened for 1 station (30′) on the southern end to avoid cool coastal current.

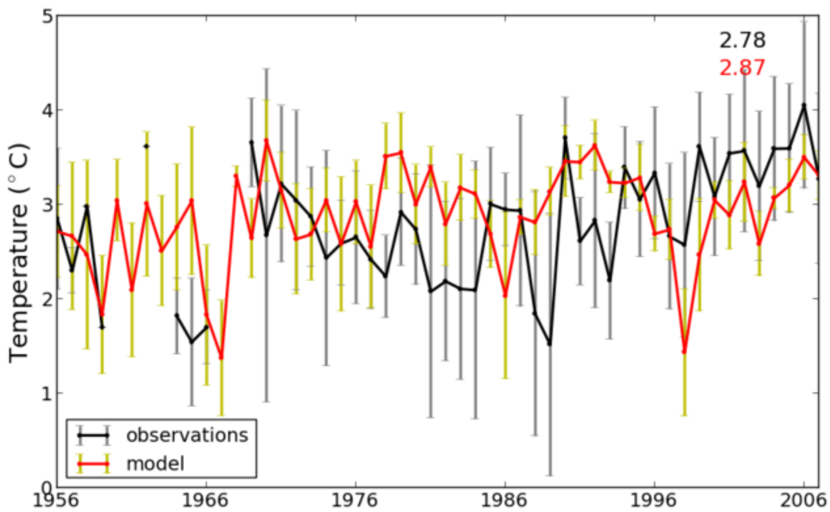

Figure 3.4: Vertical mean 50-500 m summer temperature in the WSC. The temporal mean from 1958 to 2007 is printed in the colors corresponding to the legend. Error bars denote one standard deviation. For observations no error is provided for years with less than five measurements.

and Holliday, 2006) from 1956 to 2007. For each station, the vertical mean of 50-500 m was obtained after interpolating temperature linearly to fixed depths in 10 m steps. Station means were averaged over each summer (May-October). By choosing a large depth interval we captured the whole WSC core in the observations and in our model. Fig. 3.4 shows a reasonable match of simulated and observed temperature. Despite some differences in the late 1970s and 1980s, the model depicts a warm phase in the 1990s, followed by a cool phase and the strong warming period in recent years.

Despite a bias in the sea ice extent and the Kola temperature time series the overall performance is reasonable. The model can therefore be used for the planned sensitivity study.

3.4 Sea ice

P* is an empirical value that describes the minimum force upon a block of sea ice needed to deform it. By reducing P* the sea ice internal stress reduces and sea ice becomes less resistant to the external forces from the atmosphere and ocean.

Fig. 3.5 shows the difference of several sea ice parameters between the CTRL and the WEAK experiment. All maps are March means (1968-2007) as the differences between the runs are largest at the sea ice winter maximum extent and thickness. Differences based on the annual means are similar to the winter patterns (not shown). On Fig. 3.5 panels a, b show the mean sea ice motion in CTRL and WEAK minus CTRL. In WEAK the anticyclonic motion of the sea ice in Beaufort Gyre is enhanced in comparison to CTRL, while the Transpolar Drift is somewhat slower. Overall, the ocean surface stress (wind stress plus internal ice stress) is higher in the WEAK experiment (color shading of the same panels). The highest ocean surface stresses occur in the ice free ocean and in the East Greenland Current exiting in the Fram Strait, where sea ice is the most mobile, but the highest differences between the experiments occur in the relatively slow ice of the central Arctic, with a maximum in the Kara Sea and the eastern Barents Sea.

The differences in sea ice thickness (Fig. 3.5 panels c, d) and concentration (Fig. 3.5 panels e, f) are reflecting the differences in the sea ice motion as a consequence of the fact that the lower P* in WEAK increases the compressibility of the sea ice. Due to higher dynamic growth of sea ice (not shown) we find

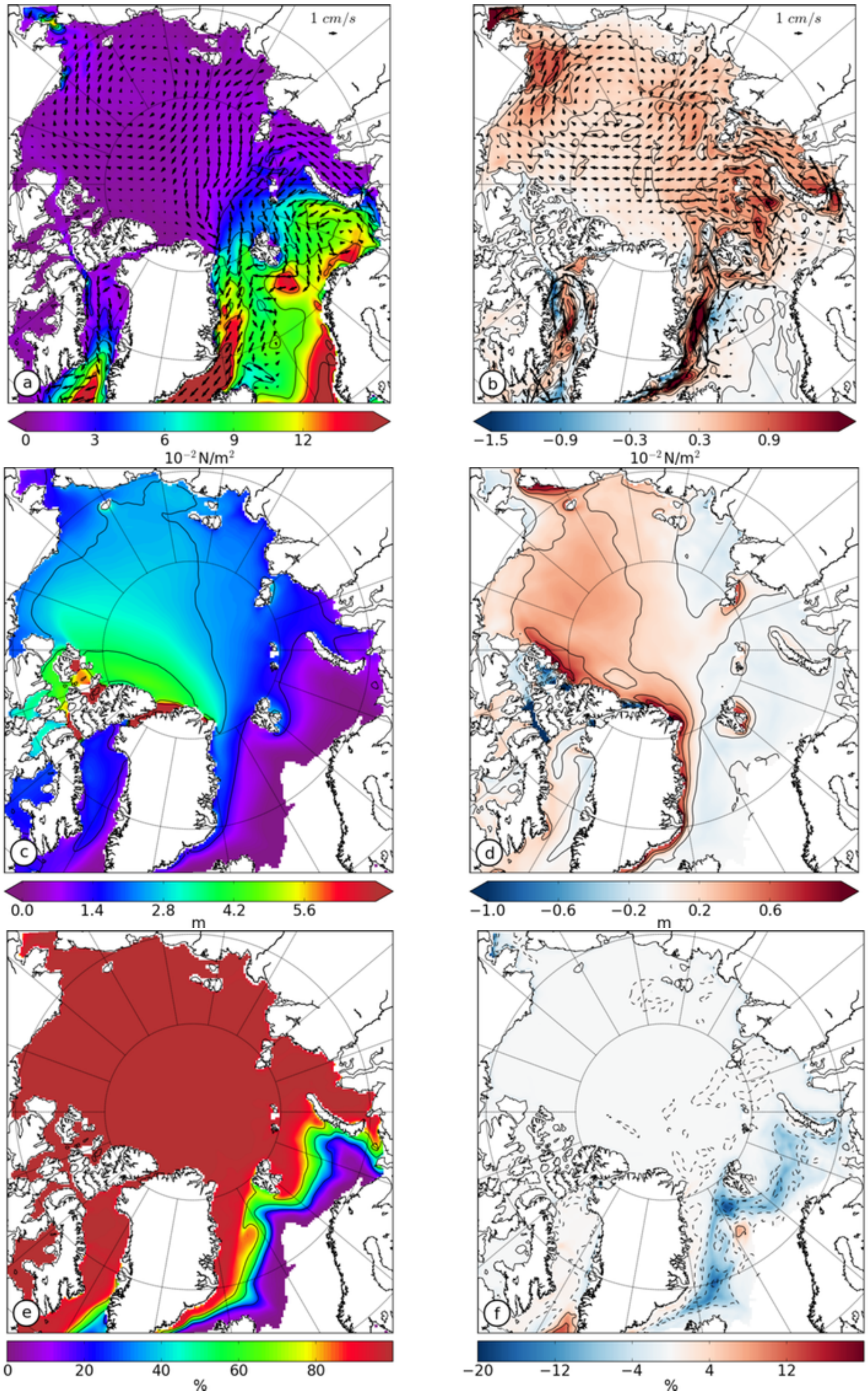

Figure 3.5: Sea ice and ocean surface properties: left - CTRL, right - WEAK minus CTRL: a,b: ocean surface stress magnitude represented by shading and sea ice drift by arrows (Only every 5th vector is shown. On panel a velocities are capped at 1 cm/s for better comprehension); c,d: sea ice thickness; e,f: sea ice concentration; g,h: surface heat fluxes. All variables are March means for the period from 1968 to 2007. Dashed contours connect negative values while solid contours connect positive values.

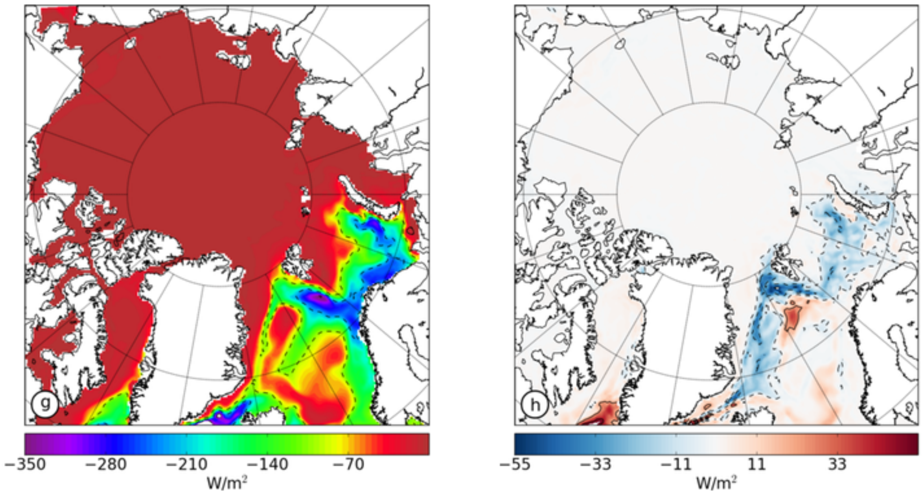

Figure 3.6: Continuation of the Fig. 3.5.

in WEAK thick ice accumulation in the Beaufort Gyre, along the Canadian Archipelago and along the Greenland coast. Some smaller areas of increased thickness are seen north of Bering Strait and south of Svalbard and Severnaya Zemlya. The MIZ in WEAK has lower sea ice concentration related to reduced sea ice export from the Arctic to the northern Nordic Seas and the Barents Sea (not shown). This pattern is reflected in the surface heat flux differences of WEAK minus CTRL (Fig. 3.5 panels g, h). Locally in the MIZ the differences amount up to 50 W/m^2.

3.5 Mid-depth ocean

Turning to the differences in the AWL (212 - 1200 m) we find all Arctic basins to be considerably cooler in the case of WEAK (Fig. 3.7). The differences are especially large in the Eurasian Basin, but the signal spreads also into the Amerasian Basin. In WEAK also the temperatures in the Nordic Seas are much lower. The AWL circulation in our simulations (arrows on Fig. 3.7) is closely following pathways described by Rudels et al (2013). In WEAK a small anticyclonic gyre develops in the Amerasian Basin between Chukchi Cap and the Lomonosov Ridge. The water mass from this gyre returns back to the Eurasian Basin. The cyclonic gyre of the AW in the Amerasian Basin is pushed away from the Eurasian shelfbreak, reduced in size, but enhanced in velocity. The loop of the AWL in the Eurasian Basin is enhanced.

The temporal development of the AWL temperatures (Fig. 3.8) reveals that

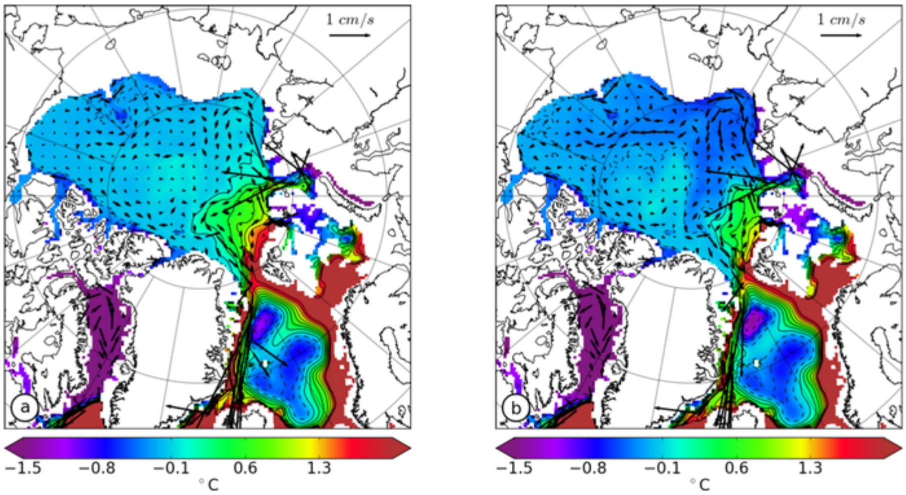

Figure 3.7: Temperature mean (1968-2007) in the AWL (212 - 1200 m): a - CTRL, b - WEAK. Dashed contours connect negative values while solid contours connect positive values. Velocities are represented by arrows. Only every 5th vector is shown. To enhance comprehension of the maps only velocities in the ice covered areas with AWL thicker than 50 m are shown.

the differences between WEAK and CTRL develop already in the first years of the simulations. During the first year (Fig. 3.8 panel a) differences occur in the Nordic Seas, mostly in the MIZ, and in the Barents Sea. During the second year (Fig. 3.8 panel b) the differences are visible in the outflow through St. Anna Trough and in the Nordic Seas recirculation of the cold signal is apparent, as well as propagation southward beyond the Denmark Strait. During the fourth year (Fig. 3.8 panel c) the difference signal has traveled around the whole cyclonic gyre in the Nordic Seas and reached the bifurcation point of the Norwegian Current to the Barents Sea branch and Fram Strait branch north of the Scandinavian Peninsula. The propagation of the signal is superimposed with ongoing differences in the surface heat fluxes and thus local cooling, especially in the MIZ of the Barents and Nordic Seas. Fig. 3.8 panels a, b also show that the signal reaches the Eurasian Basin partly through Fram Strait and partly through the St. Anna Trough and through the strait between Svalbard and Franz-Josef Land. Integrated over the entire basins a cooling trend is apparent in both basins, though significantly more pronounced, and with an earlier onset in the Eurasian basin as compared to the Amerasian Basin (Fig. 3.8 panel d). The cooling that develops off the Barents Sea shelf spreads with the cyclonic circulation of the AWL throughout the Eurasian Basin. After 4 to 5 years the time series north of Severnaya Zemlya (downs. SAT on Fig. 3.8 panel d) show the arrival of a strong cooling. The signal recirculates along the Siberian shelf slope and the Lomonosov Ridge and reaches the area upstream of Fram Strait 15 years into the simulation (ups. FS Fig. 3.8 panel d). The temperatures in the Fram Strait outflow (FS outflow on Fig. 3.8 panel e) remain predominately cooler after 20 years into the simulation. The temperatures in the St. Anna Trough inflow (SAT inflow on Fig. 3.8 panel e) become cooler in WEAK already during the first years of the simulation. The temperatures in the Fram Strait inflow (FS inflow on Fig. 3.8 panel e) are fluctuating and no stable offset in temperature between WEAK and CTRL occurs, but after about 10 years into the simulation the inflow is mostly colder in the case of WEAK, likely enhanced by the recirculation of the colder temperature signal in the Nordic Seas.

Mean (1968-2007) temperature sections at the St. Anna Trough and the Fram Strait (Fig. 3.9) show that at both gateways water masses are cooler in WEAK, with the exception of the uppermost layers in Fram Strait. In the St. Anna Trough the AW core which originates from the Fram Strait branch partially enters the trough on the western slope, recirculates and exits on the eastern side together with the Barents Sea Branch Water (BSBW. In the case of WEAK, the cooler Fram Strait branch thus contributes to the cooler AW leaving St. Anna Trough to feed into the AWL.

Comparing the two experiments we also find a difference in the net volume fluxes across the Arctic straits (Fig. 3.10). WEAK has stronger net Barents Sea inflow (by 0.19 Sv), weaker net Davis Strait outflow (by 0.28 Sv) and stronger net Fram Strait outflow (by 0.46 Sv) comparing to CTRL.

3.6 Connecting the sea ice and mid-depth ocean

In the Barents Sea and in the northern Nordic Seas WEAK has lower sea ice concentration than CTRL. Large areas of the ocean exposed directly to the atmosphere in the Barents Sea lead to a high heat loss at the ocean surface and to strong cooling of the AW that sinks to the bottom and forms the dense part of the BSBW (Fig. 3.11). Although the areal and temporal mean difference between CTRL and WEAK in surface heat fluxes in the Barents Sea is only 1.8 W/m^2 (Fig. 3.11 panel b), this alone can lead to a substantial difference in the bottom water temperature. Calculating the total amount of heat Q for a mean year and grid box area and inserting it to formula $Q = c_p * m * \Delta T$ (where m is mass, c_p = 3994 J/kg/K is heat capacity), will yield a temperature change ΔT of 0.07 K in a 200 m water column.

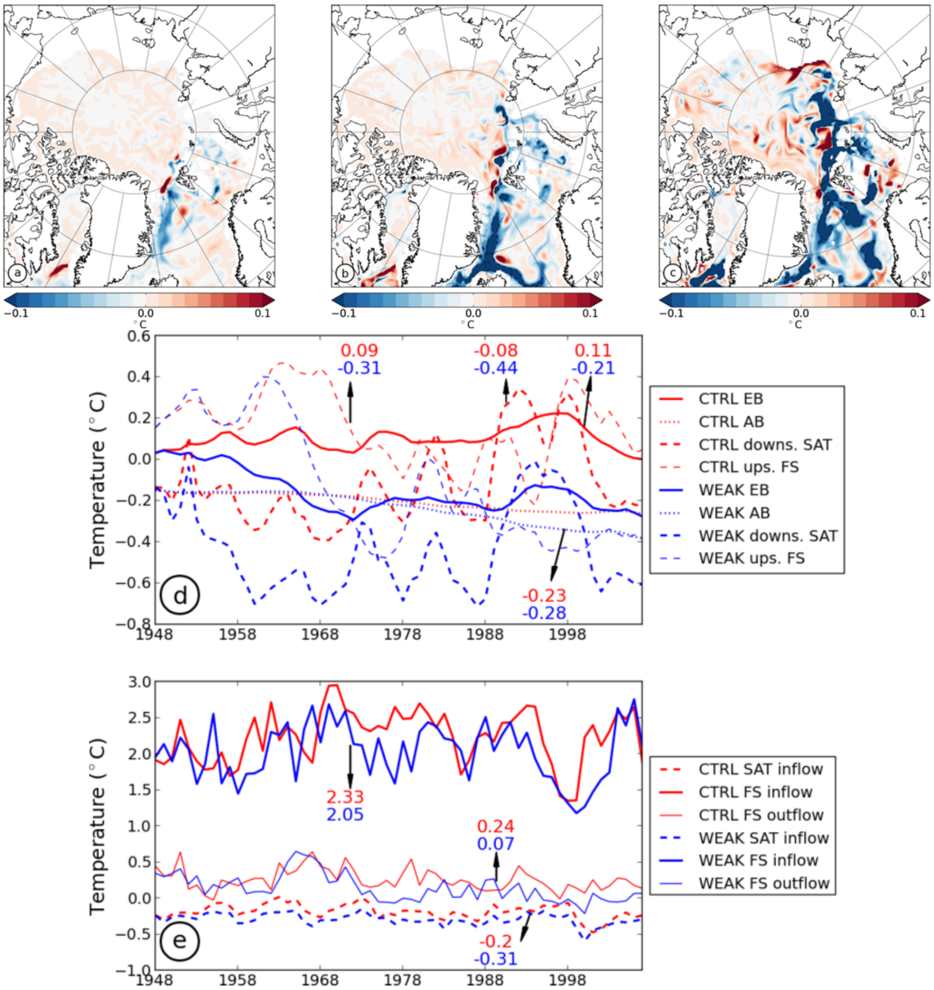

Figure 3.8: Temporal development of the AWL (212 - 1200 m) temperatures. The temperature differences WEAK minus CTRL in during: a - first, b: second and c: fourth year of the simulations, d: time series of vertically averaged temperature for the AWL in the Eurasian (EB) and Amerasian Basin (AB), box area in the Eurasian Basin downstream the St. Anna Trough (downs. SAT) and box area in the Eurasian Basin upstream the Fram Strait (ups. FS), e: time series of vertically averaged temperature for the upper AWL (212 - 700 m) inflow to the Arctic Ocean at the St. Anna Trough (SAT inflow) and Fram Strait (FS inflow) and lower AWL (700 - 1200 m) outflow at the Fram Strait (FS outflow). The temporal means 1968-2007 are printed in the colors corresponding to the legend.

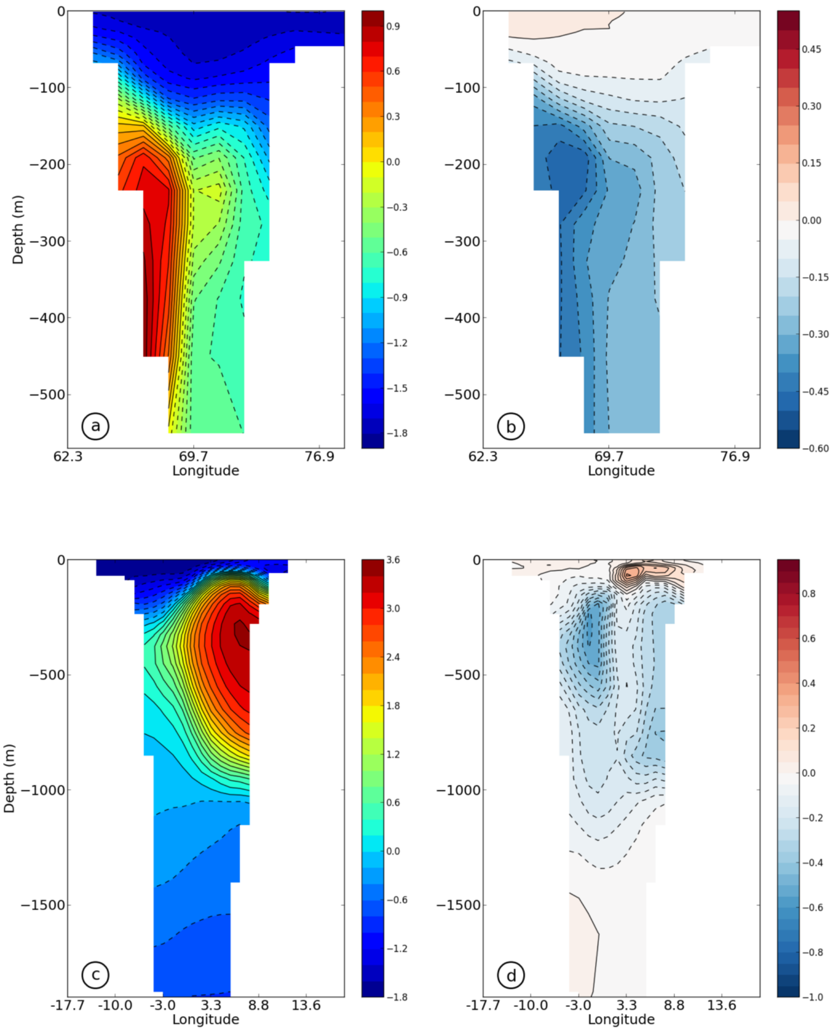

Figure 3.9: Mean temperature (1968-2007) sections at the key regions: St. Anna Trough and Fram Strait: CTRL (a,c) and WEAK minus CTRL (b,d). Both sections are oriented zonally and reader looking into the page is facing northwards.

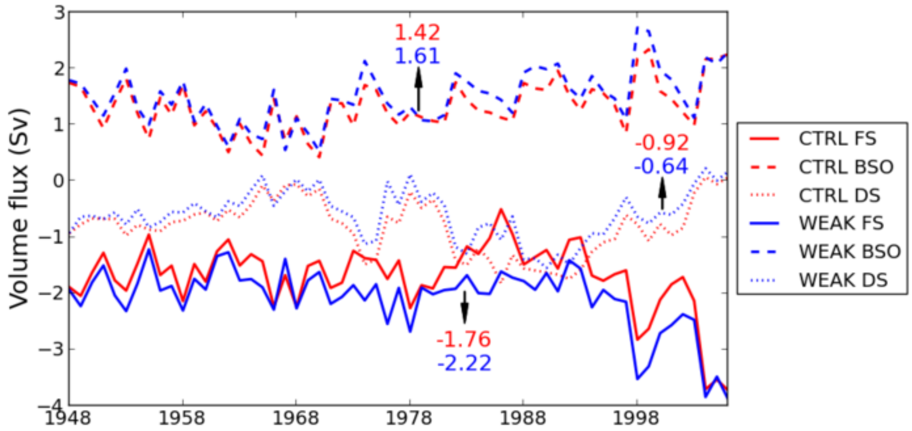

Figure 3.10: Time series of the net volume fluxes at the major Arctic Straits: Fram Strait (FS), Barents Sea Opening (BSO), Davis Strait (DS). The temporal means 1968-2007 are printed in the color corresponding to the legend.

1.8 W/m^2 is a mean annual difference, but the water masses are moving through the Barents Sea with an average velocity of about 0.01 to 0.02 m/s which results in a travel distance of about 300 to 600 km/year. The path of the BSBW over the shelf is about 1000 to 1200 km. This means that the BSBW is modified over at least two seasonal cycles. The resulting $\Delta T =$ 0.14 K is matching the mean temperature difference between WEAK and CTRL in the St. Anna Trough inflow into the Eurasian Basin (SAT inflow on Fig. 3.8 panel e). While the surface outflow from the Barents Sea into the Eurasian Basin through the section between Svalbard and Severnaya Zemlya is very similar in both runs, the deep outflow is more voluminous in WEAK than in CTRL and indicates a stronger dense water production on the Barents Sea shelf (SSZ surface and SSZ bottom on Fig. 3.11 panel d). The Barents Sea Opening volume fluxes (BSO inflow on Fig.3.11 panel d) react with stronger net inflow into the Barents Sea. The relation of stronger BSBW formation and lower sea ice extent in the Barents Sea has been pointed out in a sensitivity study by Harms et al (2005).

The Fram Strait inflow in WEAK is cooled by enhanced surface heat loss, northern Nordic Seas, just as the BSBW is conditioned in the Barents Seas. The cooling in the northern Nordic Seas in case of WEAK is apparent down to the deep part of the Fram Strait inflow (700-1200m). This is a consequence of cooling of the whole boundary current in Nordic Seas (Fig. 3.8 panels a,b,c) and the recirculation of the colder water in the Nordic Seas. When the colder

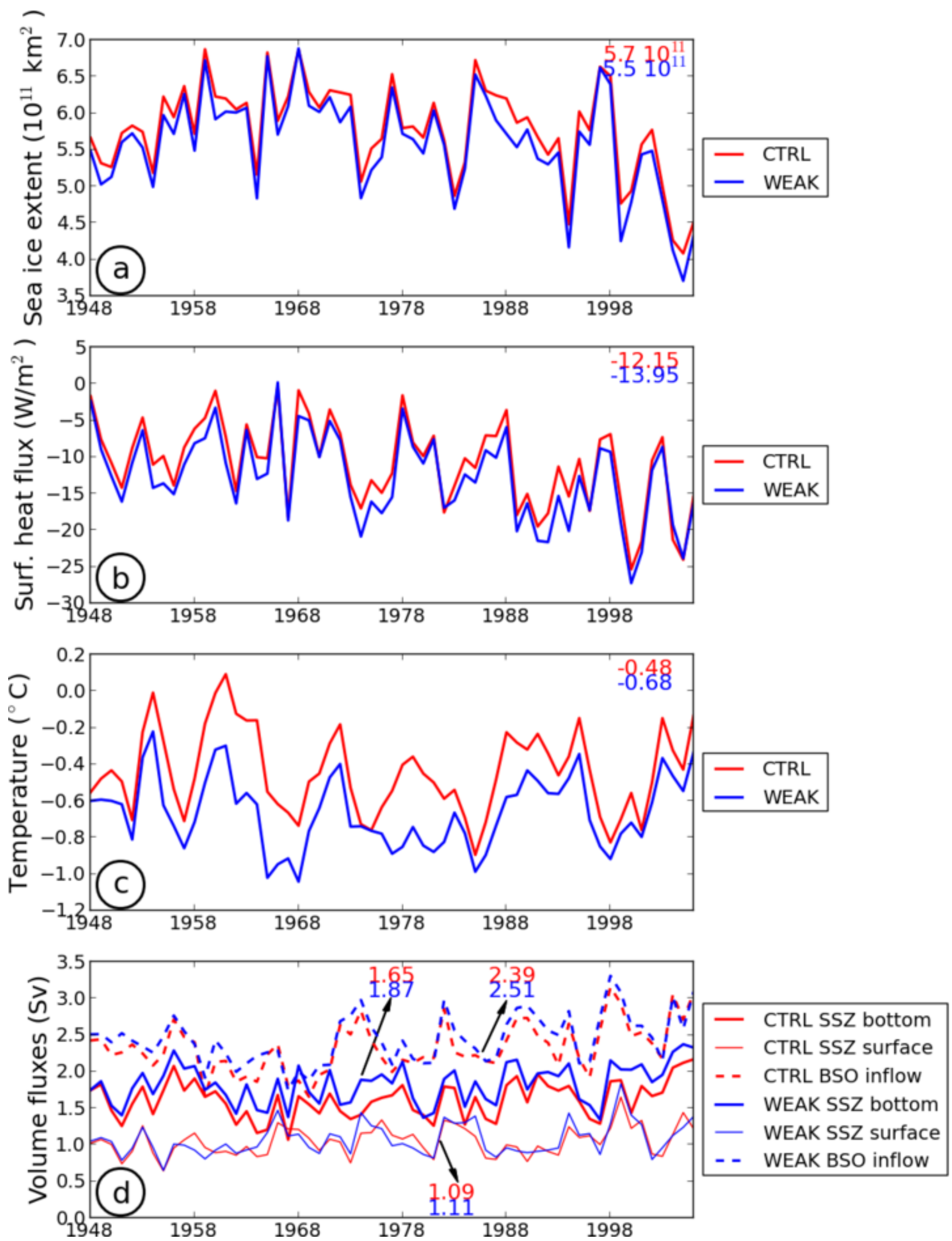

Figure 3.11: Time series of the annual mean sea ice and ocean variables for the Barents Sea: a - sea ice extent, b - surface heat flux, c - bottom (170-212 m) water temperature, d - deep (170 m - bottom) volume inflow between Svalbard and Severnaya Zemlya (SSZ deep), surface (0 - 170 m) volume inflow between Svalbard and Severnaya Zemlya (SSZ surface) and Barents Sea Opening inflow (BSO inflow). The temporal mean values 1968-2007 are printed in the colors corresponding to the legend.

water mass recirculates towards the bifurcation in the Norwegian current lead to an additional decrease in temperature. We interpret the intensified cooling in the deep WSC starting about 20 years into the simulation as consequence of the arrival of colder water from the BSBW reaching the Fram Strait as a part of the AIW. Finally the temperature difference between CTRL and WEAK in the Eurasian Basin stabilize by 0.2 K. The maximum in temperature difference between WEAK and CTRL in the WSC in the Fram Strait is at the lower AWL depth (Fig. 3.9 panel d).

The AWL circulation is not only governed by the inflow at the Arctic gateways, but also by local processes in the central Arctic, e.g. by surface stresses imposed by the combination of wind stress and sea ice motion. In WEAK the faster sea ice drift in the anticyclonic Beaufort Gyre (Fig. 3.5 panel b) leads to an intensification of the oceanic Beaufort Gyre (Fig. 3.12 panel a). Yang (2009) observed a faster sea ice motion and a gradual intensification of the Beafourt Gyre in the 1977-2006 that could not be attributed to the changes in the wind stress, but rather to the changes in the sea ice dynamical properties. The intensification of the Beaufort Gyre is accompanied with a steepening of the slope in the halocline and as a consequence of Ekman pumping also a deepening of the halocline (see e.g. Rabe et al (2011) and Karcher et al (2012)). This leads to a hampering of the underlying cyclonic circulation of the AW boundary current. A similar process has been described by Karcher et al (2012). They found that a strong anticyclonic Beaufort Gyre in the Amerasian Basin after 2004 led to a reduction and partial stopping of AW inflow from the Eurasian Basin into the Amerasian Basin. Instead, an intensification of the recirculation of AW in the Eurasian Basin along the interior ridges took place. A similar situation appears in our study where a part of the AW entering Amerasian Basin from the Eurasian Basin is returned due to a small anticyclonic gyre that develops in the Amerasian Basin between Chukchi Cap and the Lomonosov Ridge (Fig. 3.12 panels b, c and Fig. 3.7 panels a, b). Also here the loop of the AWL in the Eurasian Basin is enhanced and leading to an intense BSBW core marked by cool temperatures looping along the Eurasian Basin side of the Lomonosov Ridge towards the Fram Strait. We submit that the arrival of this plume about 20 years into the simulation (Fig. 3.8 panels d, e) triggers an adjustment in the fluxes through Fram Strait, together with the recirculation signals in the Nordic Seas. Thus, the net volume flux through both entrances to the Arctic, Fram Strait and the Barents Sea Opening change and necessarily lead to an adjustment of the volume fluxes through Davis Strait. The decrease of the Davis Strait outflow follows the increase in the East and then West

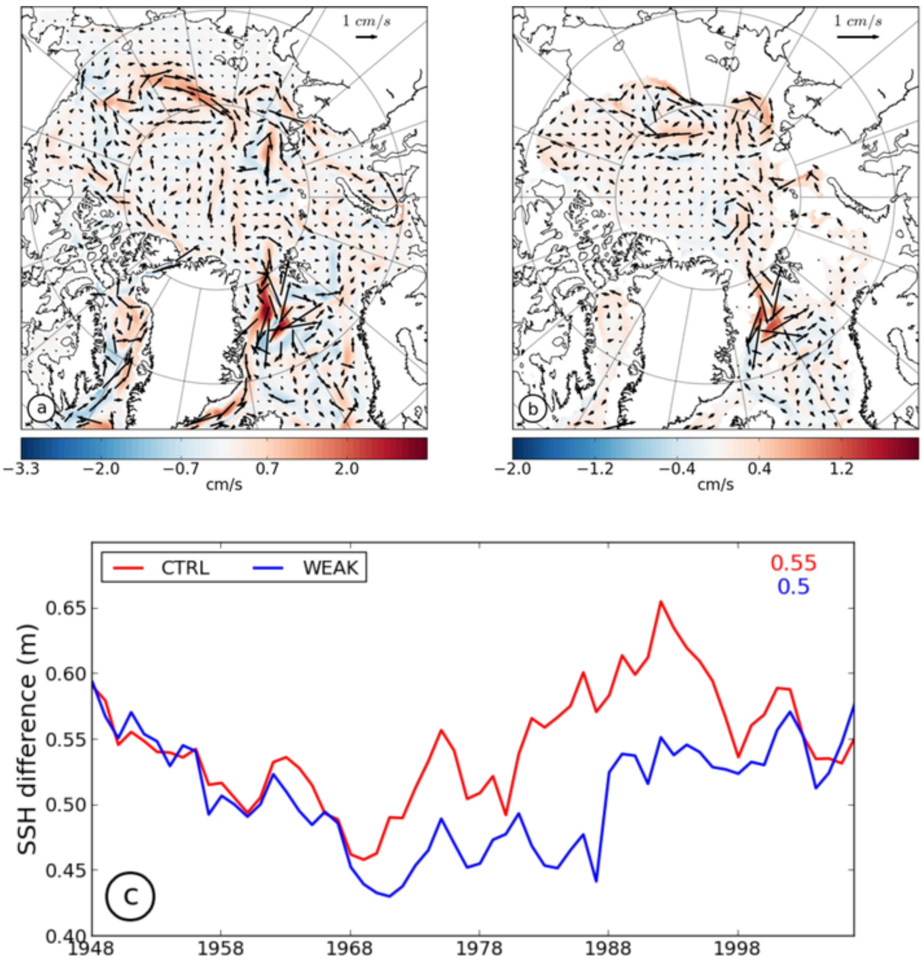

Figure 3.12: Speed mean (1948-2007) difference between WEAK and CTRL in the: a - surface 50 m, b - AWL (212-1200 m). Velocity differences are represented by arrows. Only every 5th vector is shown. To enhance comprehension of the maps only velocities in areas with the surface layer and AWL thicker than 50 m are shown. c - sea surface height difference between the Arctic Ocean north of the Canadian Archipelago and the Labrador Sea. The temporal mean values 1968-2007 are printed in the colors corresponding to the legend.

Greenland Current fluxes originating from the Fram Strait outflow and the resulting sea surface rise in the Labrador Sea (Fig. 3.12 panel e), as described by McGeehan and Maslowski (2012).

3.7 Summary and conclusions

We have presented a study in which we reduce the ice strength parameter P* to investigate the sensitivity of the ocean circulation to this change. It is motivated by the desire to investigate the potential consequences of a weaker, more mobile sea ice in an Arctic Ocean such as already observed in recent years by Rampal et al (2009) and Spreen et al (2011) and likely to continue as a consequence of climate change (Stroeve et al, 2012). Further reductions in the sea ice strength may have consequences for the the coupled climate system, which, however, are difficult to disentangle in coupled climate model simulations which take into account also other anticipated changes. While in nature the sea ice strength reduction is a consequence of sea ice thickness reduction (Zhang et al, 2012), we achieve it in our simulation by changing the P*.

As a result of the reduction in the ice strength parameter P*, we find a number of modifications of the Arctic Ocean circulation from the surface down to lower AWL depths in the central Arctic. Primary results of the imposed reduction of ice strength is a lower sea ice concentration in the MIZ and more mobile sea ice in the central Arctic. This leads to an enhanced surface heat loss in the MIZ, the formation of a colder and denser BSBW that cascades down the St. Anna Trough and is fed by an intensified inflow from the Barents Sea Opening. The Fram Strait branch in the WSC, which is warmer than the BSBW, is also experiencing enhanced surface heat loss in the MIZ. This leads to a cooling of the Eurasian Basin of about 0.2 K. In addition cooling of the mid-depth Nordic Seas along the entire basins margin, including the Denmark Strait sill region takes place, a consequence of an intensified heat loss in the Nordic Seas MIZ plus a colder BSBW signal which after recirculation in the Arctic reaches Fram Strait as a part of the AIW. The loop closes when after recirculation inside the Nordic Seas, the part of the cooling signal which moves into the WSC enters the Arctic Ocean and is another contributor to the cooler AWL there.

In the interior Arctic Ocean the reduced sea ice strength leads to a more mobile sea ice in the central Arctic which leads to an enhancement of the anticyclonic Beaufort Gyre circulation in the sea ice and the upper ocean. The latter suppresses the cyclonic AW circulation in the Amerasian Basin and reduces the flow of the AW boundary current beyond the Lomonosov Ridge. Instead the shorter loop of the AW in the Eurasian Basin enhances. Changes also apply for the volumetric balance between the Arctic straits. In the case of the weaker sea ice a stronger net inflow (by 0.19 Sv) in the Barents Sea takes place in conjunction with a stronger net outflow (by 0.46 Sv) in the Fram Strait and a weaker net outflow (by 0.28 Sv) in the Davis Strait. The transport adjustments in the Fram Strait are a reaction to the intensified BSBW production and circulation in the Eurasian Basin and lead to further adjustments in the Davis Strait transports when the West Greenland Current reaches the Labrador Sea and rises the local sea surface height. Using an atmosphere-ice-ocean coupled model Wu et al (2006) and Rinke et al (2013) demonstrated a connection of the Barents Sea sea ice cover reduction to the Beaufort Sea atmospheric circulation. In the present study sea ice concentration in the Barents Sea and ice-ocean circulation in the Beaufort Gyre are triggered solely by changes in the sea ice strength parameter.

In addition to the local changes in the circulation and hydrography in the Arctic Ocean as a consequence of changes in ice strength, we found changes in the mid depth AIW exiting the Arctic Ocean in the Fram Strait and changes in the southward boundary current in the Nordic Seas from Fram Strait to the Denmark Strait. These may have an impact on the Atlantic Meridional Overturning Circulation (AMOC) since they directly feed into overflows over the Greenland-Scotland sills. The discovered change in the ratio of the Fram and Davis Strait volume transports might result in a change of the water mass characteristics in the deep water formation areas in the Labrador Sea that also feed the AMOC.

Acknowledgments

We would like to thank Wilken-Jon von Appen and Karel Castro Morales, both Alfred Wegener Institute for the help with the observational data comparison. We are grateful to Karel, Martin Losch and Kathrin Riemann-Campe, also Alfred Wegener Institute who have contributed to the model development. Polona Itkin's PhD studies have been partially supported by a grant of the Municipality of Ljubljana, Slovenia. Michael Karcher and Rüdiger Gerdes acknowledge support from the project 'RACE - Regional Atlantic Circulation and Global Change' funded by the German Ministry for Education and Research (BMBF).

Chapter 4

Role of the landfast ice for the Arctic halocline stability

Abstract

Landfast ice covers large surfaces of the winter Siberian Seas. With its immobile cover landfast ice limits the sea ice dynamical growth, decouples the winter river plume in the coastal sea from the atmosphere and positions the flaw polynya offshore. Still, state-of-the-art numerical models are not able to represent landfast ice. We present a simple parametrization of landfast ice based on bathymetry and internal sea ice strength and demonstrate its effect on the Arctic Ocean in a sensitivity study. Our simulations suggest that the landfast ice impact the Arctic halocline stability through the enhanced brine production in the offshore flaw polynyas and through reduced river water freeze-up into the sea ice.

4.1 Introduction

The Arctic Ocean has a fresh and cold surface layer that is maintained close to the freezing point by a seasonal sea ice melting - freezing cycle. In contrast, the ocean temperature at mid-depth is up to several degrees above zero. This warm and saline Atlantic water enters the ocean from the Nordic Seas. The cold and fresh surface layers are decoupled form the mid-depth Atlantic water layer by a strong halocline that is presumably maintained by the cold brines formed on the shelf seas (Aagaard et al, 1981; Martin and Cavalieri, 1989; Cavalieri and Martin, 1994a; Winsor and Björk, 2000a) and by winter convection north of the Barents Sea (Rudels et al, 1996). The cold and fresh waters flow off the shelves and sink along the shelf break, where they mix with the underlying warm Atlantic water.

Landfast ice (also fast, shore-fast ice) is sea ice that is immobile and mechanically fastened to the coast or to the sea floor. As there is no compressive deformation, landfast ice grows only thermodynamically and it usually does not reach thicknesses much over 1.5 m (Romanov, 2004). It can extend a few kilometers (Beaufort Sea, Chukchi Sea, Western Laptev Sea) to several hundred from the coast (Kara Sea, Eastern Laptev Sea, East Siberian Sea). The mechanisms that determine the landfast ice formation, extent and decay are not fully understood. Further, the mechanisms change regionally. In the Chukchi and Beaufort Sea the landfast ice edge is found at relatively shallow depth of 18 m (Mahoney et al, 2007), while on the Eurasian shelf this depth is between 25 and 30 m (Dmitrenko et al, 2005b; Proshutinsky et al, 2007). In the Chukchi and Beaufort Sea the landfast ice is immobilized behind a row of bottom reaching

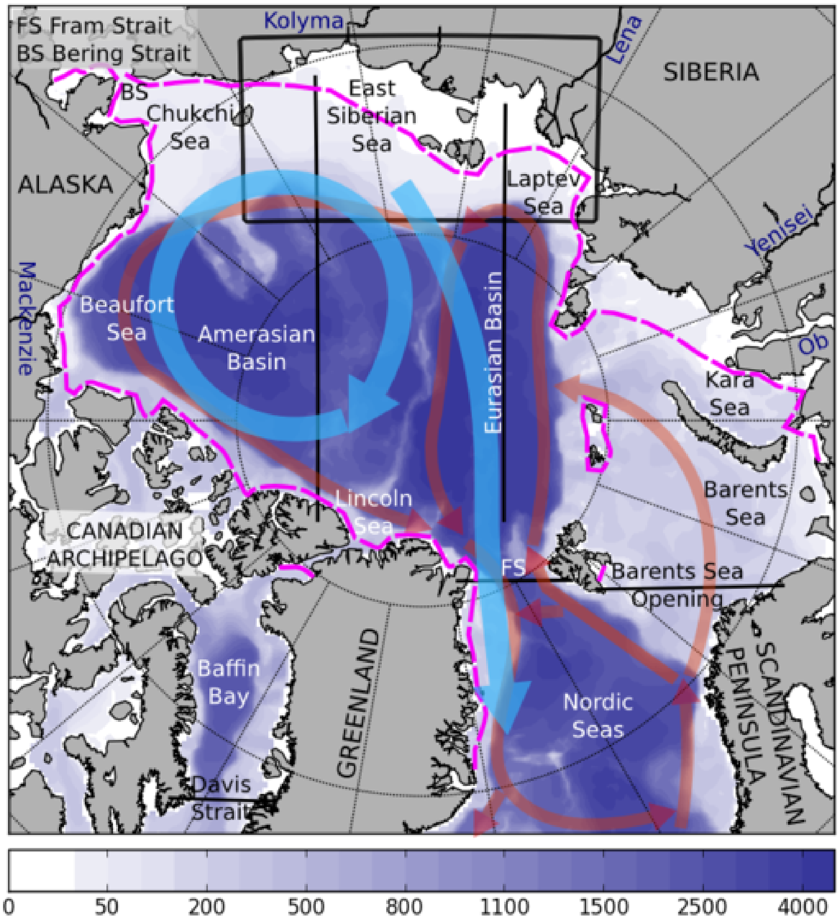

Figure 4.1: The Arctic Ocean and its marginal seas. The sea ice and surface circulation is schematically represented by light blue and mid-depth circulation by red arrows (simplified from Rudels et al (2013)), respectively. The landfast ice edge is depicted by the magenta dash line. The black lines and box mark the sections and regions used in the model analysis.

pressure ridges (Mahoney et al, 2007). In Kara Sea the landfast ice is formed behind a row of small islands parallel to the coast (Divine et al, 2004). In the Laptev Sea and East Siberian Sea, there are no pressure ridges at the landfast ice edge (Reimnizy et al, 1994). Proshutinsky et al (2007) proposed that the landfast ice edge occurs at the location where the warm intermediate Atlantic water reaches the surface after upwelling at the shelfbreak. König Beatty and Holland (2010) attributed the landfast ice extent to the mechanical properties of the sea ice. Strong freshwater and brackish sea ice (Dethleff et al, 1993; Eicken et al, 2005) formed in low salinity shelf seas with high river water content might ground at wide and shallow sand banks (Dethleff et al, 1993; Reimnizy et al, 1994) and extend with long tongues toward the landfast ice edge. Tides are also reported to have a role in the maximal extent and break-up of the landfast ice (Lieser, 2004).

Especially in the Siberian Seas, where it covers the largest surface, landfast ice has a threefold role:

1. it lowers the sea ice production by exclusively thermodynamical sea ice growth. The importance of the landfast ice for the correct simulation of the sea ice thickness has been demonstrated recently by Johnson et al (2012);

2. its immobile lid effectively decouples the inner shelf from the atmosphere and has a role in the river water redistribution. The shallow Siberian Seas are largely influenced by the seasonal river runoff of the great Siberian rivers: Ob, Yenisei and Lena. In a summer with strong onshore winds large parts of the summer maximal discharge can be preserved on the inner shelf until winter (Dmitrenko et al, 2005a);

3. its extent positions the flaw polynya seaward from the coast, where water is more saline and more brine is rejected during freezing. For drifting sea ice, the landfast ice edge forms an advanced winter shore line where during prevailing offshore winds flaw polynyas occur. During formation of nearly fresh sea ice from the saline ocean water, cold brine is rejected into the ocean. The role of the flaw polynyas in forming dense shelf waters (Dmitrenko et al, 2005b; Bauch et al, 2009; Krumpen et al, 2011) and its possible contribution to the Arctic halocline formation was addressed by many authors (Aagaard et al, 1981; Martin and Cavalieri, 1989; Cavalieri and Martin, 1994a; Winsor and Björk, 2000a).

The landfast ice is not represented in state-of-the-art sea ice-ocean models.

The importance of the landfast ice for the accurate simulation of the sea surface height and sea ice thickness has been demonstrated by Proshutinsky et al (2007) and Johnson et al (2012), respectively. In this sensitivity study we aim to show the importance of the landfast ice for the Arctic Ocean properties, with a focus on the Arctic halocline.

The outline of this paper is as follows. In section 4.2 we describe the numerical model we apply. In Section 4.2.1 we describe the details of our landfast ice parametrization. In sections 4.3, 4.4 and 4.5 we present and discuss our results. A summary of our findings and final remarks are in section 4.6.

4.2 Model setup

Our model is a regional coupled sea ice - ocean model based on the Massachusetts Institute of Technology General Circulation Model code - MITgcm (Marshall et al, 1997) with a model domain covering the Arctic Ocean, Nordic Seas and northern North Atlantic. The horizontal resolution of is 1/4° (∼28 km) on a rotated grid with the grid equator passing through the geographical North Pole. The model has 36 vertical levels unevenly distributed in a way that the top 500 m of the water column is divided into 20 levels and the depths below 2000 m have only 6. The shelf bottom has a realistic topography that allows flow of the dense brine downslope and off the shelf break. The very thin surface layer thickness under sea ice requires a non-linear free surface and the use of the rescaled vertical coordinate z* (Campin et al, 2008). Vertical mixing in the ocean interior is parameterized by a K-Profile Parameterization (KPP) scheme (Large et al, 1994) and tracers (temperature and salinity) are advected with an unconditionally stable seventh-order monotonicity preserving scheme (Daru and Tenaud, 2004) that requires no explicit diffusivity. The sea ice model is a dynamic-thermodynamic sea-ice model with a viscous-plastic rheology (Losch et al, 2010). The same model set-up has been used by Itkin et al (2013) except that now the background diffusivity has been lowered to 10^{-6} m^2/s as recommended by Nguyen et al (2009) to achieve a better defined Arctic halocline.

The model is initialized by the PHC climatology (Steele et al, 2001) and has initially no sea ice cover. For the spin-up we run the model for 30 years forced by the atmospheric climatology of the Coordinated Ocean Research Experiment (CORE) version 2 based on the reanalysis from the National Center for Atmospheric Research/National Centers for Environmental Prediction

(NCAR/NCEP) (Large and Yeager, 2009). Subsequently the model is driven from 1948 to 1977 by realistic daily atmospheric data also provided by CORE. Our model experiment continues from 1979 till 2010 with the atmospheric forcing NCEP - The Climate Forecast System Reanalysis (NCEP-CSFR) (Saha et al, 2010). Surface salinity in ice free regions is restored to a mean salinity field (PHC climatology) with a time scale of 180 days to avoid model drift. River runoff was treated like a surface volume flux and it was prescribed for the main Arctic rivers according to the Arctic Ocean Model Intercomparison Project (AOMIP, `http://www.whoi.edu/projects/AOMIP/`) protocol. Open boundaries are formulated following Stevens (1991) and are located at 50°N in the Atlantic and just south of the Bering Strait. Temperature and salinity at the open boundaries are taken from the PHC climatology. The Barents Strait inflow is prescribed as 0.8 Sv and the stream function at open boundary in the Atlantic Ocean is formulated in way that it compensates the sea surface height fluctuations in the model domain.

In this study we are comparing two identical experiments that differ only in the landfast ice parameterization described in the next section:

- control run (CTRL): no landfast ice parametrization
- landfast ice run (LF): with landfast ice parameterization

4.2.1 Landfast ice Parameterization

The mechanisms that determine the landfast ice formation and extent depend of the specific region and not fully understood. There have been many attempts to model or parameterize landfast ice. Lieser (2004) developed a parameterization based on the of sea ice thickness and total water column. The grid cells assigned as landfast ice remained at rest and surface momentum flux into the ocean was set to zero while all thermodynamic calculations were performed as usually. His approach in a 1/4° (28 km) model resulted in too thick landfast ice which survived the summer. A similar procedure was used in higher horizontal resolution models (3-12 km) by Rozman et al (2011) and Johnson et al (2012). Both studies use prescribed landfast ice areas which does not allow any internannual variability. In the Kara Sea, where the landfast ice forms over deep waters behind a row of coastal islands, Olason (2012) successfully modeled landfast ice by adjusting the internal sea ice strength parameters in the viscous-plastic rheology of Hibler III (1979). In the Laptev Sea landfast ice might get grounded at wide and shallow sand banks (Dethleff et al, 1993;

Reimnizy et al, 1994). Our grid does not resolve small islands and shallow topographical features in the Siberian Seas therefore we decided for a simplified and uniform parametrization that takes into account water column depth and landfast ice internal strength. The latter can be justified by a sharp salinity gradient between the coastal waters and the open sea in the Kara, Laptev and East Siberian Sea. In 1992 Dethleff et al (1993) documented freshwater ice up to 100 km seaward off the Lena delta. Eicken et al (2005) defines the freshwater/brakish ice as sea ice with salinity lower than 1. The measurements in 1999 confined the freshwater sea ice to the coastal water adjacent to the Eastern Lena delta with water depth less than 10 m. For the landfast ice further offshore in the southeastern Laptev Sea they estimated a 62 % average river water content based on the sea ice core salinities. In engineering sea ice strength is commonly defined as a function of brine volume (Timco and Weeks, 2010), which depends on the sea ice temperature and salinity. In the widely used sea ice strength parametrization (e.g. Hibler III (1979); Zhang and Hibler III (1997)) compressive strength P depends just on the sea ice thickness h and concentration A:

$$P = P^* h \exp(-C^*(1 - A)), \tag{4.1}$$

where P^* and C^* - empirical sea ice strength parameters, are constants. h and A depend on temperature (through the sea ice growth), but not on salinity. This is the reason for the landfast ice formed in the narrow bays and between the mainland and the New Siberian Islands in the CTRL experiment. We hypothesize that if the model is grid is resolving all the topographical features landfast ice area increases accordingly. In LF experiment we parameterize subgird shallow ocean bottom features and the higher sea ice internal strength in the low salinity Siberian Seas by setting P^* of the region shallower than the maximal fast ice edge mark (30 m) to the double of the drift ice. Such sea ice would still fail under strong offshore wind if the distance between the coastline and this bathymetrical boundary is large. To prevent this we amended the sea ice rheology in the regions shallower than 30 m with sea ice tensile strength T as derived by König Beatty and Holland (2010):

$$\zeta = \frac{P + T}{2\Delta}, \tag{4.2}$$

$$\eta = \frac{P + T}{2\Delta e^2} = \zeta / e^2, \tag{4.3}$$

and

$$p = P - T, \tag{4.4}$$

where ζ is bulk viscosity, η is shear viscosity, e is eccentricity constant and p is pressure term. This moves the elliptical yield curve in the principal stress space into the I. quadrant (so that the value of T equals P) and leave the curve unmodified for all water columns deeper than 30 m.

4.3 Impact of the parameterization on the sea ice

In the first part of our sensitivity study we compare the winter (December-April) sea ice for the CTRL and LF simulations.

Our parametrization in LF comparing to CTRL enlarges the area of the coastal sluggish winter sea ice with speed lower than 0.2 cm/s (Figure 4.2 panels c and d). The ice is slow enough for the flaw polynyas to form at its seaside edge (Figure 4.2 a and b). For this sensitivity study we define the coastal sea ice slower then 0.2 cm/s as landfast ice. The low concentration locations in LF agree better with the landfast ice edge available at the National Snow and Ice Data Center (NSIDC) and produced by the Arctic and Antarctic Research Institute (AARI), Saint Petersburg, Russia (hereafter NSIDC-AARI data). The dataset is available only for the Eurasian shelf seas. We currently use only the data from 1997 to 2006. In the model the Laptev Sea the flaw polynya is located too far away from the coast. This might be a consequence of the coarse model resolution. In the Kara Sea our parametrization has only a minor effect.

In our model the landfast ice cover in LF forms in December, becomes fully drifting in May or June and melts in summer. For this study we thus define the winter duration from December until April. In May the landfast ice is still present, but the atmospheric temperatures are too warm to have a significant amount of brine produced in the flaw polynya. The landfast ice decays in summer because P depends exponentially on A and at atmospheric temperatures above zero and when A becomes lower than 1, sea ice looses its internal strength abruptly and the size of P^* becomes irrelevant. The landfast ice break-up might be connected also to the real volume river runoff implemented in our model. The Siberian rivers reach their maximum discharge in summer and the large freshwater flux in the grid cells at the river mouths causes gravity waves.

The effect of the parametrization is clearly visible in the sea ice thickness maps

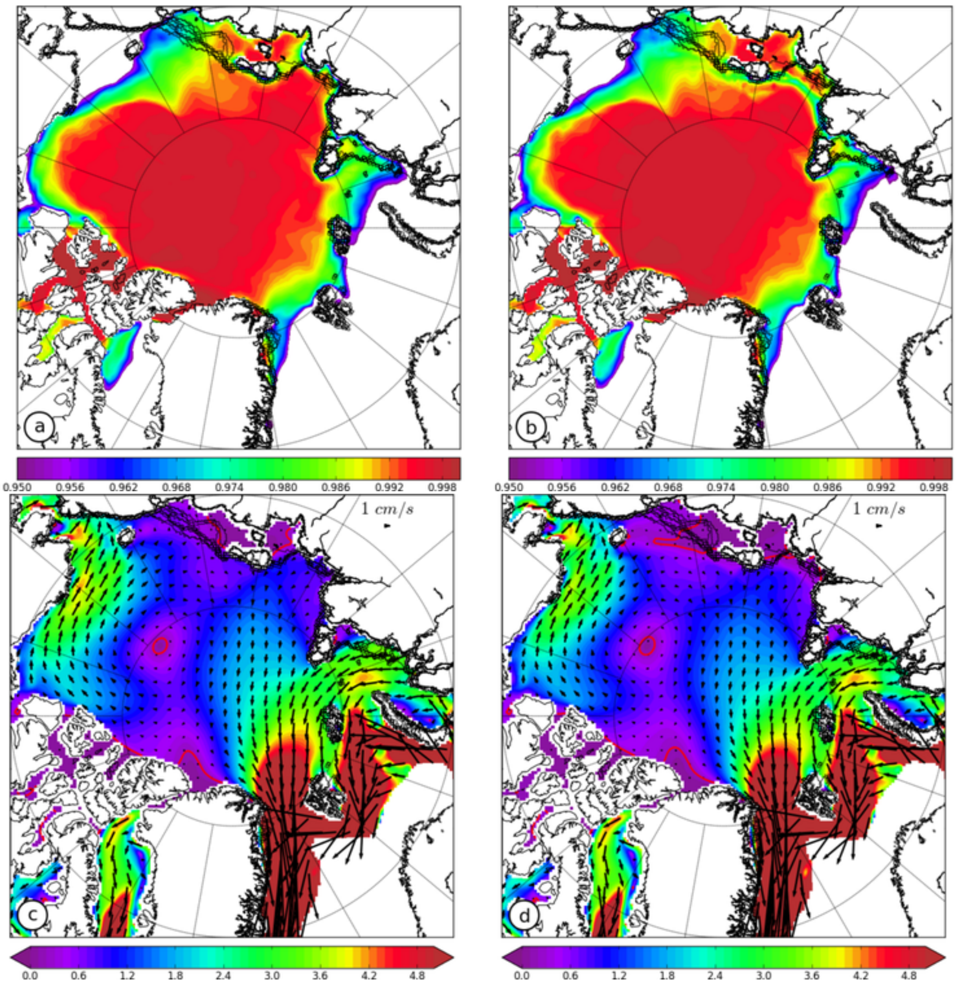

Figure 4.2: The effect of the landfast ice parametrization on the mean winter (2000-2010) sea ice concentration (a,b) and motion (c,d). a,c - CTRL, b,d - LF. Speed 0.2 cm/s is contoured by red line. Landfast edge from the NSIDC-AARI data (1997-2006) is depicted by black line.

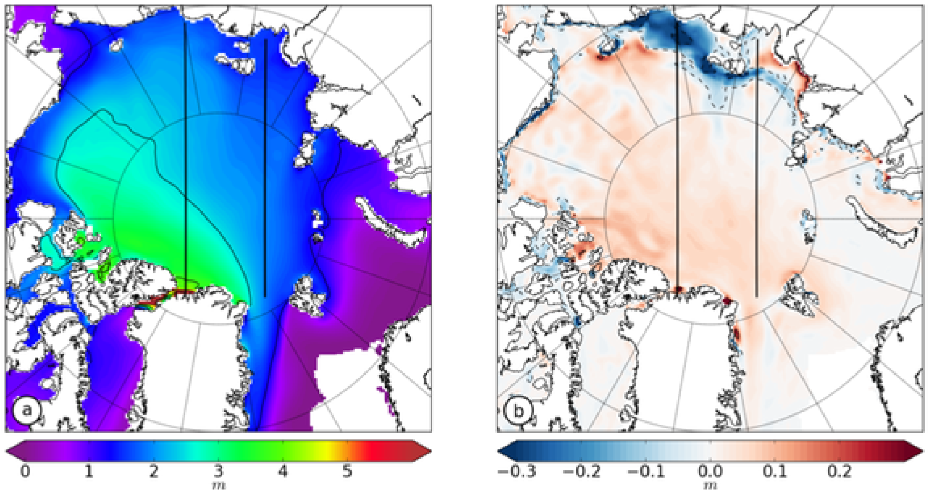

Figure 4.3: Mean winter (2000-2006) sea ice thickness: a - CTRL, b - LF minus CTRL.

(Fig. 4.3): LF has a thinner sea ice by up to 30 cm under the regions effected by the landfast ice parametrization in the Kara, Laptev, East Siberian, Chukchi and Beaufort Seas. The difference pattern matches very well with the NSIDC-AARI landfast ice extent in Fig. 4.2. Sea ice thickness in LF is reduced in the landfast ice area and in the adjacent flaw polynya. The differences are especially large at the landfast ice edge in the East Siberian and Laptev Seas. In the coastal regions of the Laptev Sea the sea ice thickness is increased in LF to correct the wrong polynya location at the coast in CTRL.

The lower sea ice thickness in the landfast ice area in LF is a consequence of exclusively thermodynamic sea ice growth in the landfast ice. The thermodynamical growth itself is also different between the runs (Fig. 4.4): in both cases the highest growth occurs in the polynyas. In LF this is further offshore than in CTRL.

Along with the thermodynamic sea ice growth salt is expelled from the water volume that is transformed into sea ice. The resulting salt flux differences resemble the difference pattern in the thermodynamic growth (Fig. 4.5). This salt flux is an order of magnitude higher and opposite in sign comparing to the salt flux generated by the sea surface salinity restoring that is enabled only for the ice free part of the model grid cell (not shown).

The largest differences in the winter sea ice cover between the runs are formed in the Laptev and East Siberian Sea. This is the area with the greatest landfast ice extent and hence our parametrization has the largest effect. The time series of the winter sea ice concentration, thickness, sea ice production, ocean surface

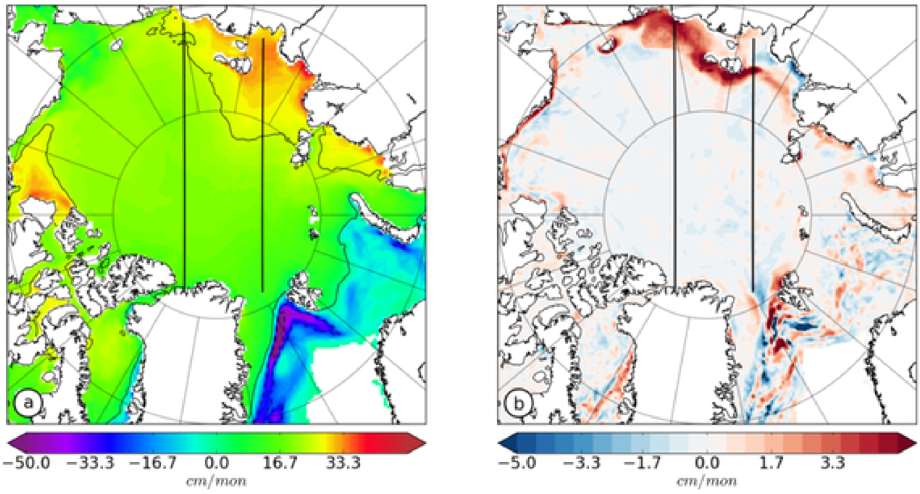

Figure 4.4: Mean winter (2000-2006) sea ice thermodynamical growth: a - CTRL, b - LF minus CTRL.

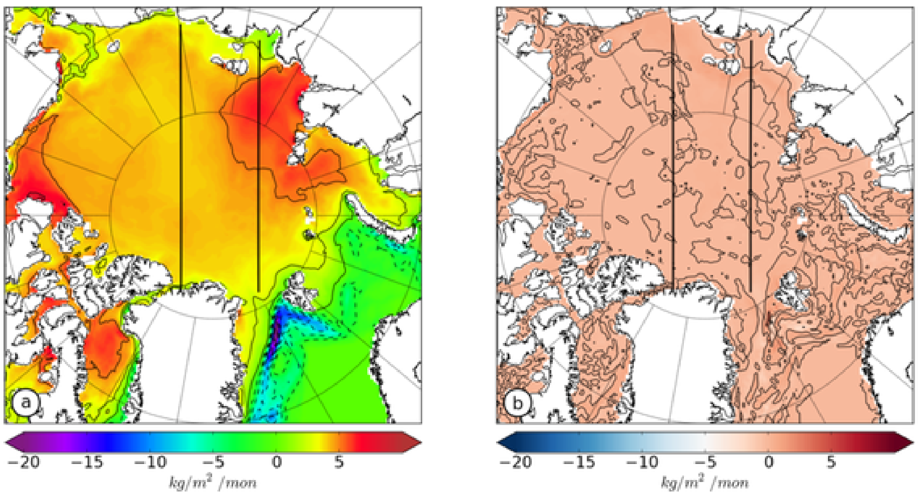

Figure 4.5: Mean winter (2000-2006) salt flux from the sea ice thermodynamical growth: a - CTRL, b - LF minus CTRL.

salinity and salt flux for the Laptev and East Siberian Sea (Fig. 4.6) facilitate the comparison of the contribution of both simulations to the winter dense shelf water production. The mean sea ice concentration over the Siberian Seas is very similar in both simulations. This is not surprising as the differences between the runs are mainly in the positioning of the polynyas within the Siberian Seas. This has only local effects and the mean sea ice extent is nearly same. The sea ice concentrations are a little lower in CTRL as the drifting sea ice allows more small leads in the area that is covered by landfast ice in LF. LF has about 10 cm thinner sea ice than CTRL. This is a consequence of no dynamical growth in the landfast ice area and less sea ice advected into the region. On contrary, there is more sea ice grown thermodynamically in LF. More sea ice production (and in more saline surface waters) leads to higher salt fluxes.

Despite the bias in polynya positioning in the Laptev Sea the differences in the sea ice production between CTRL and LF are located correctly and this sensitivity study can be used to estimate the importance of the landfast ice for the Arctic Ocean halocline.

4.4 Impact of the parameterization on the halocline

We have chosen to analyze the yearly means to verify if the landfast ice signal is strong enough to survive the summer sea ice melt and associated processes. The salinities at the top halocline (25-30 m) are higher by up to 0.5 in LF than in the CTRL (Fig. 4.7 panels a and b). The differences form in the East Siberian Sea and spread in the central parts of the Amerasian and Eurasian Basin. As also the temperatures in LF are cooler at the location where the salinity differences are the largest (Fig. 4.7 panels c and d). We attribute this saline and cool anomalies to the brines formed in the flaw polynyas of the East Siberian Sea in LF. At the rims of the deep basins and adjacent to the Laptev Sea shelf the salinities are lower in LF than in CTRL. At the same location the temperatures in LF are about 0.2 K higher than in CTRL. This warm and fresh anomaly might be attributed to the river water exported from the Laptev Sea into the Transpolar Drift and Beaufort Gyre.

To understand the relevance of these anomalies for the water column stability we show two oceanographic sections: one running from the East Siberian Sea, across the Amerasian Basin to Greenland (Fig. 4.8) and the second one from the Laptev Sea across the Eurasian Basin towards the Fram Strait (Fig. 4.9). The salinity of the surface layer in the Amerasian Basin is lower in LF than in

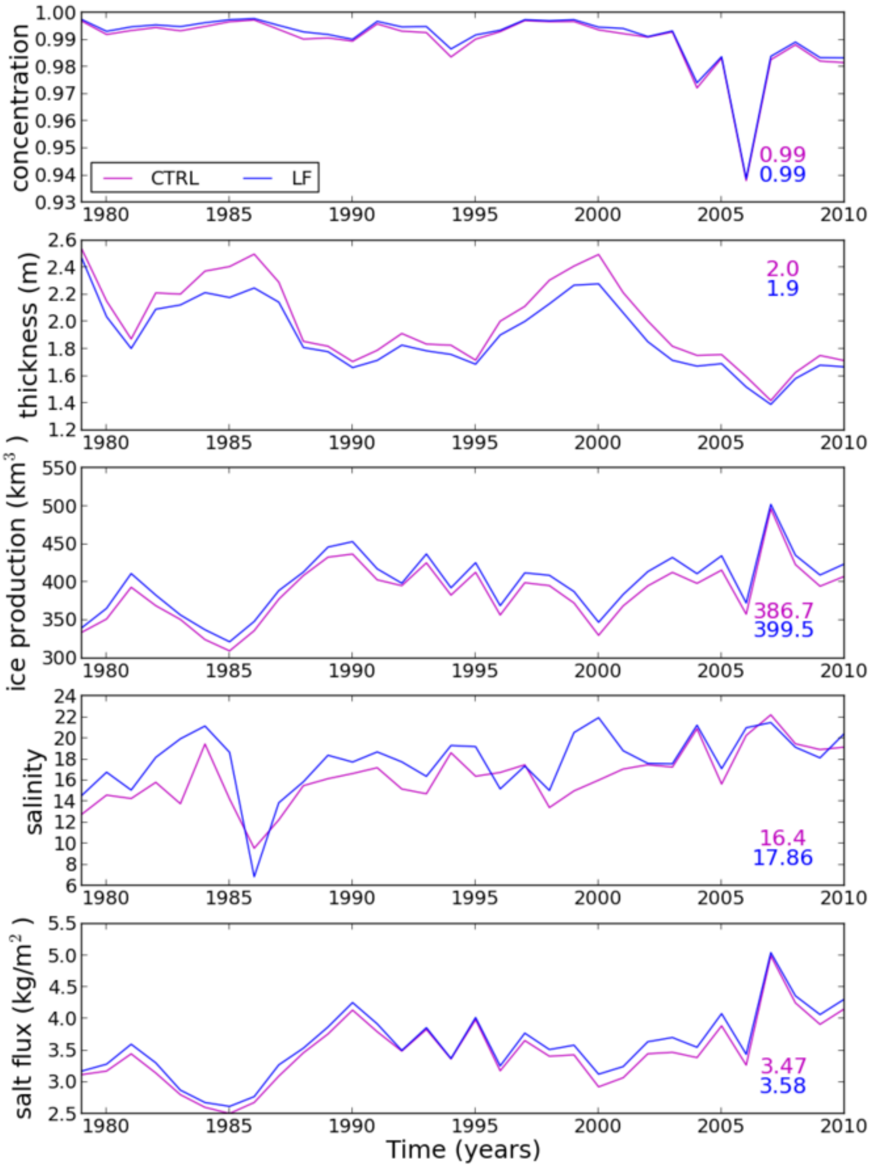

Figure 4.6: Mean winter (2000-2006) sea ice time series for the Laptev Sea and East Siberian Sea. Sea surface salinity of the areas with the mean winter production higher than 33 cm.

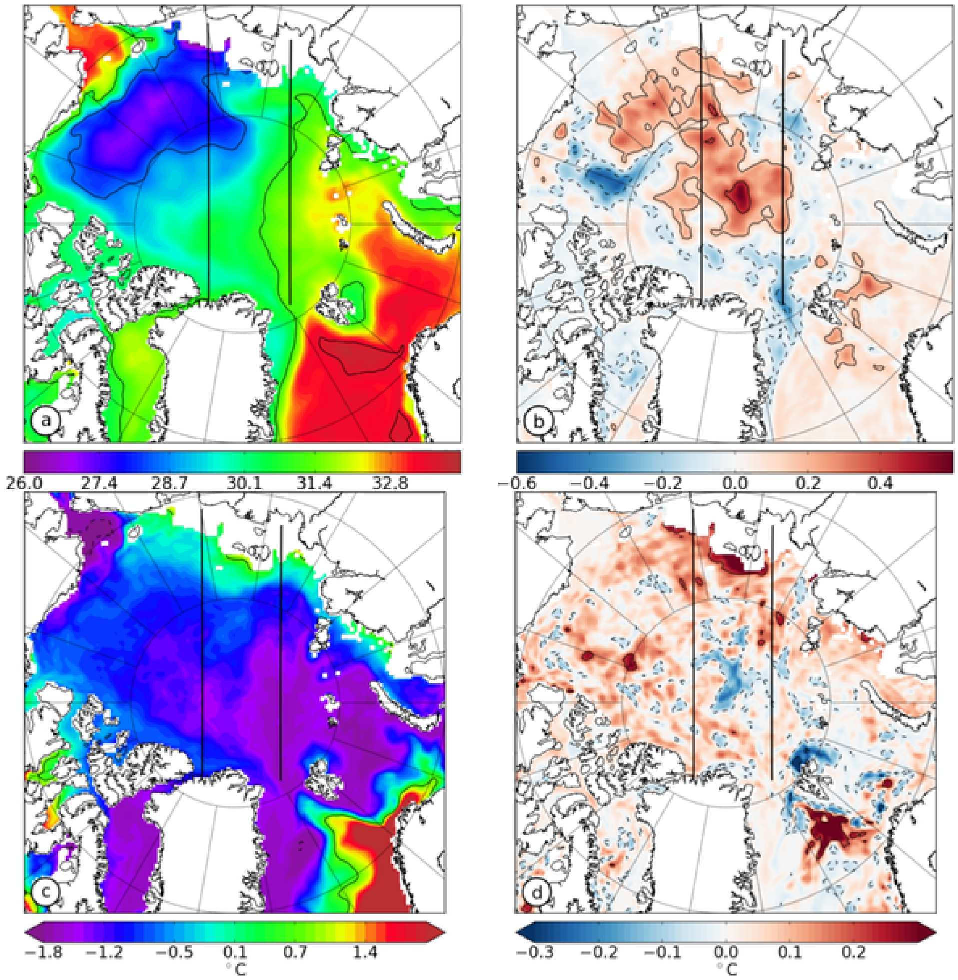

Figure 4.7: Mean yearly (2000-2010) temperature and salinity at the top halocline (25-30 m): a - CTRL, b - LF minus CTRL. Black lines mark the profile sections from the East Siberian Sea to Greenland and from the Laptev Sea to the Fram Strait.

CTRL, but the halocline is more saline and thicker (Fig. 4.8). The halocline layer is also generally warmer which suggests that the halocline waters in LF originate from the river influenced Siberian Seas. The top halocline stability is measured by buoyancy frequency N^2. The yearly mean profile is an average situation of winter mixed layer depth of about 25 m and summer stratified ocean up to the surface. The differences between LF and CTRL point to a higher stability (N^2 is more positive) at the winter mixed layer depth.

Fig. 4.9 shows a similar picture, but with a strong saline and cold anomalies in the central part of the section (closest to the North Pole). These anomalies most probably formed in the East Siberian Sea flaw polynyas and reach from the surface to the core of the halocline layer introducing instability into the halocline layer.

4.5 Discussion

Landfast ice has very little ice growth due to compressive motion (dynamical sea ice growth), but it grows almost exclusively thermodynamically. Therefore the coastal regions covered by landfast ice in LF are thinner than in CTRL. In LF the abrupt change of the the sea ice strength at the 30 m isobath causes the sea ice to fail and there occur flaw polynyas with low sea ice concentration and high sea ice production. In CTRL such areas are located directly on the coast. The shift of the polynyas from the coast in CTRL toward a realistic landfast ice edge location in LF moves the brine production in to more saline ocean area where more brine is produced per equivalent sea ice volume.

To determine if the amount of brine produced at the landfast edge is realistic we first take a look at the available sea ice production estimates for the Laptev Sea. In our study the sea ice production in LF is 144 km^3 per winter (not shown) and that is just above 94+-27km^3, the estimate given by Rabenstein et al (2013) for the southeastern Laptev Sea for winter (late December till mid-April) 2007/2008. The estimates of Willmes et al (2011) 55+-15 km^3 for the entire Laptev Sea during winter are much lower, but they only took into account ice production in the areas with sea ice thinner than 20 cm. The estimate of Dmitrenko et al (2005b) on the other hand is the total annual sea ice production in the Laptev Sea of 750 to 1450 km^3.

We can assume that the summer sea surface salinity restoring keeps the sea surface salinity in the Siberian Sea at realistic levels. Therefore the salt flux

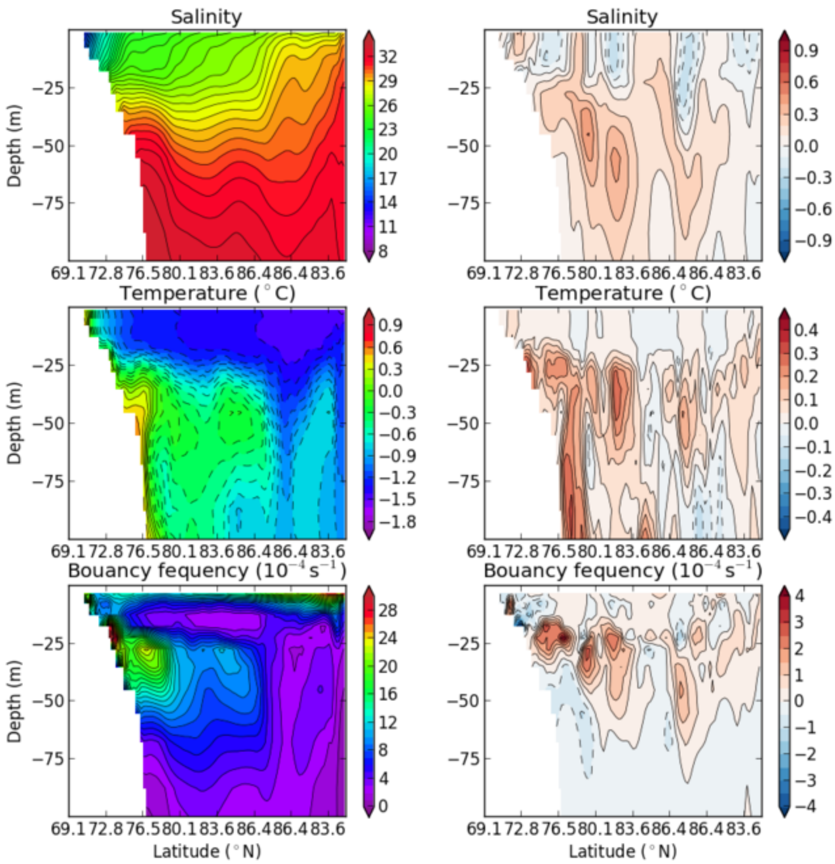

Figure 4.8: Mean yearly (2000-2010) salinity, temperature and buoyancy frequency along the section East Siberian Sea - Ellesmere Island (across the Beaufort Gyre, Amerasian Basin)

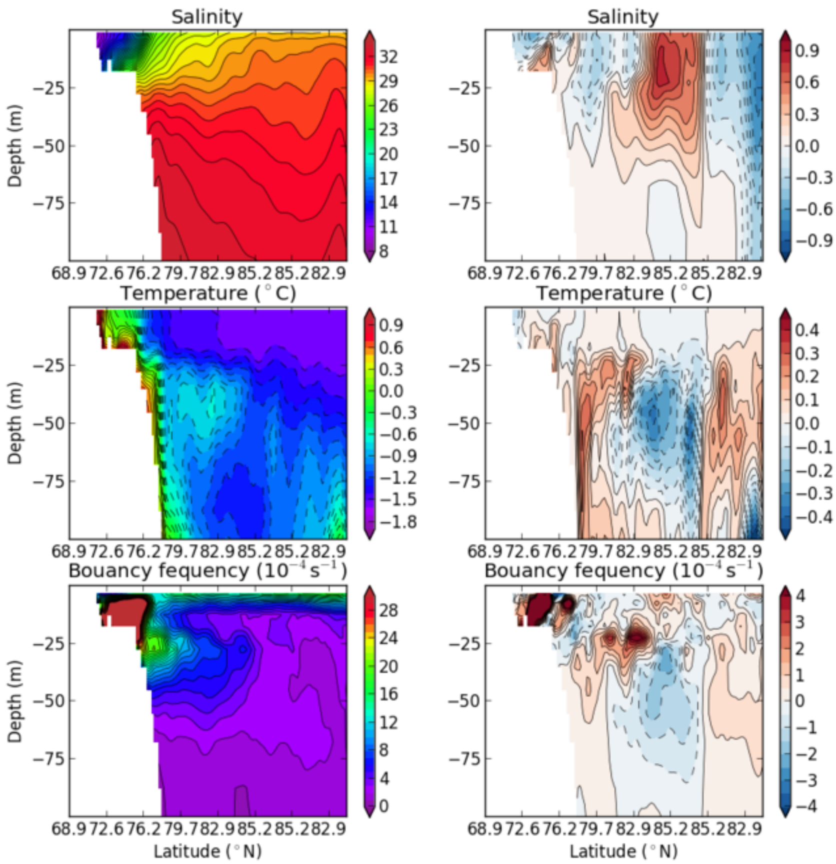

Figure 4.9: Mean yearly (2000-2010) salinity, temperature and buoyancy frequency along the section Laptev Sea - Fram Strait (along the Transpolar Drift, Eurasian Basin)

from the landfast ice edge to the Arctic halocline is also expected to be realistic. The differences between LF and CTRL in the Central Arctic Ocean show that LF has saltier and locally also colder water masses at the halocline depth. We attribute this differences to the difference in the brine production in the Siberian flaw polynyas.

Our results indicate that in LF more river water is stored in the Siberian Seas. While in CTRL more river water is removed from the ocean as it freezes into the ice and the rest is dispersed by the wind stress acting through the drifting sea ice, in LF this river water is protected from the wind by the immobile shield of the landfast ice and remains on the shelf. Then the summer offshore winds drive the river plume northward into the Central Arctic where it stabilizes the water column.

The combined effect of the increased brine export to the Central Arctic and lower river water freeze-up into the sea ice formed on the winter shelf in LF opposed to the CTRL is detectable in the Arctic halocline. The river water is only locally affecting the salinities. The dominating difference signal in salinity at the halocline depth is a positive anomaly associated with the brine while the surface layer and only locally the halocline depth have a negative salinity anomaly associated with the river water. Both, surface and halocline depth anomalies, are strengthening the halocline in LF comparing to CTRL.

The temperature anomalies are resembling the salinity anomalies only locally, at the salinity anomaly maximum, otherwise they seem to be dominated by the river water content difference between LF and CTRL. In LF the halocline is warmer than CTRL, but this does not effect the halocline stability as the affect of the salinity anomalies is dominates.

Surprisingly the positive salinity anomalies in LF in the Eurasian Basin are destabilizing the halocline. We attribute his anomaly to the high brine content and at the same time to the low river water content. Consequently the high salinities in LF occur in the water column from the surface to the halocline lower boundary and destabilize it. In the 1990s a very similar effect on the halocline in the Eurasian Basin was documented as the Great salinity anomaly (Steele and Boyd, 1998; Johnson and Polyakov, 2001). Johnson and Polyakov (2001) explained the phenomena as a consequence of a wind anomaly that caused redistribution of river water to the Amerasian Basin and increased brine production in the Great Siberian Polynya that eroded the Arctic halocline over substantial parts of the Arctic Ocean. Our study suggests that also landfast ice has a similar effect.

Mahoney et al (2007) detected negative trends in the Chukchi Seas landfast ice extent and duration. Although there is no evidence that the maximal extent of the landfast ice in the other Siberian Seas is decreasing, we speculate that the landfast ice season decreases as the sea ice season is generally getting shorter(Comiso et al, 2008; Stroeve et al, 2012). According to our study this should have implications for the halocline stability. Weakening of the halocline could permit the heat transport from the Atlantic Water layer to the surface and contribute to further rapid sea ice loss in the Arctic.

4.6 Conclusions

A simple-to-implement landfast ice parametrization generated landfast ice over extensive areas of the Laptev and East Siberian Seas. Our sensitivity study with control (CTRL) and landfast ice run (LF) show that the landfast ice has an impact on the winter sea ice and brine production. Consequently in LF more brine reaches the Arctic halocline, which is strengthened and shields the cold and fresh Arctic surface waters from the warm Atlantic Water layer underneath more effectively.

Landfast ice is also important for the river water distribution. It facilitates the positioning of the flaw polynyas, winter sea ice production zones, offshore to the landfast ice edge. Lower sea ice production in the fresh river water dominated coastal seas in when our parametrization is used and less river water freezes into ice. Consequently more river water remains in the surface layer of the ocean.

Based on our simulations we recommend to include our landfast ice parametrization to the regional numerical models that address the halocline stability and shelf - deep basin exchanges. The stratification modified by brine produced in the flaw polynyas and the river water that supplies the Arctic Ocean with sediments, nutrients, and pollutants are key factors for biogeochemical processes.

Acknowledgments

We would like to thank Valeria Selyuzhenok, Alfred Wegener Institute for her help with the observational data comparison. We are grateful to Karel Castro-Morales and Kathrin Riemann-Campe, also Alfred Wegener Institute who have contributed to the model development. Polona Itkin's PhD studies have been partially supported by a grant of the Municipality of Ljubljana, Slovenia.

Chapter 5

Summary and Concluding Remarks

In this thesis our key hypothesis was that a change in the sea ice motion causes significant changes in the ocean properties and circulation.

1. For the Siberian Seas remote sensing products give a good estimate of the sea ice drift direction, but comparing to a point in-situ measurements underestimate the sea ice drift speed. The model of a high spatial resolution as NAOSIM is able to reproduce a reasonable sea ice motion in the coastal areas.

2. Exact sea ice parametrization can be achieved by prescribing a landfast ice mask. But due to the unavailability of such mask for a climatological simulation (landfast ice exhibits internannual variability) and unknown trends of the landfast ice extent in the future we decided for a more dynamical landfast ice parameterization where the sea ice in the shallow regions has tensile strength (resistance to divergence) and a doubled compressive strength (resistance to convergence and deformation).

3. Landfast ice in the model simulation shifts the flaw polynya, location of strong winter sea ice and brine production away from the coast in the more saline ocean waters and more brine reaches the Arctic halocline. This strengthens the halocline that shields cold surface waters and sea ice from the warm AWL underneath.

4. A general change in the sea ice internal strength leads to substantial changes in the ocean properties and circulation. Under weaker and more

mobile sea ice AWL temperatures are reduced by 0.2 K. The Eurasian basin circulation in the AWL is increased and this leads to the volume transports adjustments at the Arctic Straits.

5. The results from this sensitivity study can be understood as test of the two modes in the Arctic sea ice: prior to the recent climate change and thereafter.

This confirms our hypothesis. The slowing down and stopping of the sea ice motion over parts of the Siberian Seas by the means of the landfast ice results in changes of salinity of the Arctic halocline layer. The increase in the sea ice motion by means of decreasing the sea ice internal strength (P) results in changes of the AWL temperature and volume transports across the Arctic Straits. The latter effect shows that the Arctic sea ice properties and motion are not only important for the Arctic ocean, but may have consequences also for the global ocean circulation.

5.1 Outlook

A logical continuation of the work done for this thesis would be to downscale the MITgcm to a higher resolution and preform first a validation of the sea ice motion for the whole Arctic and then also a similar validation of the near coast sea ice motion in the Siberian Seas as it was done with NAOSIM in the Paper 1.

The landfast ice parametrization should be tested and possibly adjusted for the high resolution of the MITgcm. Further improvements towards a more physically based landfast ice parametrization would be to define the P* parameter as a function of the brine volume. In engineering sea ice strength is commonly defined as a function brine volume v_b (Timco and O'Brien, 1994; Timco and Weeks, 2010) in the empirical formulas:

$$v_b = S_i(\frac{49.185}{|T_i|} + 0.532), \tag{5.1}$$

where S_i and T_i are the sea ice salinity and temperature, respectively. The uniaxal sea ice compressive strength σ_c for a horizontally loaded first year columnar ice is defined as:

$$\sigma_c = 37(\dot{\epsilon})^{.22}(1 - \sqrt{\frac{v_T}{270}}), \tag{5.2}$$

where $\dot{\epsilon}$ is the strain rate and $v_T = v_b + v_a$ is the total porosity which takes into account also the volume of the air bubbles in the ice (v_a). The tensile strength σ_t for horizontally loaded samples is approximated by:

$$\sigma_t = 4.278{v_T}^{-.6455}. \tag{5.3}$$

Another interesting task would be to check for the trends in the landfast ice duration and extent in the scope of the future climate changes. The current parametrization is sea ice concentration dependent which is in turn a function of the air temperature. This means that in the future warmer climate the landfast ice season would be appropriately shortened. The atmospheric forcing for the future climate could be obtained from one of the Coupled Model Intercomparison Project (CMIP5, `http://cmip-pcmdi.llnl.gov/cmip5/`) coupled climate models participating in the Intergovernmental Panel for Climate Change (IPCC) assessment reports.

Our research focuses of the importance of the sea ice internal stress for the sea ice mobility, but the sea ice motion depends on other factors as well. In the sea ice momentum balance equation 1.3 sea ice motion depends on the τ_a and τ_o - air and ocean stress. The intensity of the air-ice and ocean-ice is defined by the drag coefficients. While in nature the sea ice surface and underside are roughed by ridges, melt ponds and ice floe edges, in the state-of-the-art climate models the drag coefficients are kept constant in time and space without considering their dependence on the ice surface and bottom topography. Changing this values should have a significant influence on the sea ice motion.

Bibliography

Aagaard K, Coachman L, Carmack E (1981) On the halocline of the Arctic Ocean. Deep Sea Research Part A Oceanographic Research Papers 28(6):529–545

Abrahamsen E, Meredith M, Falkner K, Torres-Valdes S, Leng M, Alkire M, Bacon S, Laxon S, Polyakov I, Ivanov V (2009) Tracer-derived freshwater composition of the Siberian continental shelf and slope following the extreme Arctic summer of 2007. Geophysical Research Letters 36:L07,602

Adams S, Willmes S, Heinemann G, Rozman P, Timmermann R, Schröder D (2011) Evaluation of simulated sea-ice concentrations from sea ice-ocean models using satellite data and polynya classification methods. Polar Research 30(0)

Alexandrov V, Martin T, Kolatschek J, Eicken H, Kreyscher M, Makshtas A (2000) Sea ice circulation in the Laptev Sea and ice export to the Arctic Ocean: Results from satellite remote sensing and numerical modeling. Journal of Geophysical Research-Oceans 105(C7)

Bauch D, Dmitrenko I, Wegner C, Hölemann J, Kirillov S, Timokhov L, Kassens H (2009) Exchange of Laptev Sea and Arctic Ocean halocline waters in response to atmospheric forcing. Journal of Geophysical Research-Oceans 114(C5):C05,008

Belliveau D, Bugden G, Eid B, Calnan C (1990) Sea ice velocity measurements by upward-looking Doppler current profilers. Journal of Atmospheric and Oceanic Technology 7(4):596–602

Campin J, Marshall J, Ferreira D (2008) Sea ice-ocean coupling using a rescaled vertical coordinate z*. Ocean modelling 24(1-2):1–14

Castro-Morales K, Kauker F, Losch M, Hendricks S, Riemann-Campe K, R

G (submitted) Sensitivity to realistic ice thickness distributions and snow parameterizations of simulated arctic sea ice. xx

Cavalieri D, Martin S (1994a) The contribution of Alaskan, Siberian, and Canadian coastal polynyas to the cold halocline layer of the Arctic Ocean. Journal of Geophysical Research-Oceans 99(C9)

Cavalieri D, Martin S (1994b) The contribution of Alaskan, Siberian, and Canadian coastal polynyas to the cold halocline layer of the Arctic Ocean. Journal of Geophysical Research-Oceans 99(C9)

Comiso J, Parkinson C, Gersten R, Stock L (2008) Accelerated decline in the Arctic sea ice cover. Geophys Res Lett 35(1):L01,703

Cordey R, Desnos Y, Rosich B (2004) ASAR Wide-Swath Single-Look Complex Products: Processing and Exploitation Potential. In: Proceedings. of ESA FRINGE workshop 2003, vol 3, pp 1–5

de Couet T, Maurer T (2009) Surface Freshwater Fluxes into the World Oceans. Tech. rep., Global Runoff Data Centre. Koblenz: Federal Institute of Hydrology (BfG), URL `http://www.bafg.de/GRDC/EN/03_dtprdcts/31_FWFLX/freshflux_node.html`

Daru V, Tenaud C (2004) High order one-step monotonicity-preserving schemes for unsteady compressible flow calculations. JOURNAL OF COMPUTATIONAL PHYSICS 193(2):563–594, DOI {10.1016/j.jcp.2003.08.023}

Dethleff D, Nürnberg D, Groth E (1993) East siberian arctic region expedition'92: the laptev sea: its significance for arctic sea-ice formation and transpolar sediment flux/by d. dethleff... Berichte zur Polarforschung (Reports on Polar Research) 120

Divine D, Korsnes R, Makshtas A (2004) Temporal and spatial variation of shore-fast ice in the Kara Sea. Continental Shelf Research 24(15):1717–1736

Dmitrenko I, Kirillov S, Eicken H, Markova N (2005a) Wind-driven summer surface hydrography of the eastern Siberian shelf. Geophys Res Lett 32

Dmitrenko I, Tyshko K, Kirillov S, Eicken H, Hölemann J, Kassens H (2005b) Impact of flaw polynyas on the hydrography of the Laptev Sea. Global and planetary change 48(1-3):9–27

Dmitrenko I, Polyakov I, Kirillov S, Timokhov L, Frolov I, Sokolov V, Simmons H, Ivanov V, Walsh D (2008) Toward a warmer Arctic Ocean: Spreading of the early 21st century Atlantic Water warm anomaly along the Eurasian Basin margins. Journal of Geophysical Research 113(C5):C05,023

Dmitrenko IA, Kirillov SA, Tremblay LB, Bauch D, Hlemann JA, Krumpen T, Kassens H, Wegner C, Heinemann G, Schrder D (2010) Impact of the arctic ocean atlantic water layer on siberian shelf hydrography. Journal of Geophysical Research: Oceans 115(C8), DOI 10.1029/2009JC006020

Eicken H, Reimnitz E, Alexandrov V, Martin T, Kassens H, Viehoff T (1997) Sea-ice processes in the Laptev Sea and their importance for sediment export. Continental Shelf Research 17(2):205–233

Eicken H, Dmitrenko I, Tyshko K, Darovskikh A, Dierking W, Blahak U, Groves J, Kassens H (2005) Zonation of the Laptev Sea landfast ice cover and its importance in a frozen estuary. Global and planetary change 48(1-3):55–83

Eldevik T, Straneo F, Sand AB, Furevik T (2005) Pathways and Export of Greenland Sea Water, American Geophysical Union, pp 89–103. DOI 10.1029/158GM08

Ezraty R, Ardhuin F, Croizé-Fillon D (2006) Sea ice drift in the Central Arctic using the 89 GHz brightness temperatures of the Advanced Microwave Scanning Radiometer (AMSR-E). User's Manual, Version 2 p 21

Fieg K, Gerdes R, Fahrbach E, Beszczynska-Möller A, Schauer U (2010) Simulation of oceanic volume transports through Fram Strait 1995-2004. Ocean Dynamics 60(3):491–502

Fisher N (1996) Statistical analysis of circular data. Cambridge Univiversity Press

Frolov I, Ashik I, Kassens H, Polyakov I, Proshutinsky A, Sokolov V, Timokhov L (2009) Anomalous variations in the thermohaline structure of the Arctic Ocean. In: Doklady Earth Sciences, Springer, vol 429-2, pp 1567–1569

Gerdes R, Karcher M, Kauker F, Schauer U (2003) Causes and development of repeated Arctic Ocean warming events. Geophysical Research Letters 30(19):doi:10.1029/2003GL018,080

Girard-Ardhuin F, Ezraty R (2005) Validation of Arctic sea ice drift with IABP buoys p 7, URL `http://www.ifremer.fr/docelec/doc/2005/acte-1292.pdf`

Govorucha L, Gerasimov I (eds) (1970) Sovetskaja Arktika - Morja i ostrova Severnogo Ledovitogo okeana (Soviet Arctic - Seas and islands of the Arctic Ocean). Nauka, Moscow

Haas C, Pfaffling A, Hendricks S, Rabenstein L, Etienne J, Rigor I (2008) Reduced ice thickness in Arctic Transpolar Drift favors rapid ice retreat. Geophysical Research Letters 35(17):1–L17,501

Harder M, Lemke P, Hilmer M (1998) Simulation of sea ice transport through Fram Strait: Natural variability and sensitivity to forcing. Journal of Geophysical Research 103(C3):5595–5606

Harms IH, Schrum C, Hatten K (2005) Numerical sensitivity studies on the variability of climate-relevant processes in the barents sea. Journal of Geophysical Research: Oceans 110(C6), DOI 10.1029/2004JC002559

Hibler WD, Bryan K (1987) A diagnostic ice ocean model. Journal of Physical Oceanography 17:987–1015

Hibler WD, Walsh JE (1982) On Modeling Seasonal and Interannual Fluctuations of Arctic Sea Ice. Journal of Physical Oceanography 12:1514–1523, DOI 10.1175/1520-0485(1982)012⟨1514:OMSAIF⟩2.0.CO;2

Hibler III W (1979) A dynamic thermodynamic sea ice model. Journal of Physical Oceanography 9(4):815–846

Hölemann J, Kirillov S, Klagge T, Novikhin A, Kassens H, Timokhov L (2011) Near-bottom water warming in the Laptev Sea in response to atmospheric and sea ice conditions in 2007. Polar Research 30(0)

Hughes SL, Holliday NP (2006) Ices report on ocean climate 2005. ICES

Hunke E, Dukowicz JK (1997) An ElasticViscousPlastic Model for Sea Ice Dynamics. Journal of Physical Oceanography 27:1849–1867, DOI doi:10.1175/1520-0485(1997)027⟨1849:AEVPMF⟩2.0.CO;2

Instruments R (1996) Acoustic doppler current profilers principles of operation: A practical primer. RD Instruments

Itkin P, Karcher M, R G (2013) Is weaker Arctic sea ice changing the Atlantic water circulation? Journal of Geophysisical Research submitted

Ivanov V, Alexeev V, Repina I, Koldunov N, Smirnov A (2012) Tracing atlantic water signature in the arctic sea ice cover east of svalbard. Advances in Meteorology 2012, DOI 10.1155/2012/201818

Jakobsson M, Macnab R, Mayer L, Anderson R, Edwards M, Hatzky J, Schenke H, Johnson P (2008) An improved bathymetric portrayal of the Arctic Ocean: Implications for ocean modeling and geological, geophysical and oceanographic analyses. Geophysical Research Letters 35(7):doi:10.1029/2008GL033,520

Jammalamadaka S, Sengupta A (2001) Topics in circular statistics. World Scientific Publishing, London

Johnson M, Polyakov I (2001) The Laptev Sea as a source for recent Arctic Ocean salinity changes. Geophys Res Lett 28(10):2017–2020

Johnson M, Proshutinsky A, Polyakov I (1999) Atmospheric patterns forcing two regimes of arctic circulation: A return to anticyclonic conditions? Geophysical Research Letters 26(11):1621–1624

Johnson M, Proshutinsky A, Aksenov Y, Nguyen AT, Lindsay R, Haas C, Zhang J, Diansky N, Kwok R, Maslowski W, Haekkinen S, Ashik I, de Cuevas B (2012) Evaluation of Arctic sea ice thickness simulated by Arctic Ocean Model Intercomparison Project models. JOURNAL OF GEOPHYSICAL RESEARCH-OCEANS 117, DOI {10.1029/2011JC007257}

Kanamitsu M, Ebisuzaki W, Woollen J, Yang S, Hnilo J, Fiorino M, Potter G (2002) NCEP–DOE AMIP-II Reanalysis (R-2). Bulletin of the American Meteorological Society 83(11):1631–1643

Karcher M, Gerdes R, Kauker F, Köberle C (2003) Arctic warming: Evolution and spreading of the 1990s warm event in the Nordic seas and the Arctic Ocean. Journal of Geophysical Research 108(C2):doi:10.1029/2001JC001,265

Karcher M, Beszczynska-Mller A, Kauker F, Gerdes R, Heyen S, Rudels B, Schauer U (2011) Arctic Ocean warming and its consequences for the Denmark Strait overflow. Journal of Geophysical Research: Oceans 116(C2), DOI 10.1029/2010JC006265

Karcher M, Smith JN, Kauker F, Gerdes R, Smethie WM (2012) Recent changes in Arctic Ocean circulation revealed by iodine-129 observations and modeling. Journal of Geophysical Research 117(C8):C08,007+, DOI 10.1029/2011jc007513

Kattsov VM, Walsh JE (2000) Twentieth-Century Trends of Arctic Precipitation from Observational Data and a Climate Model Simulation. Journal of Climate 13:1362–1370

Kattsov VM, Ryabinin VE, Overland JE, Serreze MC, Visbeck M, Walsh JE, Meier W, Zhang X (2010) Arctic sea-ice change: a grand challenge of climate science. Journal of Glaciology 56(200):1115–1121, DOI doi:10.3189/002214311796406176

Kauker F, Kaminski T, Karcher M, Giering R, Gerdes R, Vobeck M (2009) Adjoint analysis of the 2007 all time arctic sea-ice minimum. Geophysical Research Letters 36(3), DOI 10.1029/2008GL036323

König Beatty C, Holland DM (2010) Modeling landfast sea ice by adding tensile strength. Journal of Physical Oceanography 40(1):185–198

Kreyscher M, Harder M, Lemke P, Flato G (2000a) Results of the Sea Ice Model Intercomparison Project: Evaluation of sea ice rheology schemes for use in climate simulations. Journal of Geophysical Research-Oceans 105(C5):11,299–11,320

Kreyscher M, Harder M, Lemke P, Flato GM (2000b) Results of the sea ice model intercomparison project: Evaluation of sea ice rheology schemes for use in climate simulations. Journal of Geophysical Research: Oceans (1978–2012) 105(C5):11,299–11,320

Krumpen T, Hölemann J, Willmes S, Maqueda M, Busche T, Dmitrenko I, Gerdes R, Haas C, Heinemann G, Hendricks S, et al (2011) Sea ice production and water mass modification in the eastern laptev sea. Journal of Geophysical Research 116(C5):C05,014

Kwok R, Rothrock D (2009) Decline in arctic sea ice thickness from submarine and icesat records: 1958–2008. Geophysical Research Letters 36(15)

Kwok R, Schweiger A, Rothrock D, Pang S, Kottmeier C (1998) Sea ice motion from satellite passive microwave imagery assessed with ERS SAR and buoy motions. Journal of Geophysical Research 103(C4):8191–8214

Kwok R, Cunningham G, Wensnahan M, Rigor I, Zwally H, Yi D (2009) Thinning and volume loss of the Arctic Ocean sea ice cover: 2003-2008. Journal of Geophysical Research 114(C7):C07,005

Large W, Yeager S (2009) The global climatology of an interannually varying air-sea flux data set. Climate Dynamics 33(2-3):341–364, DOI 10.1007/s00382-008-0441-3

Large WG, McWilliams JC, Doney SC (1994) Oceanic vertical mixing: A review and a model with a nonlocal boundary layer parameterization. Reviews of Geophysics 32(4):363–403, DOI 10.1029/94RG01872

Lavergne T, Eastwood S, Teffah Z, Schyberg H, Breivik LA (2010) Sea ice motion from low-resolution satellite sensors: An alternative method and its validation in the arctic. Journal of Geophysical Research: Oceans 115(C10), DOI 10.1029/2009JC005958

Lemke P, Hibler W, Flato G, Harder M, Kreyscher M (1997) On the improvement of sea-ice models for climate simulations: the Sea Ice Model Intercomparison Project. Annals of Glaciology 25:183–187

Lieser J (2004) A numerical model for short-term sea ice forecasting in the Arctic= Ein numerisches Modell zur Meereisvorhersage in der Arktis. Berichte zur Polar-und Meeresforschung= Reports on polar and marine research 485:93

Losch M, Menemenlis D, Campin JM, Heimbach P, Hill C (2010) On the formulation of sea-ice models. part 1: Effects of different solver implementations and parameterizations. Ocean Modelling 33(1):129–144

Mahoney A, Eicken H, Gaylord A, Shapiro L (2007) Alaska landfast sea ice: Links with bathymetry and atmospheric circulation. J Geophys Res 112:C02,001

Marshall J, Adcroft A, Hill C, Perelman L, Heisey C (1997) A finite-volume, incompressible Navier Stokes model for studies of the ocean on parallel computers. J geophys Res 102(C3):5753–5766

Martin S, Cavalieri D (1989) Contributions of the Siberian Shelf Polynyas to the Arctic Ocean intermediate and deep water. Journal of Geophysical Research 94(C9)

Martin T, Gerdes R (2007) Sea ice drift variability in Arctic Ocean Model Intercomparison Project models and observations. J Geophys Res 112(C04S10):doi:10.1029/2006JC003,617

McClelland J, Holmes R, Peterson B, Stieglitz M (2004) Increasing river discharge in the Eurasian Arctic: Consideration of dams, permafrost thaw, and fires as potential agents of change. Journal of geophysical research 109(D18):D18,102

McGeehan T, Maslowski W (2012) Evaluation and control mechanisms of volume and freshwater export through the canadian arctic archipelago in a high-resolution pan-arctic ice-ocean model. Journal of Geophysical Research: Oceans 117(C8), DOI 10.1029/2011JC007261

Meier W, Maslanik J, Fowler C (2000) Error analysis and assimilation of remotely sensed ice motion within an Arctic sea ice model. Journal of Geophysical Research-Oceans 105(C2):3339–3356

Münchow A, Weingartner T, Cooper L (1999) The Summer Hydrography and Surface Circulation of the East Siberian Shelf Sea*. Journal of Physical Oceanography 29:2167–2182

Nguyen AT, Menemenlis D, Kwok R (2009) Improved modeling of the Arctic halocline with a subgrid-scale brine rejection parameterization. Journal of Geophysical Research-Oceans 114, DOI {10.1029/2008JC005121}

Olason EÖ (2012) Dynamical modelling of kara sea land-fast ice. PhD thesis, University of Hamburg

OSI-SAF (2013) Eumetsat ocean and sea ice satelitte application facility. global sea ice concentration reprocessing dataset 1978-2009 (v1.1, 2011). URL `http://osisaf.met.no`

Overland J, Wang M (2005) The Arctic climate paradox: The recent decrease of the Arctic Oscillation. Geophys Res Lett 32(6)

Overland J, Wang M (2010) Large-scale atmospheric circulation changes are associated with the recent loss of Arctic sea ice. Tellus A 62(1):1–9

Pacanowski R (1995) MOM 2 documentation, users guide and reference manual. GFDL Ocean Group Tech Rep 3:232

Perovich DK, Richter-Menge JA, Jones KF, Light B (2008) Sunlight, water, and ice: Extreme arctic sea ice melt during the summer of 2007. Geophysical Research Letters 35(11), DOI 10.1029/2008GL034007

Peterson B, Holmes R, McClelland J, Vorosmarty C, Lammers R, Shiklomanov A, Shiklomanov I, Rahmstorf S (2002) Increasing river discharge to the Arctic Ocean. Science 298(5601):2171

Polyakov I, Beszczynska A, Carmack E, Dmitreko I, Fahrbach E, Frolov I, Gerdes R, Hansen E, Holfort J, Ivanov V, et al (2005) One more step toward a warmer Arctic. Geophysical Research Letters 32:L17,605

Polyakov I, Timokhov L, Alexeev V, Bacon S, Dmitrenko I, Fortier L, Frolov I, Gascard JC, Hansen E, Ivanov V, Laxon S, Mauritzen C, Perovich D, K S, H S, Sokolov V, Steele M, Toole J (2010) Arctic ocean warming contributes to reduced polar ice cap. Journal of Physical Oceanography 40:2743–2756, DOI 10.1175/2010JPO4339.1

Prange M (2003) Einfluss arktischer süßwasserquellen auf die zirkulation im nordmeer und im nordatlantik in einem prognostischen ozean-meereis-modell= influence of arctic freshwater sources on the circulation in the arctic mediterranean and the north atlantic in a prognostic ocean-sea ice model. Berichte zur Polar-und Meeresforschung (Reports on Polar and Marine Research) 468

Prange M, Gerdes R (2006) The role of surface freshwater flux boundary conditions in Arctic Ocean modelling. Ocean modelling 13(1):25–43

Proshutinsky A, Johnson M (1997) Two circulation regimes of the wind-driven Arctic Ocean. Journal of Geophysical Research 102(C6):12,493

Proshutinsky A, Ashik I, Häkkinen S, Hunke E, Krishfield R, Maltrud M, Maslowski W, Zhang J (2007) Sea level variability in the Arctic Ocean from AOMIP models. Journal of Geophysical Research 112(C4):C04S08

Rabe B, Karcher M, Schauer U, Toole JM, Krishfield RA, Pisarev S, Kauker F, Gerdes R, Kikuchi T (2011) An assessment of arctic ocean freshwater content changes from the 1990s to the 20062008 period. Deep Sea Research Part I: Oceanographic Research Papers 58(2):173 – 185, DOI http://dx.doi.org/10.1016/j.dsr.2010.12.002

Rabenstein L, Krumpen T, Hendricks S, Koeberle C, Haas C, Hoelemann JA (2013) A combined approach of remote sensing and airborne electromagnetics to determine the volume of polynya sea ice in the Laptev Sea (vol 7, pg 947, 2013). Cryosphere 7(4):1107–1108, DOI {10.5194/tc-7-1107-2013}

Rampal P, Weiss J, Marsan D (2009) Positive trend in the mean speed and deformation rate of arctic sea ice, 19792007. Journal of Geophysical Research: Oceans 114(C5), DOI 10.1029/2008JC005066

Reimnizy E, Dethleff D, Nurnberg D (1994) Contrasts IN Arctic shelf sea-ice regimes and some implications - Beaufort Sea versus Laptev Sea. Marine Geology 119(3-4):215–225, DOI 10.1016/0025-3227(94)90182-1, 4th International Conference on Paleoceanography (ICP IV), KIEL, Germany, Sep. 21-25, 1992

Rigor I, Colony R (1997) Sea-ice production and transport of pollutants in the Laptev Sea, 1979–1993. Science of the Total Environment, The 202(1-3):89–110

Rigor I, Wallace J, Colony R (2002) Response of sea ice to the Arctic Oscillation. Journal of Climate 15:2648–2663

Rinke A, Dethloff K, Dorn W, Handorf D, Moore JC (2013) Simulated arctic atmospheric feedbacks associated with late summer sea ice anomalies. Journal of Geophysical Research: Atmospheres 118(14):7698–7714, DOI 10.1002/jgrd.50584

Rollenhagen K, Timmermann R, Janjic T, Schröter J, Danilov S (2009) Assimilation of sea ice motion in a finite-element sea ice model. Journal of Geophysical Research 114(C05007):doi:10.1029/2008JC005,067

Romanov I (2004) Morphometric Characteristics of Ice and Snow in the Arctic Basin: Aircraft Landing Observations from the Former Soviet Union, 1928-1989. National Snow and Ice Data Center, Boulder, CO, digital media[Available online at http://nsidc org/data/g02140 html]

Rosich B, Meadows P (2004) Absolute calibration of ASAR level 1 products generated with PF-ASAR. ESA Document, Frascati, Italy

Rothrock D (1975) The mechanical behavior of pack ice. Annual Review of Earth and Planetary Sciences 3(1):317–342

Rozman P (2009) The Role of the Fast Ice in an Arctic Sea Ice - Ocean Coupled Model. Master's thesis, Bremen University, Bremen, Germany

Rozman P, Hlemann J, Krumpen T, Gerdes R, Kberle C, Lavergne T, Adams S, Girard-Ardhuin F (2011) Validating satellite derived and modelled sea-ice drift in the laptev sea with in situ measurements from the winter of 2007/08. Polar Research 30(0)

Rudels B, Anderson L, Jones E (1996) Formation and evolution of the surface mixed layer and halocline of the Arctic Ocean. Journal of Geophysical Research 101(C4):8807–8821

Rudels B, Jones EP, Anderson LG, Kattner G (2013) On the Intermediate Depth Waters of the Arctic Ocean, American Geophysical Union, pp 33–46. DOI 10.1029/GM085p0033

Saha S, Moorthi S, Pan HL, Wu X, Wang J, Nadiga S, Tripp P, Kistler R, Woollen J, Behringer D, Liu H, Stokes D, Grumbine R, Gayno G, Wang J, Hou YT, Chuang HY, Juang HMH, Sela J, Iredell M, Treadon R, Kleist D, Van Delst P, Keyser D, Derber J, Ek M, Meng J, Wei H, Yang R, Lord S, Van den Dool H, Kumar A, Wang W, Long C, Chelliah M, Xue Y, Huang B, Schemm JK, Ebisuzaki W, Lin R, Xie P, Chen M, Zhou S, Higgins W, Zou CZ, Liu Q, Chen Y, Han Y, Cucurull L, Reynolds RW, Rutledge G, Goldberg M (2010) The NCEP Climate Forcast System Reanalysis. Bulletin of the American Meteorological Society 91(8):1015–1057, DOI {10.1175/2010BAMS3001.1}

Schauer U, Fahrbach E, Osterhus S, Rohardt G (2004) Arctic warming through the Fram Strait: Oceanic heat transport from 3 years of measurements. Journal of geophysical research 109(C6):C06,026

Schauer U, Beszczynska-Mller A, Walczowski W, Fahrbach E, Piechura J, Hansen E (2008) Variation of measured heat flow through the fram strait between 1997 and 2006. In: Dickson R, Meincke J, Rhines P (eds) ArcticSubarctic Ocean Fluxes, Springer Netherlands, pp 65–85, DOI 10.1007/978-1-4020-6774-7_4

Schmitz WJ, McCartney MS (1993) On the north atlantic circulation. Reviews of Geophysics 31(1):29–49, DOI 10.1029/92RG02583

Shimada K, Kamoshida T, Itoh M, Nishino S, Carmack E, McLaughlin F, Zimmermann S, Proshutinsky A (2006) Pacific ocean inflow: Influence on catastrophic reduction of sea ice cover in the arctic ocean. Geophysical Research Letters 33(8), DOI 10.1029/2005GL025624

Slanina S (2007) Permafrost in the Arctic. Tech. rep., available at www.eoearth.org

Spreen G, Kwok R, Menemenlis D (2011) Trends in arctic sea ice drift and role of wind forcing: 19922009. Geophysical Research Letters 38(19), DOI 10.1029/2011GL048970

Steele M, Boyd T (1998) Retreat of the cold halocline layer in the Arctic Ocean. Journal of Geophysical Research 103(C5):10,419

Steele M, Morley R, Ermold W (2001) Phc: A global ocean hydrography with a high-quality arctic ocean. Journal of Climate 14:2079–2087, DOI 10.1175/1520-0442(2001)014⟨2079:PAGOHW⟩2.0.CO;2

Steele M, Ermold W, Zhang J (2008) Arctic Ocean surface warming trends over the past 100 years. Geophys Res Lett 35:L02,614

Stevens D (1991) The open boundary condition in the United Kingdom fine-resolution Antarctic model. Journal of Physical Oceanography 21(9):1494–1499

Stevens DP (1990) On open boundary conditions for three dimensional primitive equation ocean circulation models. Geophysical & Astrophysical Fluid Dynamics 51(1-4):103–133

Stroeve JC, Kattsov V, Barrett A, Serreze M, Pavlova T, Holland M, Meier WN (2012) Trends in arctic sea ice extent from cmip5, cmip3 and observations. Geophysical Research Letters 39(16), DOI 10.1029/2012GL052676

Swift JH (1984) The circulation of the denmark strait and iceland-scotland overflow waters in the north atlantic. Deep Sea Research Part A Oceanographic Research Papers 31(11):1339 – 1355, DOI http://dx.doi.org/10.1016/0198-0149(84)90005-0

Thompson D, Wallace J (1998) The Arctic Oscillation signature in the wintertime geopotential height and temperature fields. Geophysical Research Letters 25(9):1297–1300

Thorndike A, Colony R (1982) Sea ice motion in response to geostrophic winds. Journal of Geophysical Research 87(C8):5845–5852

Timco G, O'Brien S (1994) Flexural strength equation for sea ice. Cold Regions Science and Technology 22(3):285–298

Timco G, Weeks W (2010) A review of the engineering properties of sea ice. Cold Regions Science and Technology 60(2):107–129

Timokhov L, Tanis F (1997) Environmental Working Group Joint US–Russian Atlas of the Arctic Ocean-Winter Period. Environmental Research Institute of Michigan in association with the National Snow and Ice Data Center, Arctic Climatology Project, CD-ROM

Timokhov L, Tanis F (1998) Environmental Working Group Joint US–Russian Atlas of the Arctic Ocean-Summer Period. Environmental Research Institute of Michigan in association with the National Snow and Ice Data Center, Arctic Climatology Project, CD-ROM

Tremblay LB, Hakakian M (2006) Estimating the sea ice compressive strength from satellite-derived sea ice drift and ncep reanalysis data. Journal of Physical Oceanography 36:2165–2172, DOI 10.1175/JPO2954.1

Weingartner T, Danielson S, Sasaki Y, Pavlov V, Kulakov M (1999) The Siberian Coastal Current: A wind-and buoyancy-forced Arctic coastal current. Journal of geophysical research 104(C12):29,697

Willmes S, Adams S, Schroeder D, Heinemann G (2011) Spatio-temporal variability of polynya dynamics and ice production in the Laptev Sea between the winters of 1979/80 and 2007/08. POLAR RESEARCH 30, DOI {10.3402/polar.v30i0.5971}

Winsor P, Björk G (2000a) Polynya activity in the Arctic Ocean from 1958 to 1997. Journal of Geophysical Research-Oceans 105(C4)

Winsor P, Björk G (2000b) Polynya activity in the Arctic Ocean from 1958 to 1997. Journal of Geophysical Research-Oceans 105(C4)

Wu B, Wang J, Walsh JE (2006) Dipole anomaly in the winter arctic atmosphere and its association with sea ice motion. Journal of Climate 19:210–225, DOI doi:10.1175/JCLI3619.1

Yang J (2009) Seasonal and interannual variability of downwelling in the beaufort sea. Journal of Geophysical Research: Oceans 114(C1), DOI 10.1029/2008JC005084

Zhang J, Hibler III W (1997) On an efficient numerical method for modeling sea ice dynamics. Journal of Geophysical Research C Oceans 102:8691–8702

Zhang J, Lindsay R, Schweiger A, Rigor I (2012) Recent changes in the dynamic properties of declining arctic sea ice: A model study. Geophysical Research Letters 39(20), DOI 10.1029/2012GL053545

Zhang X, Sorteberg A, Zhang J, Gerdes R, Comiso J (2008) Recent radical shifts of atmospheric circulations and rapid changes in Arctic climate system. Geophysical Research Letters 35(22):L22,701

Acknowledgements

I would like to express my gratitude towards my supervisor Prof. Rüdiger Gerdes, AWI. Ruediger has been a great supervisor. He managed to guide me in my research and yet left me a lot of scientific freedom. His door has always been open and he always had 'a couple of minutes' for me.

I am grateful to Prof. Laurenz Thomsen, Jacobs University who agreed to be my second referee.

Martin Losch, AWI, my referee as an external member has been of a great help to me with the MITgcm. His friendly, detailed and on-spot explanations of the model code and physics have been not only helpful but very inspiring.

Michael Karcher, AWI and O.A.Sys - Ocean Atmosphere Systems, has acted as my advisor during the last year of my graduate studies. His good mood and relaxed communication have encouraged me through the hardest moments.

Cornelia Köberle supervised and supported my first steps into the numerical modeling and coding. She kindly showed me around the NAOSIM code.

Prof. Ursula Schauer, AWI, Jens Hölemann, AWI and IFM-GEOMAR and Frank Kauker, AWI and O.A.Sys - Ocean Atmosphere Systems have together with Ruediger, Martin, Michael and Cornelia attended my regular POLMAR PhD Panel Meetings and guided my scientific work.

I am very grateful to Claudia Hanfland and Claudia Sprengel from the POLMAR graduate school at AWI. Both have not only organized appealing courses, but advised me and helped with many technical and personal issues.

I would like to thank Marcel Nicolaus, AWI and Chris Petrich, Norut Narvik - Nothern Research Institute Narvik, Norway (at that time International Arctic Research Center, Fairbanks, Alaska) who made possible my only hands-on sea ice experience during the SIZONet field campaign in May 2010, Barrow, Alaska.

Furthermore i would like to thank everybody at AWI who is encouraging the life-work balance guideline of the institute. Winfried Hebold-Heitz, Ursula Schauer (also former AWI women's representative), Beate Meinardus and Andrea Bleyer have all been very supportive whenever I encountered difficulties.

I am grateful for the opportunity to work along with Priska Hunkeler, Thomas Krumpen, Valeria Selyuzhenok, Stefan Hendricks, Lasse Rabenstein, Vera Fofonova, Giulia Castellani, Karel Castro-Morales, Kathrin Riemann-Campe, Hiroshi Sumata, Malte Thoma, Hartmut Hellmer, Verena Haid, Ralph Timmermann, Jürgen Determann, Wee Cheah and many other present and former AWI colleagues from the Sea ice physics group and from the Climate Sciences division who helped to create a relaxed and productive working environment.

My graduate studies have been partially supported by a grant of Municipality of Ljubljana, Slovenia.

Finally, I would like to thank my family for their unfailing love, patience and support.

Statement of Source

Declaration

I declare that this thesis is my own work and has not been submitted in any form for another degree or diploma at any university or tertiary institution of tertiary education. Information derived from published or unpublished work of others has been acknowledged in the text.

Date and Signature